The Pennsylvania State University

The Graduate School

College of Earth and Mineral Sciences

SELECTIVE CATALYTIC REDUCTION OF NO_X BY NH_3 FOR DIESEL EXHAUST AFTERTREATMENT

A Thesis in

Energy and Mineral Engineering

by

Christopher H. Sokolowski

Submitted in Partial Fulfillment
of the Requirements
for the Degree of

Master of Science

August 2014

The thesis of Christopher H. Sokolowski was reviewed and approved* by the following:

Yongsheng Chen
Assistant Professor of Energy and Mineral Engineering
Thesis Advisor

Sarma V. Pisupati
Associate Professor of Energy and Mineral Engineering

Jonathan P. Mathews
Associate Professor of Energy and Mineral Engineering

Luis F. Ayala H.
Associate Professor of Petroleum and Natural Gas Engineering
Associate Department Head for Graduate Education of the Department of Energy and Mineral Engineering

*Signatures are on file in the Graduate School

ABSTRACT

The increasing price of liquid fuels and an increased focus on fuel efficiency has driven vehicle engine manufacturers toward diesel and other lean burn engines at the cost of increased emissions of nitrogen oxides (NO_X), which contribute to pollution such as smog, ground level ozone, and acid deposition. Within the past thirty years, increasingly stringent NO_X emission standards have forced engine manufacturers to develop novel ways to reduce these emissions. With the implementation of the latest American and European NO_X emission standards, Selective Catalytic Reduction (SCR) has become the most prominent NO_X reduction method in lean-burn engines.

In the present work, a method is developed to test the performance of commercial SCR catalyst coated monoliths and probe the deactivation mechanisms. A monolith testing apparatus is constructed for these purposes. Necessary design features included a programmable gas mixing system, a steam generator, a temperature control system, and an analysis system based upon Fourier-transformed infrared spectroscopy. It is found that a high flow rate of carrier gas as well as a method to generate a water mist and prevent dripping is essential to ensure a stable supply of steam and repeatable results.

Important SCR reactions, namely the standard, fast, and slow SCR reactions as well as NH_3 adsorption and performance of a zeolite catalyst coated monolith were investigated at three temperatures – 250 and 300 °C representing engine operation at normal operating conditions and 400 °C representing engine operation at high load. The amount of NH_3 adsorbed decreased with temperature in line with previous studies while NO_X reduction performance increased with higher temperatures at all inlet compositions tested. A transient drop in NO conversion performance was observed upon introduction of NH_3 without the presence of NO_2 consistent with previous studies suggesting an NH_3 inhibition mechanism. When supplied with 1:1 and 1:3 ratios of NO:NO_2 at 250 °C, the catalyst reduced more NO_X than NH_3 suggesting that part of the NO_X reduction was proceeding

through an ammonium nitrate intermediate and generating nitric acid. In addition, NH_3 oxidation into N_2O was prevalent at 300°C in an excess of NO_2. The SCR reaction results indicate that both transient effects and side reactions play an important role in an NH_3 SCR system, particularly one that is designed to operate under continuously changing conditions.

Catalyst aging mechanisms were investigated by comparing catalytic performance, material structure, and surface composition of a new and a used zeolite catalyst monolith for the fast SCR reaction. Physical analysis of the catalyst monoliths through X-ray Photoelectron Spectroscopy (XPS), X-ray Diffraction (XRD), and Scanning Electron Microscopy (SEM) with Energy-Dispersive X-ray Spectroscopy (EDS) indicated four aging mechanisms. Both the new and used catalyst monoliths performed at least 95% NO_X reduction in the fast reaction at all temperatures tested. Despite the similar NO_X reduction performance, the used catalyst monolith exhibited lower NO oxidation performance, increased NH_3 oxidation, and a lower quantity of adsorbed NH_3 compared to the new catalyst monolith. Dealumination is likely the primary cause of the used catalyst monolith's lower NO_X reduction performance with promoter metal deactivation, poisoning by sulfur and phosphorous, and mechanical failure of the catalyst coating on the monolith also contributing to the decreased performance. The results do not find evidence of carbon coking. This investigation into catalyst aging mechanisms confirms the efficacy of the commercial SCR catalyst monolith over long time periods.

TABLE OF CONTENTS

LIST OF FIGURES

LIST OF TABLES

Acknowledgments

I would like to thank all the faculty and staff who have assisted me greatly with this project including my advisor Dr. Yongsheng Chen for providing me with this thesis project and donating his time towards helping me succeed. I would like to also thank my committee - Dr. Sarma Pisupati and Dr. Jonathan Mathews – for their time and effort in reviewing my thesis.

This project would not have been possible with the tremendous help of the Earth and Mineral Sciences Energy Institute staff including laboratory assistants David Johnson and Mamoru Fuji. Without the dozens of hours of assistance from David and Mamoru, I would have had neither the components nor the expertise to complete this project. A special thanks goes to Cindy Anders of the Energy Institute for guiding me through the different procedures at the Institute and her patience with my seemingly unending requests for ordering supplies such as the oodles of compressed gas cylinders needed over the course of this project.

Chapter 1

Diesel Engines and Selective Catalytic Reduction

1.1 Introduction

The industrial revolution was marked by ever increasing combustion of fossil fuels, starting with coal and later progressing to petroleum and natural gas. While this transition has added many new technologies to society and increased quality of life tremendously, it has not been without cost. Among the costs of industrialization has been air pollution related to the combustion of these fuels. As the world has become more and more industrialized, ever increasing amounts of air pollutants are expelled with cities in developing countries such as China recording unprecedented levels of smog [1]. Even in countries such as the United States with strict pollution controls, there is a desire to continue to reduce air pollution as evidenced by continuous revisions of the Clean Air Act [2].

Compression ignition (diesel) engines are today one of the most prevalent engine designs [3]. Diesel engines power most heavy transportation including trucks, trains, ships, construction equipment, and increasingly passenger cars throughout the world [4-6]. Diesel engines are expected to increase in popularity over the coming decades. While diesel fuel accounted for about 30% of the worldwide transportation fuel supply in 2010, between the period of 2010 and 2040, transportation fuel demand is expected to increase worldwide by 40% with 70% of that increase being met by diesel [7, 8]. While fuel demand for personal transportation will decrease over that 40-year period [7, 8], heavy duty transportation, a sector overwhelmingly powered by diesel engines [9], is expected to grow 65% over that same period [7]. In the United States, demand for diesel fuel is expected to increase by 0.8 million

barrels per day to 4.3 million barrels per day in 2040, a 23% increase over 2011; in contrast, gasoline use is expected to drop by 1.6 million barrels per day over the same time period [6].

As with all combustion systems, diesel engines' exhaust contributes to air pollution. Modern emissions control schemes have been developed to curtail these emissions, with an intense focus beginning in 1970 with the passage of the Clean Air Act in the United States and later with air pollution standards in the European Union [2, 10]. These standards are being continually tightened [10] due to a desire to improve public health as well as the increasing number of combustion sources contributing to pollution [3].

Developing methods to reduce the output of these pollutants from diesel engines to reduce environmental impact and comply with regulations has become a focus area for combustion and catalyst research. Considering the large predicted growth in the heavy duty transportation sector over the coming years, it is especially important to consider heavy duty diesel applications when designing emissions control measures.

1.2 The Diesel Engine

Two engine types dominate ground transportation [9, 11]. *Spark ignition* (SI) engines use the Otto cycle and most commonly consume gasoline fuel while compression ignition (CI) engines use the diesel cycle and most commonly consume diesel fuel [11]. Both engine types operate on similar thermodynamic cycles; however, compression ignition engines present inherent efficiency advantages over spark ignition engines.

The *compression ratio*, the volume of the exhaust gases compared to the volume of the compressed air-fuel mixture, is a major factor in the efficiency of heat engines [12]. One can increase efficiency by increasing compression of the air-fuel mixture [12], but since adiabatic compression

increases temperatures, as compression ratio increases, gas temperature increases. Since spark ignition engines intake air-fuel mixtures, the fuel must resist ignition at these high temperatures (until a spark is generated). While higher octane fuels improve resistance to autoignition, the instability of the gasoline at high temperature limits compression ratio and therefore the efficiency of the spark ignition engine [13, 14]. Compression ignition engines intake air only and therefore are not limited by gas temperature. Fuel is only injected shortly before maximum compression is achieved. This means that compression ratio and thus efficiency is primarily limited by the strength of materials in the engine to resist high temperatures and pressures [13]. Compression ignition engines also achieve increased efficiency over spark ignition engines due to reduced pumping losses. This is primarily due to the lack of a throttle plate to regulate engine speeds [15]; in compression ignition engines, engine speed can be regulated by adjusting fuel flow.

However, the tradeoff to all these advantages is that compression ignition engines, for a given power output, can generate more pollutants such as NO_X, particulate matter, and unburnt hydrocarbons than spark ignition engines [16]. This increase in production of hydrocarbons and particulate matter is partially due to the usage of diesel fuel with long chain hydrocarbons and partially due to the lack of a homogeneous air-fuel mixture, both of which make achieving complete combustion difficult. This is improved through adding excess air to the engine thus resulting in a “lean-burn” cycle, but adding excess air results in the generation of different pollutants such as NO_X. There has been decades of research into reducing emissions both through use of alternative, less polluting fuels [17] (for example dimethyl ether [18]) and through use of homogeneous charge compression ignition [19, 20], but both of these technologies still have significant hurdles to overcome.

1.3 An Overview of Diesel Pollutants

All hydrocarbon combustion in oxygen, including diesel fuel, would ideally produce only CO_2 and H_2O. In reality many side reactions occur producing undesirable and toxic byproducts. Three pollutants are caused by incomplete combustion - carbon monoxide, unburned hydrocarbons, and soot. One pollutant, NO_X, is caused primarily by high temperature combustion in air. Finally, other combustion byproducts such as sulfur dioxide can arise from impurities in the fuel.

1.3.1 Incomplete Combustion Byproducts

Carbon monoxide is generated through incomplete oxidation of carbon atoms in the fuel. In humans, the protein hemoglobin binds to oxygen and transports it throughout the body. Carbon monoxide reacts with hemoglobin to form the stable compound carboxyhemoglobin, which cannot perform this oxygen transportation function [21]. As a result, carbon monoxide exposure leads to oxygen deprivation (hypoxia) [22].

Unburned hydrocarbons (HC) are hydrocarbon vapors that remain after incomplete combustion of a hydrocarbon fuel. In addition to being toxic, these hydrocarbon vapors participate in reactions that form ground level (tropospheric) ozone [23], which is a respiratory irritant and contributes to respiratory diseases [24].

Particulate matter (PM) consists of solid particles present in exhaust. Organic particulate matter, commonly called soot, is caused by incomplete combustion of large, complex hydrocarbon molecules. Since diesel fuel is comprised of heavier, longer chain hydrocarbon molecules than gasoline, soot is a pollutant more prevalent in diesel engines than gasoline engines [4, 25]. The large hydrocarbon molecules in diesel fuel combust via diffusion flames in fuel-rich parts of combustion zone [26]. In these diffusion flames, volatile components of the fuel as well as the hydrogen atoms on the long chains

combust first leaving a slow-burning central carbon particle. Since the engine must be optimized to produce high power in a limited combustion chamber volume, it is not practical to wait for all carbon particles to slowly combust and release their energy before recharging the combustion chamber with new air and fuel. Instead, the uncombusted carbon particles are carried out by the exhaust stream as particulate matter [27]. Particulate matter has been correlated with respiratory and cardiovascular disease [28].

1.3.2 Nitrogen Oxides

Nitrogen oxides, more commonly known as NO_X, is a term referring to the sum of two pollutants, nitric oxide (NO) and nitrogen dioxide (NO_2). In combustion, NO comprises majority of NO_X emissions; NO_2 only accounts for about 5% of the total NO_X emissions [29]. Nitrogen oxides in themselves are respiratory irritants, but since they are extremely reactive, they are short lived in the environment [30]. However, NO_X readily reacts with other molecules in the atmosphere to produce longer-lived secondary pollutants. Where ultraviolet radiation is present (typically from sunlight), NO_X reacts with volatile hydrocarbons to produce ground level ozone (O_3) and aerosols (particulate matter) [31]. Nitrogen oxides also react with water in the atmosphere to produce nitric acid, which deposits on soil and surface water harming plant and animal species sensitive to pH [32]. Acid deposition also corrodes metal structures and dissolves stone structures, particularly those made of carbonate rocks such as limestone and marble [33].

Nitric oxide can form from three distinct sources. The main mechanism responsible for NO production in diesel engines is the *extended Zeldovich mechanism*; the NO_X produced from this

mechanism is also known a *thermal NO_X* due to the mechanism's dependence on high temperature [34]. This mechanism is comprised of many radical reactions with the three most important reactions being:

$$N_2 + O \rightarrow NO + N \quad (1)$$

$$N + O_2 \rightarrow NO + O \quad (2)$$

$$N + OH \rightarrow NO + H \quad (3)$$

The hydroxyl radical is generated from combustion intermediates. The initial oxygen and nitrogen radicals can be generated from intermediate stages of combustion, but they are most commonly generated through dissociation of molecular nitrogen and oxygen at high temperatures [35].

Fuel NO_X is caused by nitrogen containing impurities in the fuel. The exact mechanism for this type of NO_X generation is not completely understood and presumably dependent on the structure of the nitrogen impurity [36]. Fuel NO_X can be reduced by removing nitrogen impurities within the fuel [37].

The remaining NO_X that cannot be attributed to either thermal NO_X or fuel NO_X is known as prompt NO_X. Prompt NO_X is caused by reaction of fragments of fuel molecules with atmospheric nitrogen [38]. Prompt NO_X is the smallest contributor to NO_X emissions; however, since it is not as temperature dependent as thermal NO_X, its proportion of total NO_X emissions increases inversely to temperature [39].

Nitrous oxide (N_2O), while an oxide of nitrogen, is not considered a part of NO_X under environmental legislation. Unlike all the previous pollutants mentioned, nitrous oxide is not a natural component of diesel exhaust; rather, it is generated as a byproduct of NO_X reducing catalysts [16]. Nitrous oxide causes ozone depletion and is a powerful greenhouse gas with a global warming potential 298 times that of CO_2 [40]. It therefore is regulated under ozone depletion and global warming regulations.

1.3.3 Other Fuel Impurities

Other impurities in the fuel can produce undesirable byproducts in the exhaust. However, the majority of impurities are removed at the refinery, and exhaust treatment to prevent the remaining impurities from being released to the atmosphere is not practiced in automobiles [41]. One common impurity is sulfur, which combusts to produce sulfur dioxide. Sulfur dioxide combines with water in the atmosphere to produce sulfuric acid, which is carried down from the atmosphere as acid deposition [42]. Improved fuel standards have worked to reduce this problem. The introduction of the ultra-low sulfur diesel (ULSD) standards in Japan in 2005, the United States in 2006, and the European Union in 2009 limits sulfur content in diesel fuel to 15 ppm [43]. Removing sulfur in the fuel is also important as sulfur is a poison to many catalysts used in pollution control [44].

1.4 Emissions Control Legislation

The first NO_X emissions controls in the world were enacted in Ventura County, California in 1969 covering industrial boilers [45]. The United States' Clean Air Act of 1970 regulated vehicle emissions on a national level for the first time [2], and since then most industrialized counties have followed with their own vehicle emissions regulations. The two most widely used vehicle emissions standards today are written by the federal government of the United States and by the European Union [46].

The number of pollutants regulated, the number of vehicle types regulated, and the stringency of the requirements have all increased since the original legislation [47]. The emissions of heavy-duty highway compression ignition (diesel) engines have been regulated in the United States since model year 1974 [48]. European countries began regulating these vehicles beginning with model year 1988 vehicles [49]. In the United States, the category of heavy duty highway compression ignition engines includes all on-road vehicles weighing over 8,500 lbs and powered by compression ignition engines;

similar definitions apply throughout the world. While the United States regulations specified NO_X emissions since model year 1974, NO_X was not classified as an individual pollutant until model year 1985; prior to this, only the sum of HC + NO_X emissions was regulated [48].

Figure 1.1 shows historical NO_X regulations of the United States and the European Union for heavy duty highway compression ignition engines. The data is presented in a logarithmic scale to emphasize the relative change in each new standard. While continuous progress has been made over the 30-year period, the most recent regulations represent the largest relative reduction in pollutants. The model year 2010 emissions regulations in the United States is the largest drop. This single change, from 1.2 g/BHP-hr (0.90 g/kWh) in 2009 to 0.20 g/BHP-hr (0.15 g/kWh), reduced emissions by 83% from the previous model year. Similarly, the 2014 European Union regulations followed the United States and reduced emissions from 2.0 g/kWh in 2013 to 0.40 g/kWh in 2014. While neither law specified how the reductions needed to be achieved, their stringent requirements essentially forced all manufactures into implementing into their vehicles selective catalytic reduction technology [50].

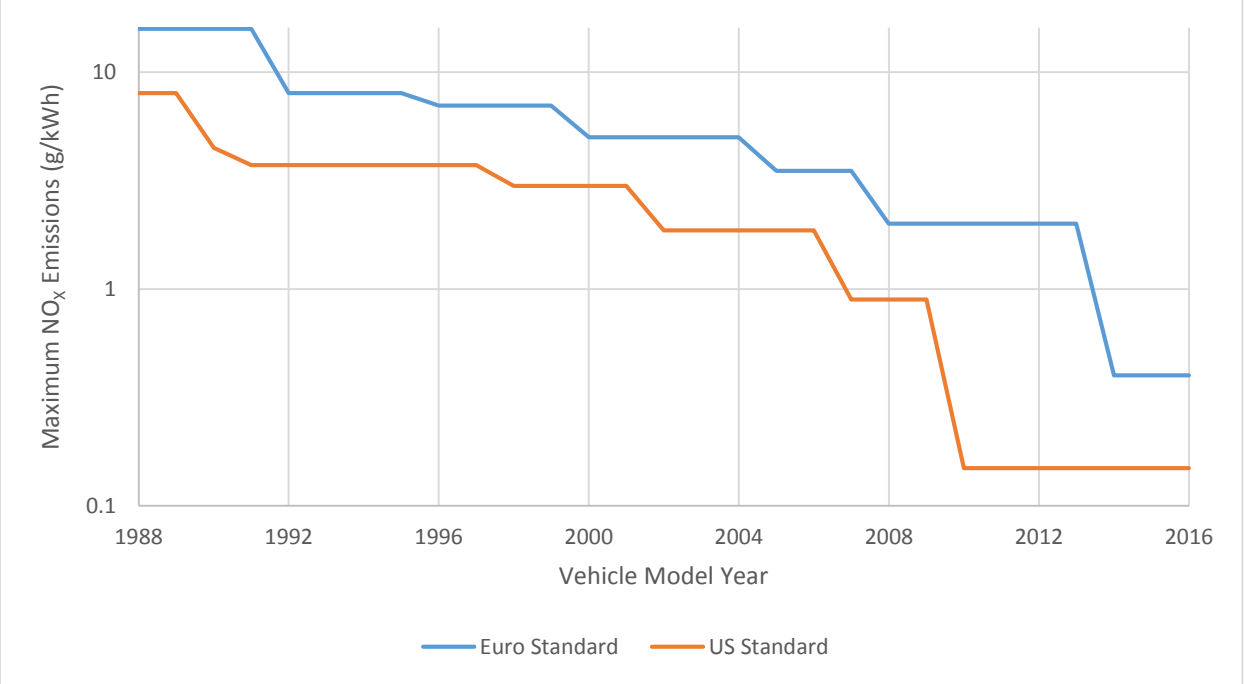

Figure 1.1: NO_X emissions standards in the United States and the European Union over time

1.5 Emissions Control Measures

The challenge in designing a vehicle's emissions control system is in balancing conflicting goals. Three conditions inhibit formation of incomplete combustion byproducts: increasing air-fuel ratio, increasing combustion temperature, and increasing the residence time of fuel in the combustion zone [51]. However, the exact opposite three conditions inhibit formation of NO_X: decreasing air-fuel ratio, decreasing combustion temperature, and decreasing the residence time of fuel in the combustion zone. In addition, the system must be compact enough to fit within a vehicle and robust enough to survive adverse vehicle conditions such as thermal cycling. All of these requirements must be balanced with the need to produce a system that is both inexpensive and requires little maintenance.

The most common method of reducing pollutants in spark ignition engines is with the *three-way catalyst*, which acts simultaneously to remove CO, HC, and NO_X [52]. As a result, the following three reactions are performed:

$$2\,NO_X \rightarrow x\,O_2 + N_2 \quad (4)$$

$$2\,CO + O_2 \rightarrow 2\,CO_2 \quad (5)$$

$$HC + O_2 \rightarrow CO_2 + H_2O \quad (6)$$

The three-way catalyst is extremely effective; however, it only works in stoichiometric air-fuel ratios, it cannot deal with particulate matter, it is expensive due to incorporating precious metals, and it is susceptible to deactivation by catalyst poisons such as sulfur [16, 52, 53]. Three-way catalysts are only reasonable to use in a vehicle burning a lighter fuel like gasoline where stoichiometric air-fuel ratios are feasible [52].

The three-way catalyst is ineffective in diesel engines. When combusting diesel fuel, a high air-fuel ratio, also known as *lean burn*, is needed to accelerate the combustion of large chain molecules and reduce the amount of soot generated [54]. However, in the presence of excess oxygen the three-way catalyst cannot perform the NO_X reduction reaction.

In these lean burn systems, different exhaust treatment measures have to be used, which consists of three stages rather than the single stage used in gasoline and light fuel combustion systems [51]. The first stage consists of an oxidation catalyst, which uses excess oxygen in the exhaust to oxidize the remaining hydrocarbons, carbon monoxide, and some of the soot to carbon dioxide and water [55]. The second stage consists of a filter to remove particulate matter. Since the particulate matter is combustible carbon soot, the particulate filter can be occasionally regenerated by heating to high temperature and burning off the captured soot particles [56].

However, NO_X is still present after the two treatment stages, and it presents a major challenge to remove. One method to eliminate NO_X is to reduce its generation. At the point of use, thermal NO_X is the first source targeted since combustion temperature is easily controllable [57]. Combustion temperature could be reduced by simply diluting the fuel with more air, but adding air results in more oxygen being present in the system, counteracting the lower temperature's NO_X reducing effects. Instead, thermal NO_X reduction in a diesel engine is achieved through engine tuning and exhaust gas recirculation (EGR) [58, 59].

In *exhaust gas recirculation* (EGR), some of the exhaust gas is recirculated into the intake stream of the engine where it dilutes the air-fuel mixture [3, 60]. The exhaust gas contains higher proportions of water and carbon dioxide and lower proportions of nitrogen and oxygen compared to air. The lower proportion of nitrogen and oxygen in the combustion chamber also serves to reduce NO_X formation. Due to the water content, the exhaust gas also has a higher specific heat than air. The high specific heat lowers combustion temperature, reducing NO_X formation in the engine [59]. The main drawback with EGR besides additional complexity of the engine is that the lowered combustion temperature produces more soot, which must be removed by exhaust treatment.

1.6 Selective Catalytic Reduction (SCR)

While EGR was very effective in meeting the first generation of NO_X emission targets, it cannot meet later standards. In modern diesel engines, the predominant method of reducing NO_X in exhaust is through EGR combined with selective reduction [46].

Selective reduction is a general term encompassing a variety of technologies whose goal is to reduce NO_X in the exhaust stream. While a recent innovation for use in vehicles, selective reduction has

been in wide use in stationary power sources for over a decade [61-63]. The goal of selective reduction is to reduce (decrease the oxidation state of) NO and NO_2 to N_2. The reaction needs to be selective because the goal is to not reduce O_2 or any other components, since doing so could generate additional NO_X and pollutants. The desired reaction is also selective because the catalyst's goal is to completely reduce NO and NO_2 into N_2 without producing N_2O, a byproduct which would be generated with incomplete reduction [64].

Thermodynamically, NO_X reduction reaction should proceed on its own at ambient conditions, since below about 900 °C, N_2 and O_2 are favored over NO and NO_2 [65] (ΔH_f = +90 kJ/mol) [16]. However, the activation energy of this reaction is too large to occur naturally in any significant amount; therefore, one of three methods may be performed. In *Direct reduction*, a catalyst is used to reduce the activation energies of the NO_X decomposition reactions and no reducing agent is added. In a second method, *selective non-catalytic reduction* (SNCR), a reducing agent such as NH_3 is added to the exhaust stream to reduce NO_X through alternate, faster reactions, but no catalyst is present. In a third method, *selective catalytic reduction* (SCR), a reducing agent such as NH_3 is added to the exhaust stream and a catalyst is present.

Selective non-catalytic reduction is popular in stationary combustion systems that operate at steady state such as boilers used for power plants [61]. These systems operate at steady state for long periods of time. Consequently, engineers can precisely predict flow conditions and tune these combustion systems to achieve very high NO_X reduction without a catalyst [66-68]. However, the exhaust treatment systems of vehicles have to deal with a wide range of engine operating conditions. For this reason, vehicular applications use catalysts.

1.6.1 Types of Catalysts

Direct reduction would be extremely desirable due to its lack of requiring a reducing agent. There has not been much study of this method due to the lack of catalysts that can adsorb NO_X and convert NO_X into N_2 and O_2, and desorb N_2 and O_2 [16, 69]. One study [70] focused on using platinum as a catalyst for this reaction as platinum causes NO to dissociate forming a Pt-O complex and N_2. However, that study found that in an oxygenated environment the oxygen never dissociates from the platinum, and eventually all platinum oxidizes, deactivating the catalyst. Current SCR catalysts are designed to use a reducing agent, which either serves to remove oxygen from the catalyst or facilitates NO_X removal through a completely different mechanism [71].

Initial research into vehicular implementations of SCR focused on using hydrocarbons to reduce NO and NO_2 on a catalyst [65], which is known as *hydrocarbon SCR* or HC-SCR. Hydrocarbon SCR is similar in principle to the mechanism of the three-way catalyst except that the catalysts being researched would work in the oxygenated environment of a lean burn engine. The advantage of HC-SCR is that the reducing agent is already present in the exhaust reducing complexity of the SCR system.

There are two approaches to HC-SCR. The simpler and older method involves catalysts that can reduce NO_X in real time with hydrocarbons in the oxygenated exhaust a diesel engine naturally produces. For these systems, the majority of laboratory research has focused on using 3-4 carbon alkanes and alkenes as reducing agents and has had promising results [72, 73]. However, these catalysts have had trouble operating in actual diesel exhaust, which contains hundreds of different hydrocarbon compounds, some of which are catalyst poisons [70]. The catalysts tested have also had very narrow ranges of operating temperatures in which activity is high [70], and the catalysts have poor activity below about 300 °C [74]. This low activity at low temperature is an issue because the temperature of diesel exhaust, the source of heat for the catalyst, is below 300 °C at engine idle. While diesel engines

only produce appreciable amounts of NO_X at high load [75], and diesel engines at high load do produce high exhaust temperatures, the engine's NO_X output increases more quickly than the catalyst heats; therefore, the catalyst must be able to deal with NO_X at idle temperature.

A more recent method is *NO_X storage-reduction* (NSR). In this method, the diesel engine operates in its conventional lean burn mode most of the time, and NO_X binds to a catalyst but does not react. When the catalyst can no longer store any more NO_X, the engine switches to a fuel-rich mode, and the excess hydrocarbons generated by the engine reduce the stored NO_X. The technology is promising, but it is still in early development and suffers from rapid catalyst degradation [74].

In current practice, NH_3 SCR is the most popular SCR implementation for lean-burn engines [76]. Due to the inherent safety issues in working with concentrated NH_3 gas, either aqueous NH_3 or more commonly pure liquid urea ($(CH_2)_2CO$) is stored. The fluid is injected into the exhaust directly upstream of the catalyst and vaporizes. In either case, NH_3 is still the reductant as urea reacts with water to form carbon dioxide and NH_3 before reaching the catalyst [77].

1.6.2 Catalyst Materials

The performance and longevity of a SCR catalyst are highly dependent on the environment in which it will be used. Vehicular exhaust systems present a large challenge for SCR catalysts, since the catalyst must operate in a wide range of conditions. A SCR catalyst should be effective in reducing NO_X at low temperatures, such as when a diesel vehicle's is warming up or idle. Simultaneously, the catalyst must be able to survive very high temperatures that occur when the engine is at high load or when the diesel particulate filter is being regenerated. It must withstand vibrations that occur during the normal operation of the vehicle, and it must remain stable in thermal cycling that occurs as the vehicle is turned

on and off. In addition, the catalyst must withstand a range of compounds present in diesel exhaust such as various hydrocarbons [78, 79] and the common catalyst poison sulfur dioxide [80].

Selective catalytic reduction catalyst materials can be grouped into three categories [57]. The initially studied SCR catalysts were supported noble metal catalysts such as Pt/Al_2O_3. A prominent commercial implementations of a supported noble metal catalyst is the three-way catalyst, and while they have been studied for hydrocarbon-SCR [70, 73], they are not used for NH_3-SCR. Later, supported metal oxide catalysts were introduced such as V_2O_5 [81], WO_3 [82], and oxides of manganese [76]. Supported metal oxide catalysts have received wide deployment in stationary NH_3-SCR systems [82]. Metal oxide catalysts provide higher resistance to poisons than the noble metal catalysts. In the past V_2O_5 catalysts had some vehicular applications in Europe in the early 2000s [83].

Metal oxide catalysts have fallen out of favor due to issues with thermal stability. The implementation of particulate filters to reduce soot emissions causes exhaust temperature to exceed 650 °C when the filter is being regenerated. The most common metal oxide catalysts, V_2O_5-WO_3/TiO_2, cannot operate above 550 °C. The TiO_2 support changes phase from anatase to rutile rendering the catalyst inactive, and above 500 °C vanadium evaporates from the surface of the catalyst forming a toxic aerosol that is discharged out of the exhaust [78].

The final and most recent category is ion-exchanged zeolite catalysts. These catalysts are currently the most studied for SCR systems. Initial research showed that copper-zeolite catalysts had NO_X conversion 50% higher at low temperatures compared to supported metal oxide catalysts; however, the copper zeolite catalysts had issues with thermal stability over long times and were easily poisoned by sulfur dioxide and water [84]. Even as recently as the early 2000s, zeolite SCR catalysts were not considered to ever become viable [65].

Research has shifted to zeolites promoted by other metals. By using novel ion exchange methods, iron-zeolite catalysts could withstand up to 20% H_2O and 150 ppm SO_2 (molar basis) without

loss of activity [85, 86]. Based on this evidence, reports concluded that the ion exchange method was the most important factor in the performance of the catalyst. Recently, there has been contention on whether preparation method is as important as previously believed; rather, researchers attribute the increased activity to the topology of the zeolite involved [87]. Because of their ability to operate over a wide variety of conditions, ion exchanged zeolite catalysts have received significant attention for vehicular SCR implementations [84, 87].

1.6.3 Reaction Mechanisms

While there is some dispute on the mechanism of NH_3-SCR, there is agreement on the overall reactions [64, 88] that occur on zeolite catalysts. All of these reactions presented below are assumed to be in an environment with free oxygen. Zeolite catalysts are designed to operate in an oxygenated environment; indeed, NO_X reduction decreases tremendously in environments without oxygen [74].

For zeolite catalysts, at high temperatures, the standard SCR reaction proceeds in the manner [89-91] shown in Figure 1.2. Free oxygen binds to metal ions. Simultaneously, two NH_3 molecules bind to two Brønsted acid sites to form NH_4^+ groups on the catalyst. A NO molecule then reacts with the oxygen bound on the catalyst to form a metal-NO_2 group. After that, the two NH_4^+ groups and the NO_2 group react to form a $(NH_4)_2NO_2$ intermediate. Another NO molecule then binds to this compound, causing it to destabilize and decompose into H_2O and N_2 and regenerate a metal site and two Brønsted acid sites. It is generally accepted that the reaction between free NO and the metal ion-oxygen complex on the surface to form NO_2 is the rate limiting step in SCR, although there is inconsistency in the explanations as to why this is the rate limiting step [92].

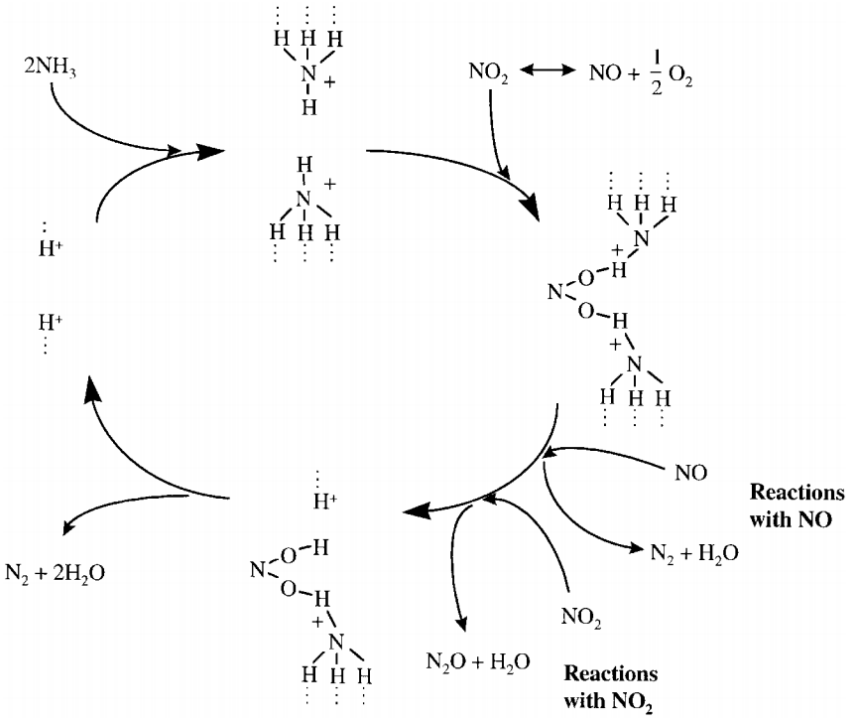

Figure 1.2: SCR reaction mechanism at moderate and high temperatures [91]

Contemporary research has focused on improving the fast SCR reaction at low temperatures, which is generally accepted to involve nitrate and nitrite intermediates [64, 87, 93] and is shown in Figure 1.3. Ammonia adsorbs onto the catalyst forming ammonium groups. NO_2 reacts with oxygen to form a nitrate on the catalyst, NO reduces nitrate to nitrite, and nitrite reacts with ammonium to form an ammonium nitrite intermediate, which decomposes to N_2 and H_2O. Undesirable byproducts are generated when nitrate reacts with ammonium instead of NO. This forms ammonium nitrate which decomposes into either N_2O or HNO_3. At close to ambient conditions, NH_3 can also poison the catalyst preventing NO from reducing nitrates [94].

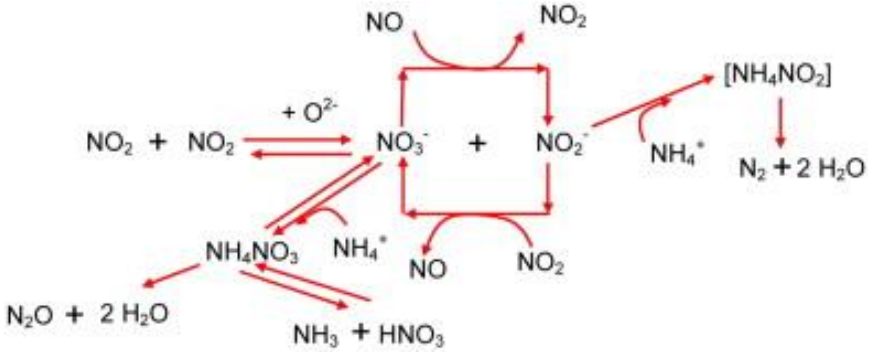

Figure 1.3: SCR reaction mechanism at low temperature.[64]

1.6.4 Catalytic Reactions

When urea is injected into the SCR system, it reacts with water to form NH_3 [77], which can then be utilized in SCR:

$$2\,(NH_2)_2CO + H_2O \rightarrow 2\,NH_3 + \,CO_2 \tag{7}$$

NO reduction proceeds through the following chemical reaction:

$$4\,NO + 4\,NH_3 + \,O_2 \rightarrow 4\,N_2 + \,6\,H_2O \tag{8}$$

Reaction (8) is the dominant reaction mechanism for a system with NO and no NO_2; this is known as the *standard reaction*. The standard reaction only proceeds at intermediate temperatures (300°C and higher) due to the limited ability to oxidize NO on the catalyst's surface at lower temperatures, a necessary step in its reaction mechanism [95].

When only NO_2 is present, the following reaction can occur [96]:

$$6\,NO_2 + 8\,NH_3 \rightarrow 7\,N_2 + \,12\,H_2O \tag{9}$$

Reaction (9) has slower kinetics than the standard SCR reaction and thus is known commonly as the *slow reaction* [97].

When both NO and NO_2 are present, the following can occur:

$$NO + \,NO_2 + 2\,NH_3 \rightarrow 2\,N_2 + \,3\,H_2O \tag{10}$$

This is referred to as the *fast reaction* due to its rapid reaction rate, which is about ten times faster than the standard reaction [95-97] and about thirteen times faster than the slow reaction [93].

As stated earlier in this chapter, NO is the dominant pollutant in NO_X. However, 1:1 NO_2:NO is desirable for the fast reaction as this ratio achieves the highest NO_X reduction. In a diesel exhaust system, the oxidation catalyst performs oxidation of NO to increase this ratio [97], and SCR catalysts are designed to further increase it as well. However, it is undesirable to exceed 1:1 NO:NO_2. Since the slow reaction is slower than the standard reaction; it is better to error on the side of having excess NO than excess NO_2. Ensuring there is no excess NO_2 is important for reducing side reactions, as will be discussed next.

One set of undesirable reactions is NH_3 oxidation. These reactions waste NH_3 that could otherwise be used for the NO_X reduction reactions. Even deeper NH_3 oxidation can actually generate NO_X instead of just wasting NH_3:

$$4\,NH_3 + 3\,O_2 \rightarrow 2\,N_2 + 6\,H_2O \quad (11)$$

$$4\,NH_3 + 4\,O_2 \rightarrow 2\,N_2O + 6\,H_2O \quad (12)$$

$$4\,NH_3 + 5\,O_2 \rightarrow 4\,NO + 6\,H_2O \quad (13)$$

$$4\,NH_3 + 7\,O_2 \rightarrow 4\,NO_2 + 6\,H_2O \quad (14)$$

These reactions are positively correlated with temperature and are responsible for the sharp drop off in efficiency of NH_3-SCR catalysts at very high temperatures as the catalyst simultaneously generates and reduces NO_X [16].

A significant set of side reactions generate nitrous oxide, N_2O:

$$4\,NH_3 + 4\,NO + 3\,O_2 \rightarrow 4\,N_2O + 6\,H_2O \quad (15)$$

$$6\,NH_3 + 8\,NO_2 \rightarrow 7\,N_2O + 9\,H_2O \quad (16)$$

$$4\,NH_3 + 4\,NO_2 + 3\,O_2 \rightarrow 4\,N_2O + 6\,H_2O \quad (17)$$

$$2\,NH_3 + 2\,NO_2 \rightarrow N_2O + N_2 + 3\,H_2O \quad (18)$$

Nitrous oxide is produced by incomplete NO_X reduction, which is caused by insufficient active sites on the catalyst for the given NO_X inlet [40].

At low temperatures, (around 150-250 °C) the SCR system can generate and decompose ammonium hydroxide (NH_4NO_3) [94, 96, 98, 99]. This provides a second reaction path for NO_2, which explains why NO_2 consumption becomes dominant at low temperatures. At 200 °C it is estimated that with about half of the NO_2 is consumed through the slow reaction and the other half through ammonium hydroxide production and decomposition [93]. In addition to performing the SCR reactions, undesirable products can be formed.

$$2\,NH_3 + 2\,NO_2 \rightarrow NH_4NO_3 + N_2 + H_2O \quad (19)$$

$$NH_4NO_3 \rightarrow N_2O + 2\,H_2O \quad (20)$$

$$NH_4NO_3 \rightarrow NH_3 + HNO_3 \quad (21)$$

$$2\,HNO_3 + NO \rightarrow 3\,NO_2 + H_2O \quad (22)$$

When water concentration high, Reaction (21) is favored and NHO_3 becomes a direct product. When water concentration is low, NHO_3 decomposes and Reactions (20) and (22) dictate the final products [64, 87, 93]. As both nitric acid and nitrous oxide are pollutants, it is important to ensure that in a commercial SCR implementation the catalyst is not operated at conditions that favor the formation of these products. Thus, research into low temperature catalysis is focused not only upon increasing reduction of NO_X but also increasing selectivity towards production of N_2 and H_2O

Chapter 2

Method Development and Experimental Apparatus

2.1 Overview

This thesis project was the initial stage of a multi-year project to test SCR catalyst monoliths. Therefore, this thesis project had three important goals. The first goal was to design a monolith testing system to be reliable, precise, and easy to use. The second goal was to test catalyst monolith samples with different aging. The third goal was to use this data to evaluate the mechanisms of catalyst aging.

The structure of this thesis provides equal weight to the design of the testing apparatus and to the experimental results. When initially attempting to design these components, it was discovered that there was a lack of literature on their construction, and the resources that provided any information only provided flow diagrams while not specifying of the equipment used or challenges involved [50]. It is the hope of the author that this thesis can serve to assist future researchers who need this information.

The experimental setup consists of three distinct sections. The first section delivers imitative exhaust gas, the second section heats the gases and passes them through the catalyst monolith, and the final section analyzes the converted gases. Each section had its own unique set of problems and solutions that needed to be solved throughout the construction process. A wide angle view of the test system in its final configuration is shown in Figure 2.1, and a process flow diagram of the final system configuration is shown in Figure 2.2.

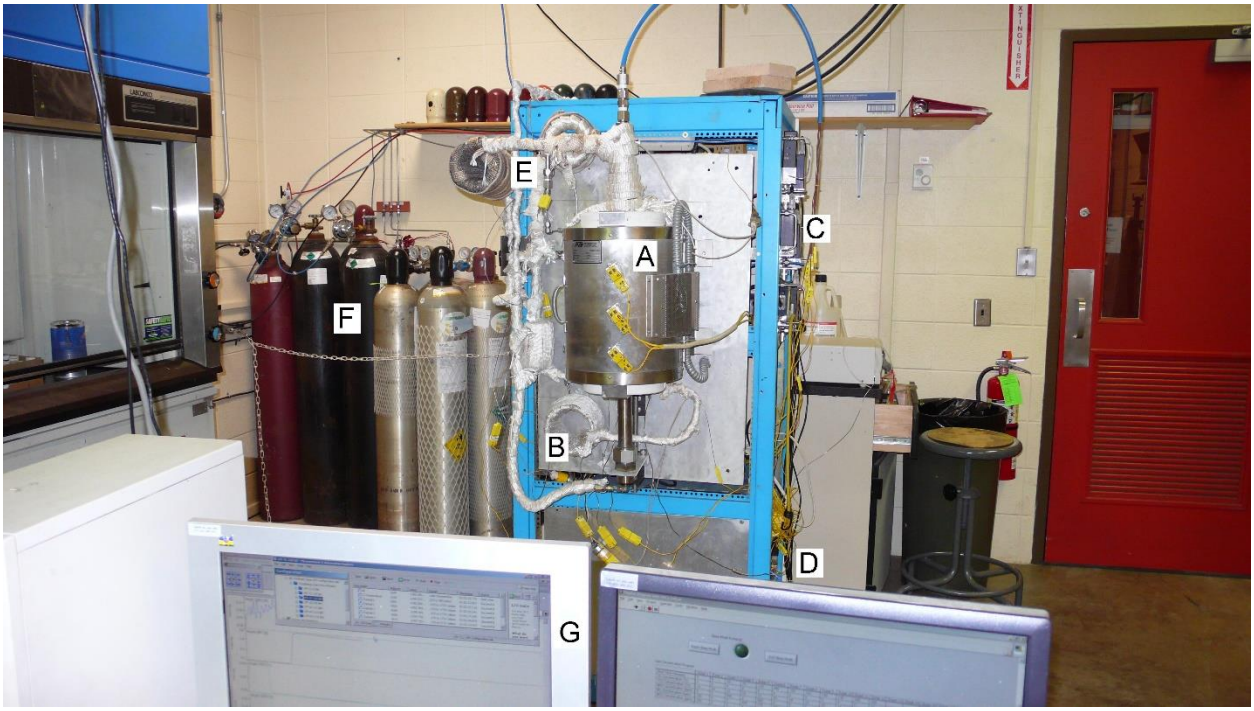

Figure 2.1: A wide angle view of the testing apparatus showing (A) furnace with monolith tube, (B) steam generation system, (C) mass flow controllers, (D) control interface and temperature monitoring, (E) gas pre-heating system, (F) gas cylinders and mixing, and (G) computer control and data acquisition system. Not shown is the FT-IR spectrometer, which is hidden behind the cabinet, the temperature controllers, which are on the left side of the cabinet, and the air compressor and dehumidifier, which are in another room.

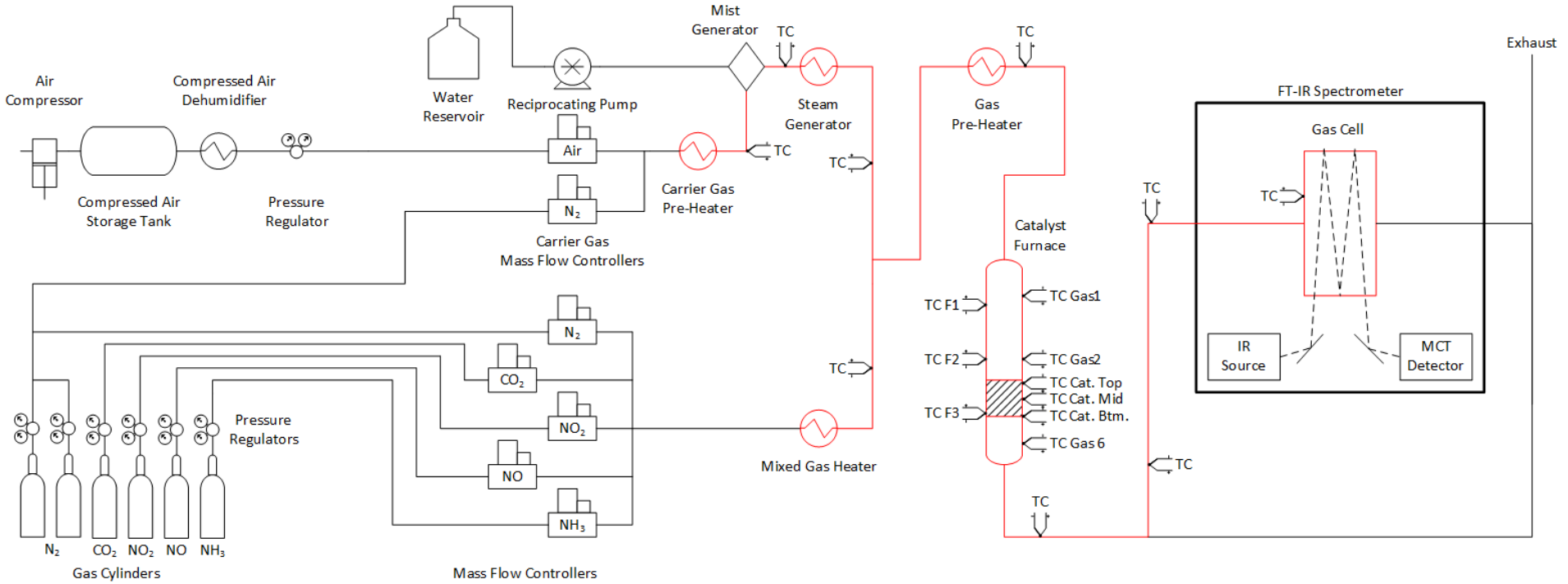

Figure 2.2: Process flow diagram of the final system configuration. Heated sections of the systems are colored red.

Gases are sourced from compressed cylinders and metered through mass flow controller. Steam is generated through a separate steam generation system, and then all of the gases are mixed together. Multiple sequential heaters increase the gas temperature to just below the desired temperature, and then the gases pass through a furnace with a SCR catalyst monolith. The products of reactions are sent through heated tubing to a Fourier-transformed infrared spectrometer equipped with a gas cell, which analyzes the composition of the gases. Finally, the gases are exhausted outside of the building.

2.2 Gas Control and Mixing

The first section of the system is focused upon generation of the imitative exhaust gas. While the catalyst monoliths being tested are intended for use in a diesel engine's exhaust system, a diesel engine is not used to generate the exhaust gas input. Instead, a gaseous mixture is generated by mixing different gases in proper proportion. This technique reduces the complexity of the testing apparatus and allows precise control of the concentration of pollutants. This approach also enables the SCR system to be tested in a variety of extreme conditions including those not achievable using a diesel engine but still useful for research into reaction mechanisms.

The gas mixture is generated to specified parameters by mixing streams of seven different gases. These seven gases include the combustion byproducts and reaction inhibitors of CO_2 and H_2O, the latter of which is added through a steam generation system that will be detailed later in this section. NO and NO_2 are added, and NH_3 is added as a reducing agent for the selective catalytic reduction reactions. A stream of air is introduced to fulfill the specified O_2 concentration, and N_2 is added to balance the mixture.

This system does not contain other common diesel pollutants such as particulate matter, hydrocarbons, CO, or SO_2. In a diesel exhaust system most of these would be filtered or catalytically

removed before reaching the SCR system, but trace amounts would reach the SCR catalyst and diminish its steady state performance [46]. Because the apparatus omits the other pollutants, the apparatus has the advantage that it does not further age catalyst samples.

Typical SCR systems intended for use on vehicles use an industry standard mixture of *diesel exhaust fluid* (32.5% urea in water) as the source of NH_3 and therefore require a vaporizer to gasify the liquid. This apparatus uses anhydrous NH_3 gas to eliminate the requirement for a vaporizer. Since NH_3 is the reactant regardless of source [77], the deviation from real world SCR systems should not affect results. However, the water concentration used in the experiments is increased from what would be expected in untreated diesel exhaust to account for the water component of the diesel exhaust fluid.

Nitric oxide, NO_2, and NH_3 were all obtained diluted in N_2 rather than pure form to reduce the hazards of these components should there be a gas leak. Initially, air was obtained in compressed gas bottles to ensure a consistent composition particularly with respect to the amount of water in the compressed air. Later, an air compressor coupled with a dehumidifier replaced the bottles of compressed air since this was less expensive to operate. This dehumidifier ensures that the dew point of the compressed air remains below 4 °C at all times thus removing the requirement of accounting for water in the air stream when calculating the water concentration in the system.

2.2.1 Gas Flow Control

Mass flow controllers (MFCs) are used in the system for accurately control gas flow rates. These mass flow controllers have electronic solenoid valves, which allow them to cut off gas flow in milliseconds, and measure gas flow by metering mass flow, which makes them insensitive to the system pressure. The precision of the mass flow controllers is very high with an error of 1% [100].

A bubble flow meter is used to calibrate each MFC to a specific gas. However, an exception was made for NO, NO_2, NH_3, and N_2O. While N_2O was not used as an input, it was still necessary to use for calibration of the FT-IR spectrometer outside of experiments. Since these gases are toxic, it would be dangerous to use an open bubble flow meter to calibrate flow rates using these gases. Instead, these MFCs are calibrated with nitrogen, and then a correction factor is applied compensating for the differing heat capacities and densities of the gas mixtures. While this correction is not perfect, the residual error is minor due to the heat capacities of the mixed gases being so similar and the low concentration of the gases in the nitrogen diluent. The correction factors for the gases are presented in Table 2.1 and are obtained using a combination of data available through the National Institute of Standards and Technology's *Chemistry WebBook* and experimental data provided by Sierra Instruments.

Table 2.1: Correction factors for mass flow controllers

Gas Controlled	Cylinder Gas Concentration (Diluted in Nitrogen)	Mixed Gas Correction Factor
NO_2	4.07%	0.9785
NO	4.10%	0.9998
NH_3	2.67%	0.9947
N_2O	0.10%	0.9994

The actual implementation of the six primary mass flow controllers is shown in Figure 2.3. Two additional mass flow controllers, one controlling the flow rate of the nitrogen carrier gas for steam and one controlling the nitrogen purge for the FT-IR spectrometer are not shown; these will be discussed later. All the controllers have integrated computers to control their valves, but they need power and a separate control signal to input their set points. In addition, they output a control signal to communicate the current gas flow rate. To send and read this data, two pieces of equipment are

assembled. Shown in Figure 2.4 is a custom built control box. This box aggregates the signals from the individual controllers and groups them into inputs and outputs. These inputs and outputs are connected to a National Instruments Compact FieldPoint Module CFP-2110 with backplane, pictured in Figure 2.5. MFC Inputs are attached to an AI-112 input card on the backplane and MFC outputs are attached to an AO-100 output card on the backplane. In addition, two TC-120 cards are used for thermocouple inputs, another AO-100 output card is used to control the temperature set points of the furnace zones, and an AI-112 card receives information from the toxic gas sensors in the room signaling the system to perform a controlled shutdown in the event of an alarm.

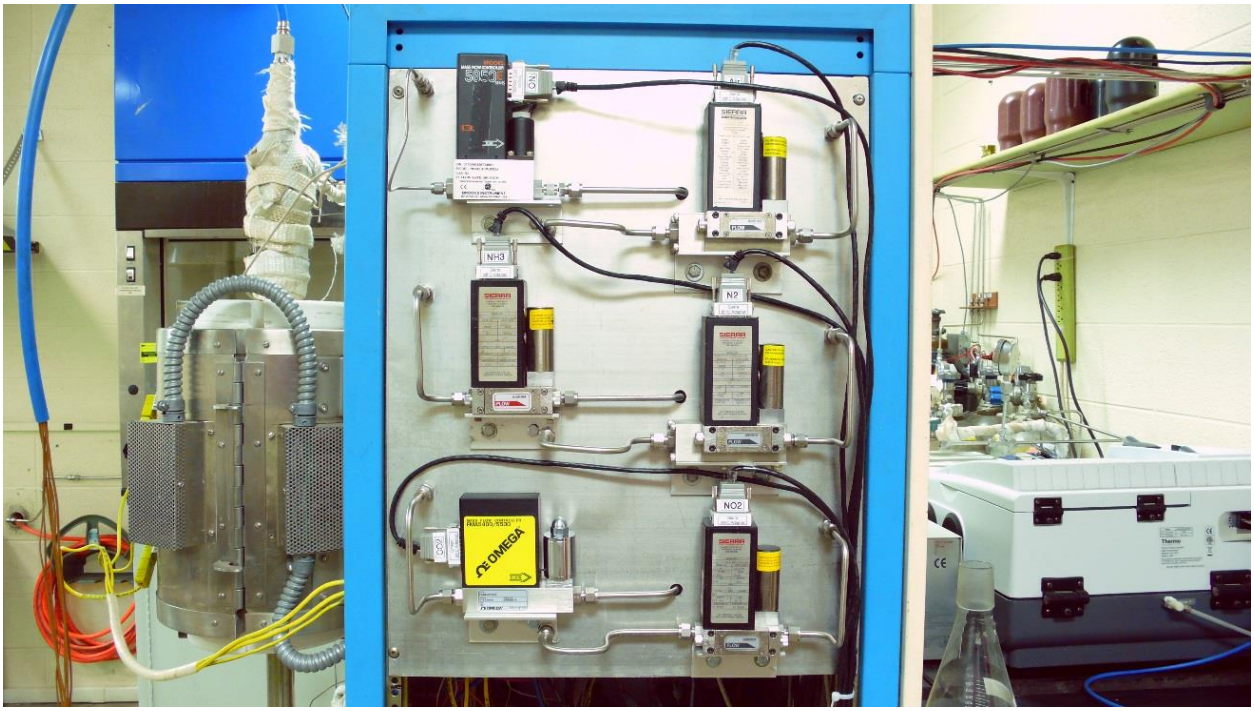

Figure 2.3: The mass flow controller system showing the six primary MFCs. Not shown are a MFC controlling the flow rate of the nitrogen carrier gas for steam and a MFC controlling the nitrogen purge for the FT-IR spectrometer.

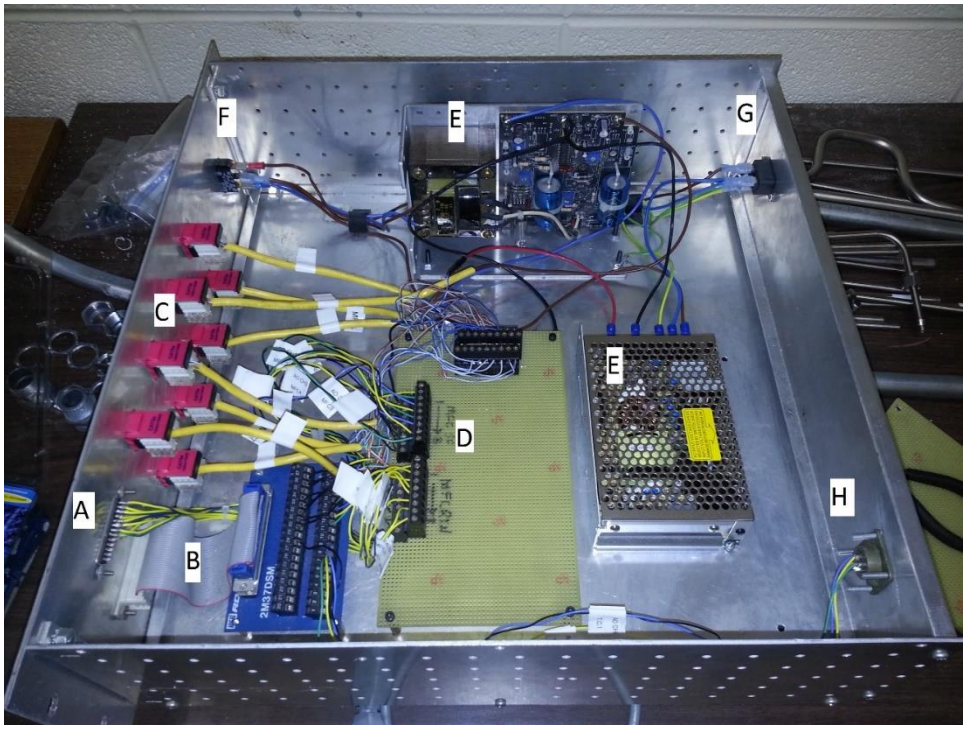

Figure 2.4: The MFC control box, showing major components: MFC Flow readings output (A), MFC set points input (B), Connections for individual MFCs (C), Signal and power distribution board (D), Power supplies (E), Main power switch (F), AC power input (G), and Furnace temperature set points (H)

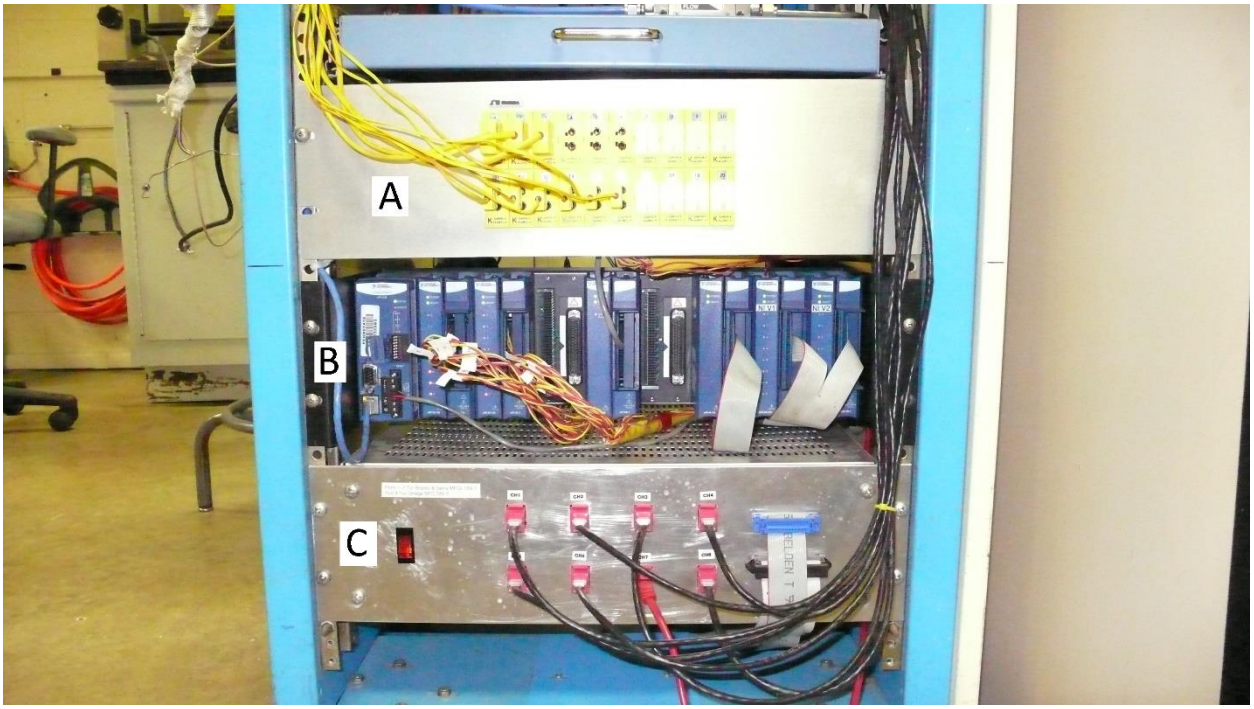

Figure 2.5: The input/output section of the apparatus showing (A) thermocouple inputs, (B) compact Fieldpoint module with add-in cards and (C) MFC control box

2.2.2 Steam System

Generating and controlling steam presented the largest challenge in assembling the catalyst monolith testing apparatus. The steam system went through five separate iterations before achieving a consistent supply of steam. In all cases, water was injected into the system at a fixed rate by a HPLC pump, initially a Waters model 515 and later an Alltech model 616 (used after the Waters pump failed). However, the method through which this water was converted to steam evolved significantly throughout the course of the project. The main issue with controlling steam was that the system would not produce steam at a constant rate; instead, bursts of steam would occur. This caused the overall gas flow rate of the system to fluctuate and thus the concentration of the other gases to fluctuate as well. This manifested itself as noisy data. Generating a constant supply of steam was key to reducing noise in the data.

The first revision of the steam control system involved a heated tube through which water flowed upward. This implementation is shown in Figure 2.6. The water was pumped into an unheated tube and slowly made its way up a heated coil of tubing. The water level would stabilize at the point in the coil where the water had gained enough heat to boil. The remaining tubing would superheat the steam.

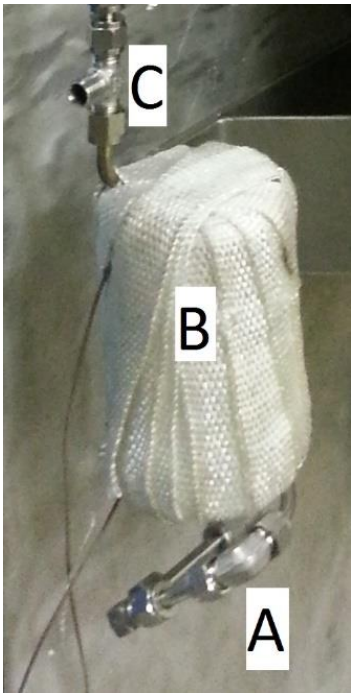

Figure 2.6: The first revision of the steam generation system showing the water inlet (A), heated coil (B), and thermocouple port and steam outlet (C)

This design presented two issues. The system had a complicated startup procedure. If the water level was too high before turning on the heater, the heater could not inject enough heat to boil all the water. In this case it acted as a water heater rather than a steam generator, flooding the rest of the system with hot water. However, this problem could not be avoided just by starting the system with no water. The heat input to the steam coil was controlled based upon the measurement of the steam temperature exiting the coil. When starting up, there would be no steam for the temperature controller to monitor. The lack of steam would cause the temperature controller to assume the system was too cold and instruct the heater to run at 100% duty cycle, even if the lack of steam was due to a lack of water rather than a lack of heat. At this point the heater exceeded 500 °C, and the problem would not resolve itself. Any water that touched the very hot coil would flash boil resulting in bursts of steam that were too small and quick for the controller to detect (and realize that the temperature was too high).

However what ultimately led to the replacement of this system was that even when the system was operating properly, steam would still be generated in pulses. Even when operating at steady state,

steam concentration in the system would vary by 45%, as seen in the FT-IR data in Figure 2.7. This was clearly unacceptable and had to be resolved before any reliable experiments could be recorded. The working hypothesis was that nucleate boiling, bubbles of steam, was generating these pulses; nucleate boiling had to be eliminated to reduce variability in steam concentration.

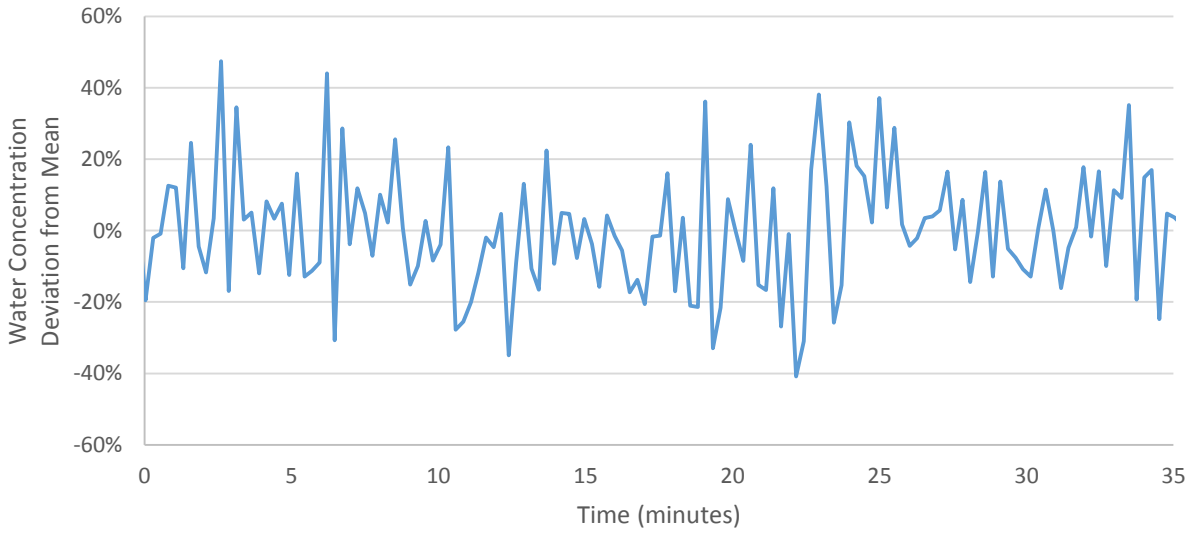

Figure 2.7: Plot of the water concentration in the system over time (relative to mean concentration) as generated by the second revision of the steam system.

The deficiencies of the first system led to a second revision, in which the pool of water was eliminated. This system is shown in Figure 2.8. The goals of this second revision was to eliminate nucleate boiling and to reduce the number of variables affecting the rate of steam generation. The previous system had two variables that affected the rate of steam production, water input rate and heat input rate, and these two parameters had to be perfectly balanced to maintain a steady state. In the new system, the goal was to ensure that the water input was the limiting factor in steam generation. That way, heat input and temperature did not need to be controlled as precisely; as long as the temperature was above the vapor temperature and enough heat was being input, water would evaporate exactly at the rate of injection.

In this system, water was injected through a small tube into the center of a wick, composed of a porous ceramic. A constant stream of nitrogen gas, around 4 L/min and preheated to just above the dew point, would then pass around this wick and evaporate the water. After the wick, the nitrogen/steam mix would pass through a coil to superheat the mixture prior to combining with the other gases within the system.

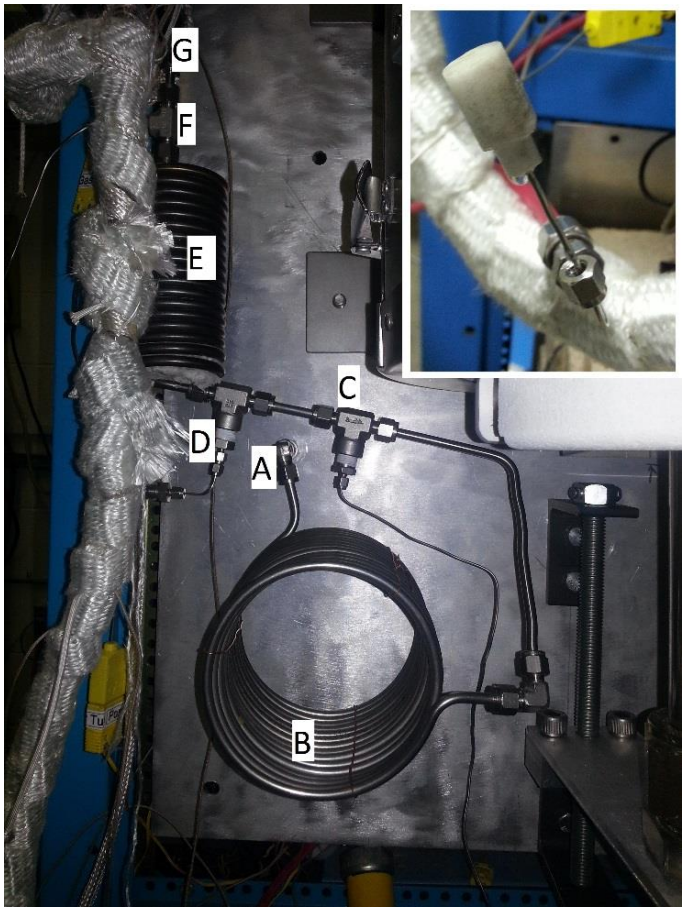

Figure 2.8: The second revision of the steam generation system showing nitrogen inlet (A), nitrogen pre-heater (B), pre-heater thermocouple (C), wick and water injection system (D), steam super heater (E), super heater thermocouple (F), and steam/nitrogen outlet (G). In the inset is the ceramic wick that is part of D in the main image. Not pictured is the heating tape and insulation normally present on all tubes and the mass flow controller controlling the nitrogen flow rate.

This second system resolved the issues with system startup and control. Since there would always be a flow of gas even if there was no water, the thermocouples would always be reading the correct gas temperature and could adjust the heaters' outputs accordingly to prevent overheating. The

flooding condition was avoided because the system could now be started dry and the water added only once the system reached the proper temperature. However, the second steam system still did not solve the fluctuations in the water concentration. Upon further investigation, it was determined that the surface tension of the water exiting the small tube within of the wick caused water to enter the wick in large droplets as opposed to a steady stream. This deficiency led to a third revision in the design of the steam system as shown in Figure 2.9.

The third steam system design attempted to eliminate these large droplets. The major change from the second system was the elimination of the wick and replacement with a nozzle on the end of the water tube that would generate a constant stream of water. Preventing droplets is a significant challenge at low water flow rates since at these low flow rates breaking the surface tension of the water requires a large energy input relative to the energy needed to simply pump the water. After some experimentation, it was found that reducing the nozzle size increased the pressure enough to break the surface tension of the water outside of the apparatus. Compressing the end of the tube to reduce the nozzle size from 0.03” to below 0.005” was enough to increase the water pressure from 10 to 40 psi. This change created a stream of water, which when tested in conjunction with a carrier gas formed a mist instead of droplets.

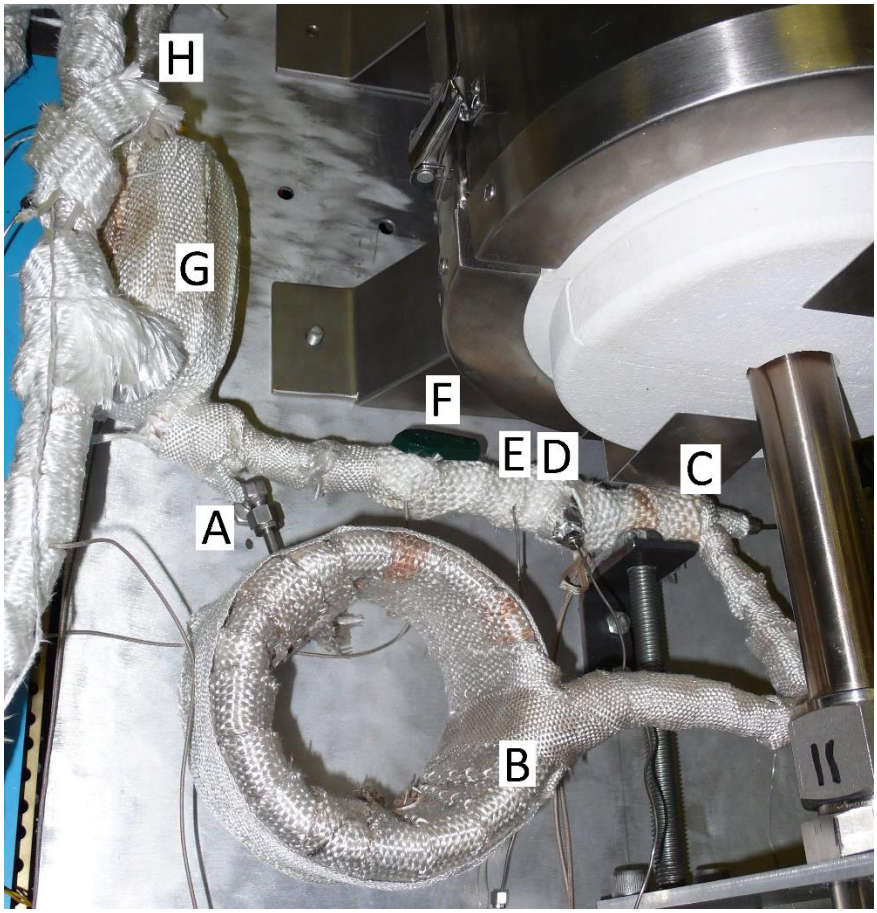

Figure 2.9: The third through fifth revisions of the steam generation system showing nitrogen carrier gas inlet (A), nitrogen carrier gas pre-heater (B), water injection system (C), post injection gas temperature thermocouple (D), post injection tube wall temperature thermocouple (E), stem system cutoff valve (F), steam super heater (G), and super heater thermocouple (H)

While it was initially assumed that creating this stream of water carried by nitrogen would improve the stability of the steam, the stream of water did not resolve the steam fluctuations. The heat capacity of the carrier gas alone at the 130 °C set point was likely not enough to vaporize the incoming water. The third (and second) revision of the steam system had been designed based on the assumption that the heat contained within the nitrogen carrier gas would be enough to vaporize all the water. If this assumption was incorrect, droplets would form inside the main tube and be carried along until being vaporized later in the system. This hypothesis was supported by two observations. The wall temperature of the tube immediately after the water injection was about 65 °C, which indicated that much of the heat was absorbed and that condensation could occur. In addition, increasing the

temperature set point of the gas reduced the steam fluctuations, which indicated that the system could benefit from more heat.

To resolve this situation, the location of a heater control thermocouple was moved. In the third steam system revision, the gas pre-heater was controlled by a thermocouple measuring the gas temperature immediately before the water injection. The fourth steam system revision had the gas pre-heater controlled by a thermocouple measuring the tube wall temperature. The tube walls would be the coldest parts of the steam system in direct contact with water, so it could be inferred that as long as the tube wall was above 100 °C, there was enough heat being input to vaporize the water as it contacted the wall of the tube. In an initial test, the lack of heat was confirmed to be a problem, as the tube wall temperature was unable to reach the 100 °C wall temperature set point even with the heater at 100% duty cycle. To alleviate this, the two 150W heating tapes were replaced with a 600W heating tape. However, even with these two modifications, the behavior of the system did not change; the steam still varied by up to 10%.

Without any clear ideas as to the cause of the problem, more data was needed to diagnose the issue. It was decided that a more granular record of steam temperatures was needed. The standalone temperature controller only monitored temperatures every 2 seconds. To get a better record of performance, the thermocouples in the steam system were connected to a computer, which read and recorded the temperature every 0.1 seconds, 20 times faster than the standalone temperature controller. This data showed a very important trend that was expected as shown in Figure 2.10.

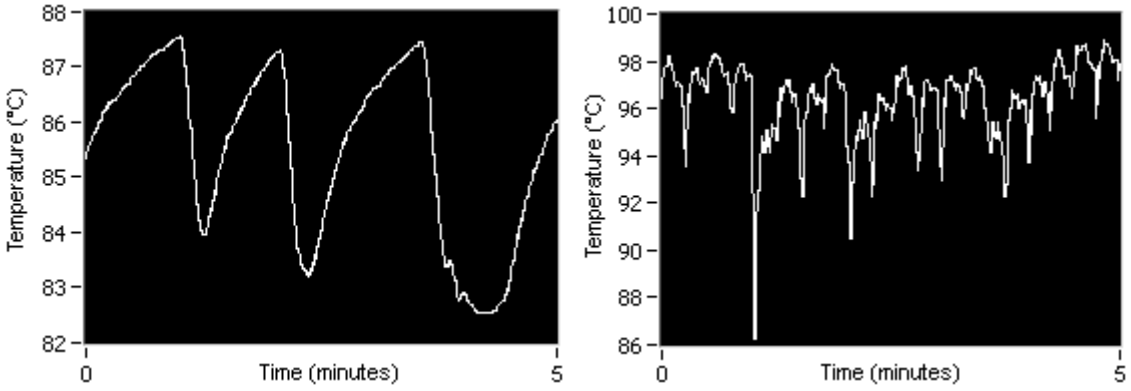

Figure 2.10: Temperature charts of the steam system (revision 4) showing tube wall temperature (left) and gas temperature (right)

The gas temperature remained slightly below 100 °C, but this was not an issue since the dew point for the given amount of water used was calculated at 76 °C. The important information was the tube wall temperature; the temperature was oscillating but not in a sine curve. If the oscillations were a sine curve, then this would indicate a poorly tuned temperature controller. Instead, the oscillations had sharp edges to them, which indicated the dripping of water from the inlet rather than the stream of water that was expected. The hypothesis for the observed behavior was that the wall temperature increases to a set point exponentially, but just before it reaches the set point, a droplet of water falls on the tube. This absorbs the tube wall's stored heat causing a sharp drop in tube wall temperature. Once the entire droplet has evaporated, the wall temperature bottoms out, begins to recover, and the cycle repeats.

At this point it was unclear whether the drops were due to a lack of heat to evaporate the water at the point of injection or if the only issue was the design of the water injection system. To probe this behavior further, the water injection section of the steam system was taken apart and tested piece by piece. At experimental conditions (1.894 mL/min water) the 4L/min carrier gas was observed to be insufficient to break the surface tension of water, and dripping was occurring. In retrospect, it was clear

that estimate of the flow rate of carrier gas used to test the mist generation idea was much higher than the actual flow rate provided. A much higher gas speed was needed in the steam generation system.

The original carrier gas tube, 0.25" in diameter with wall thickness of 0.038", was only producing a gas velocity of 12.8 m/s at 4 L/min carrier flow rate. To increase this velocity, the tube was replaced with one of 0.125 inch diameter and wall thickness of 0.028 inches. This produced a gas velocity of 86.8 m/s at 4L/min carrier flow rate. When tested, this was an improvement, with water no longer dripping. However, the water was carried away in large droplets, which was still considered a problem. Since even smaller diameter tubing was not available (nor would it be practical to install), the mass flow controller supplying the carrier gas was replaced with one of larger capacity. The same system was tested with increasing flow rates, and it was found that 10 L/min was the minimum flow rate needed to ensure a water mist.

Due to the design of the system and the lack of spare mass flow controllers, the only way to achieve a 10 L/min minimum steam carrier flow rate was to rearrange the gas flow in the system. Previously, a small fixed flow rate of nitrogen would pass through the steam system and a large variable flow rate of nitrogen and air (carrying the pollutant gases) was added after the steam system. This was reversed to have a large variable flow rate of nitrogen and air pass through the steam system and a small fixed flow rate of nitrogen (carrying the pollutant gases) added after the steam system. While this gas flow rate through the steam system would be variable depending on the concentration of pollutants, at the 40000 hr^{-1} space velocity used in the experiments, the small relative volume of pollutants meant that the carrier gas flow rate would never drop below 10 L/min.

This change finally solved the steam system issues. As seen in Figure 2.11, the dripping behavior was no longer present. There were still oscillations in tube wall temperature due to the temperature controller. A side effect of the increased carrier gas flow rate was that the temperatures of the system were over 70 °C higher. This was attributed to the higher flow rate of the gas, which distributed heat

throughout the tube more evenly. Most importantly, the FT-IR spectrometer was now reporting water fluctuations of ±2% as shown in Figure 2.12.

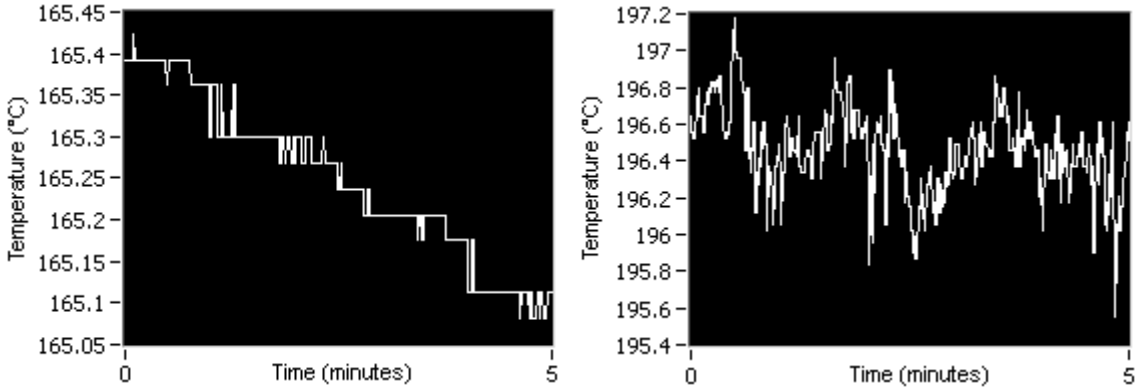

Figure 2.11: Temperature plots of the steam system (revision 5) showing tube wall temperature (left) and gas temperature (right)

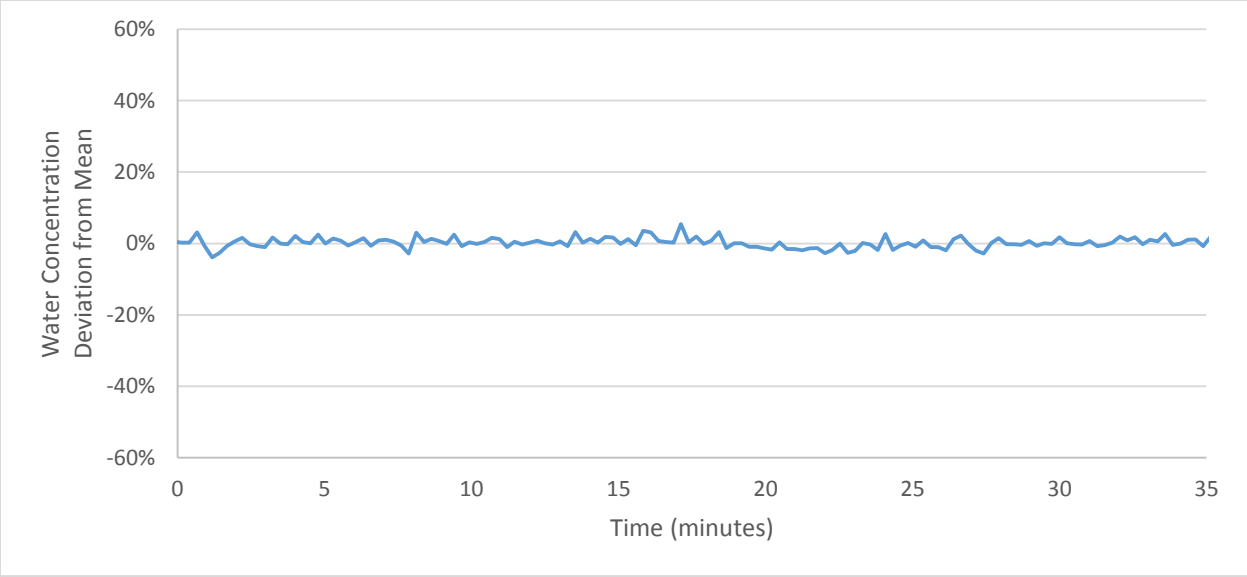

Figure 2.12: Plot of the water concentration in the system over time (relative to the mean concentration) as generated by the fifth revision of the steam system.

2.3 Heating System

Testing parameters specify catalyst operating temperatures between 250 and 400 °C depending on the test, although the heating system needs to be flexible to reach catalyst temperatures between 150 and 500 °C. In addition, all tubing between the steam generator and the analysis equipment needs to be kept above the steam dew point to prevent condensation and ensure consistent gas composition. To achieve this temperature, a furnace, heating equipment, temperature controllers, and temperature monitoring are part of the system.

Together, the system requires eleven temperature controllers and seventeen thermocouples. These eleven temperatures controllers are divided among four zones at medium temperature (around 200 °C) prior to the furnace to preheat the gas, three zones within in the furnace to bring the gas up temperature and to heat the monolith, and four zones after the furnace at low temperature (around 100 °C) to keep the steam from condensing before analysis. The seventeen thermocouples are comprised of six monitoring the monolith temperature, three monitoring the furnace temperature, and eight monitoring the temperatures of tubing outside the furnace.

2.3.1 System Tubing

All tubing between the steam system and the analysis equipment was wrapped with heating tape. After each heating tape, a thermocouple, placed within the gas stream, was added to monitor the temperature of the flowing gas. This temperature data was sent to a PID temperature controller, which controlled the duty cycle of the heating tape to regulate temperature.

The entirety of piping (with the exception of the tube holding the monolith samples) is constructed of ¼" outside diameter 316 stainless steel tubes. This diameter of tubing was selected to ensure that the maximum system pressure remained below 20 psig at all times, approximating a

automotive exhaust system. This low pressure also minimizes the chances of the gas composition changing between the reaction zone and the analysis equipment due to the possibility of having different equilibriums at different pressures.

2.3.2 Furnace and Tube Reactor

The system is designed to test 3" long x 1" diameter cylindrical samples. Since automotive SCR catalyst monoliths are much larger than these dimensions, the samples tested are cores cut out of the original monolith. The furnace used is an Advanced Test Systems furnace with three 750 W heating zones. The monolith itself is housed within a stainless steel tube, which is placed within the furnace. Originally, quartz glass tubes were used, but the tube material has changed to stainless steel after initial testing determined that the glass shattered under the combination of heat and pressure present during the experiment. The tube has a washer inserted to hold the monolith in the lower third of the furnace. This allows the upper two zones of the furnace to act as gas heaters while the lower third keeps the monolith at operating temperature. Five thermocouples are placed within the monolith, each approximately 1/5 of the length of the monolith apart. The monolith thermocouples are shown in Figure 2.13. One additional thermocouple is placed immediately prior to the monolith to monitor the temperature of the gas entering the monolith.

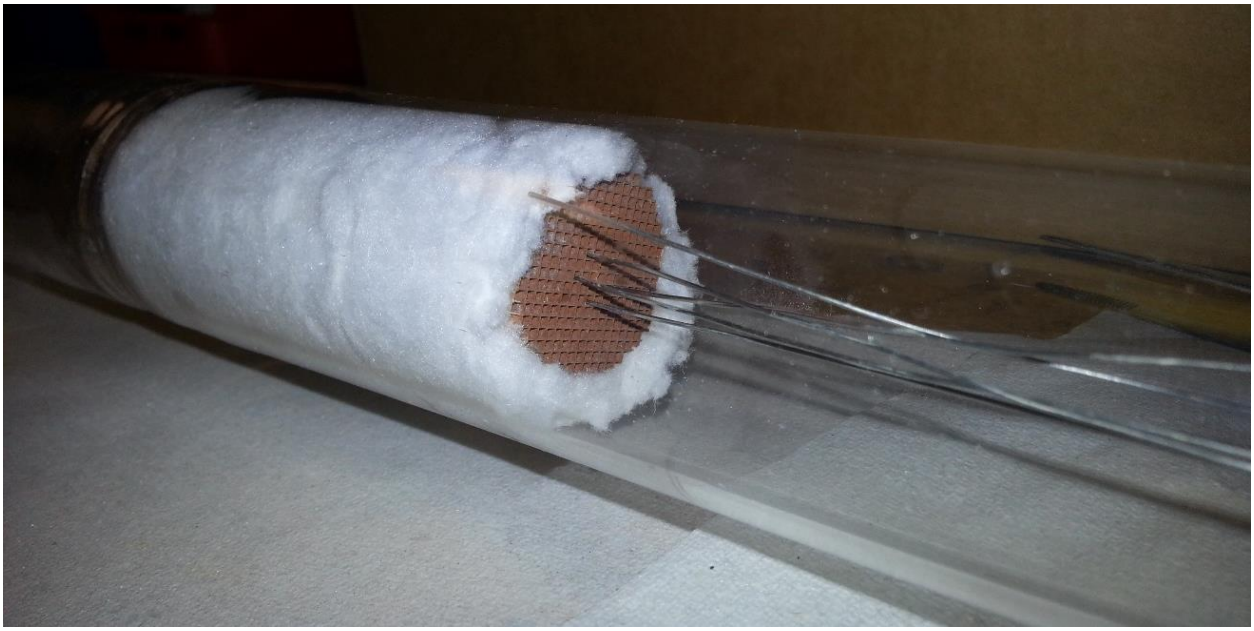

Figure 2.13: Monolith in the monolith tube with thermocouples inserted. The monolith is held in place with insulating wool. This picture is from an early experiment using a glass tube.

The low heat capacity of the gas presents a different problem within the furnace. The monolith is housed with a stainless steel furnace tube, with gaps of gas between the furnace and the stainless steel furnace tube as well as between the monolith and furnace tube. The number of thermal interfaces makes the monolith temperature very insensitive to the heat applied by the furnace. Around one hour is needed between a control input to the furnace heaters and the time the monolith finally reaches the set point. The temperature controllers attached to the furnace heaters are set to monitor the temperature of the gas between the monolith tube and the furnace as opposed directly monitoring to the temperature of the monolith. This is because if the temperature controllers monitored the temperature of the monolith to control the heaters, then due to the long response time they would overshoot the set point by hundreds of degrees Celsius. This long response time is still a major flaw to the temperature control system.

2.4 Gas Analysis

Gas analysis is performed using a Thermo Nicolet 6700 Fourier-transformed infrared (FT-IR) spectrometer equipped with a MCT detector. A Nicolet 2 m gas cell with ZnSe windows is placed in the beam path. A spectral resolution of 0.5 cm^{-1} is used with 4 scans per spectrum. The gas cell attenuates the beam significantly, so the spectrometer's aperture is set to 17%, which is the largest aperture recommended by the spectrometer software for the given resolution. These settings produce an absorbance spectrum every 16 s.

Every IR absorbing compound has a characteristic absorbance spectrum. According to Beer's law, as concentration increases, absorbance increases proportionate to the product of the path length, the specific absorbance of the compound, and the concentration of the absorbing compound. Therefore, the concentration of a gas can be determined using FT-IR spectroscopy by creating a calibration chart that correlates absorbance (at any given wavenumber) with concentration. Theoretically, this fit is linear for all concentrations; however, detector characteristics limit this linear regime to only low concentrations; at high concentrations, little light reaches the detector and the response becomes more polynomial [101].

When multiple compounds are present, their absorbances add together. It is easiest to separate these individual component spectra from a spectrum of mixed compounds if each component's contribution can be determined using characteristic absorbance peaks. These characteristic absorbance peaks are peaks in the mixture's spectrum that can be solely attributed to one compound; they do not overlap with the peaks of other compounds present in the sample. In situations where multiple peaks overlap, then they can be separated through subtraction of the compounds contributing to the peak.

2.4.1 Calibration

Calibration of the spectrometer is performed by measuring the mid-infrared absorbance of set quantities of the four gases to be analyzed – NO, NO_2, NH_3, and N_2O. Because a change in the density of the gas within the gas cell can influence the absorbance and thus the reported gas concentration, the calibration is performed at the experimental conditions. The space velocity of the gas is held at 40000 hr^{-1}, the temperature of the gas cell is kept at 130 °C, and the pressure of the gas cell is maintained at 3 psig. The mass flow controllers are set to pass through specified concentrations of individual gases diluted in nitrogen as nitrogen is transparent to infrared radiation. All IR spectra are recorded between the wavenumbers of 650 cm^{-1} to 4000 cm^{-1} and in 50 ppm intervals from 50 to 500 ppm for NO, NO_2, NH_3, and N_2O.

2.4.2 Choosing Characteristic Peaks

Figure 2.14 presents overlapping spectra of 250 ppm NO, 250 ppm NO_2, 500 ppm NH_3, and 150 ppm N_2O all with balance nitrogen. NH_3 exhibits peak splitting and shows three absorbance regions: one between 3100-4000 cm^{-1} with a peak near 3320 cm^{-1}, one between 1850-1375 cm^{-1} with a peak near 1650 cm^{-1}, and one between 1250-650 cm^{-1} with a peak near 965 cm^{-1}. However, the peak near 1650 cm^{-1} overlaps with the NO_2 peak, so for simplicity this peak is not used to characterize NH_3 because it requires first determining NO_2's contribution and then subtracting it. This subtraction also adds additional error into the calculation; avoiding the subtraction reduces experimental error. Of the remaining two peaks, the peak near 950 cm^{-1} is considerably more intense than the peak near 3350 cm^{-1} and thus is the choice to characterize NH_3 concentration. Since noise in the data is constant, a signal with higher absorbance will produce data with a higher signal to noise ratio.

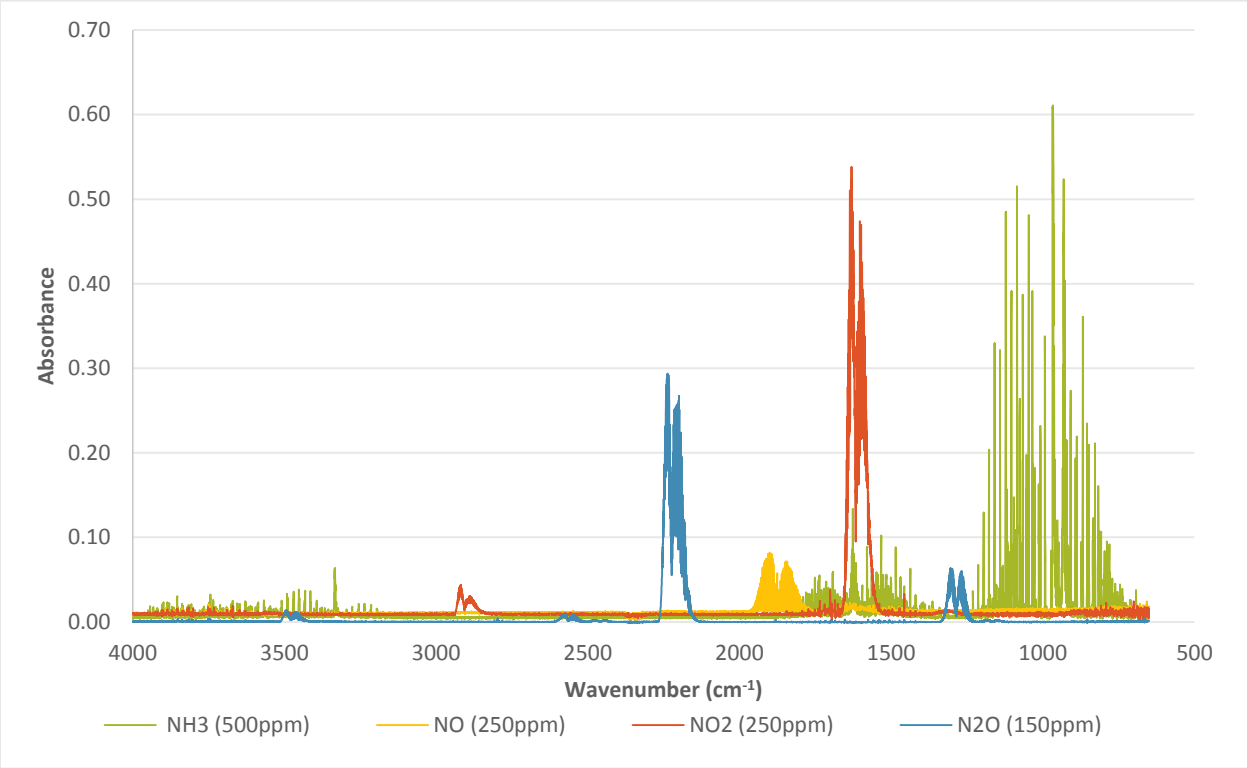

Figure 2.14: IR spectra of the three analyzed gases

The NO_2 shows two absorbance regions – one between 2950-2800 cm^{-1} with peak near 2910 cm^{-1} and one between 1650-1500 cm^{-1} with peak near 1630 cm^{-1}. The NO_2 absorbance peak near 1630 cm^{-1} is not convenient to use because it overlaps with other compounds; therefore, the non-overlapping smaller peak near 2910 cm^{-1} is the one that is used to characterize NO_2 concentration. While this smaller peak intensity does mean that the signal to noise ratio is lower, the subtraction that would be needed with the other peak would complicate analysis and introduce more noise into the data.

The two other gases presented challenges in characterization due to the contributions of H_2O and CO_2. Figure 2.15 presents the same data as Figure 2.14 except with water and carbon dioxide shown. It is immediately obvious while the peaks selected for NH_3 and NO_2 do not overlap with those of water, all regions of NO and N_2O overlap with H_2O and CO_2. While it is possible to subtract the contribution of these two compounds to the spectrum (by taking a background spectrum), this is not an

ideal solution. Conceivably one would want to subtract a fixed background since the concentration of H_2O and CO_2 should be constant throughout the experiment (disregarding the negligible amount of water generated by SCR). However, the large absorbance of H_2O and CO_2 relative to that of NO and N_2O means that even slight changes in the concentration of H_2O and CO_2 will drastically affect the relative amplitude of the NO and N_2O peaks. Therefore, it is best to use the peak with the smallest contribution from H_2O and CO_2 even if that peak is not the one with the largest amplitude.

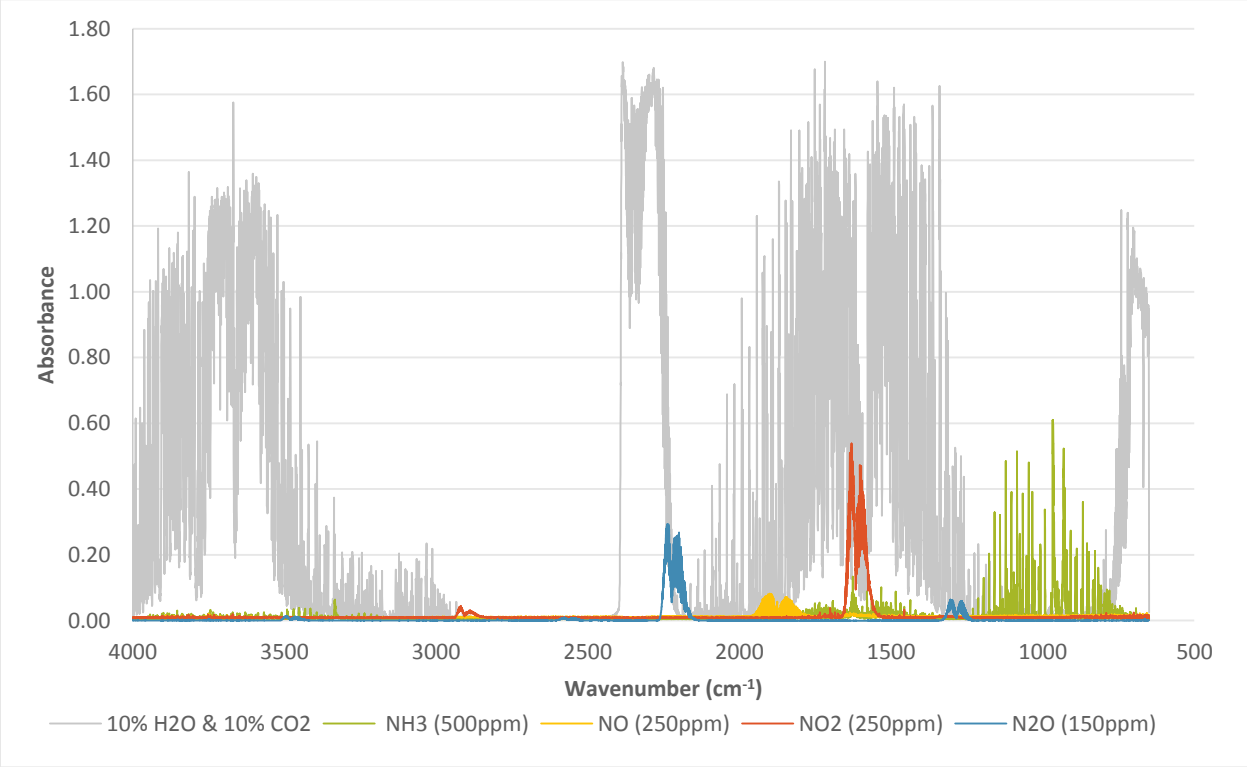

Figure 2.15: Absorbance of the six infrared active components

There are multiple N_2O regions; the two largest are between 2250-2100 cm^{-1} with absorbance peaks near 2230 cm^{-1} and 2200 cm^{-1} and between 1375-1200 cm^{-1} with peaks near 1300 cm^{-1} and 1260 cm^{-1}. While neither region overlaps with the other three important compounds, both regions overlap with H_2O and CO_2. Of the four peaks noted, the peak near 2200 cm^{-1} is the peak with the least influence from H_2O and CO_2 and therefore is the one utilized for characterization of N_2O.

An important point to note is that the 150 ppm N_2O concentration shown in the plot is well above what would be expected in an experiment; a typical experiment would only experience N_2O concentrations around 20 ppm. In early experiments, the imprecision in control of CO_2 concentration meant that N_2O concentration had a signal to noise ratio of about 1:1, and all data of N_2O concentration was too noisy for analysis. For this reason N_2O concentration was omitted in the early results. As the apparatus was refined, the precision of CO_2 concentration improved allowing precise measurements of N_2O in later experiments.

The NO signal presents only one absorbance region between 1950-1750 cm^{-1} with absorbance peaks near 1900 cm^{-1} and 1860 cm^{-1}. The peak near 1860 cm^{-1} overlaps slightly with the NH_3 and H_2O regions making it undesirable. The peak near 1900 cm^{-1} could be considered the best to characterize NO, but the presence of H_2O complicates this. The next section will focus upon dealing with H_2O in the NO peak.

2.4.3 Resolving the NO Characteristic Peak

The conventional method to deal with a peak that overlaps another is to obtain a reference spectrum of the offending compound and obtain the height of a characteristic peak of the offending compound. Then, one scales the reference spectrum to the height of the characteristic peak and subtracts that spectrum from the experimental data. While this can be used to remove water's influence from the NO region, this approach introduces additional experimental error into the data due to the use of calibration data with inherent error. Since the absorbance for 250 ppm NO is only 0.0035, the ±0.0001 noise in absorbance already results in a NO concentration fluctuation of ±7 ppm. Introducing additional error into the data is unacceptable.

Instead of attempting to subtract the water spectrum from the largest NO peak, an alternative approach is used. While at first glance the regions of NO and water appear to overlap, upon closer inspection both NO and H_2O exhibit peak splitting. The data is comprised of many narrow peaks, some of which are distinct to NO and others to water. If one can find a peak that is characteristic to NO but not water, then it can be used to characterize NO. Note that this does not mean that the absorbance of water has to be zero in the region where the desired NO peak lies. As long as the NO peak is narrower than the water trough, one can measure the height of the trough and use it as a baseline for the NO peak. This method still requires subtraction, but since there is no reference spectrum and no calibration curve for water, experimental error is reduced.

The technique is tested by taking two spectra, one with water and the other with water and NO. If peaks show up in one spectrum but not in the other, then it is known that the peaks are unique to NO. At the initial spectral resolution chosen, 2 cm^{-1}, these water and NO peaks are indistinguishable. A higher spectral resolution is needed to distinguish these peaks.

When choosing infrared spectroscopy parameters, there are three important parameters that must be balanced – spectral resolution, the number of scans, and time per sample. Since this data could be used for research on reaction kinetics, time resolution is important. Doubling the spectral resolution increases the amount of time needed to obtain a spectrum by a factor of the square root of two, but each spectrum is sharper. Similarly, doubling the number of scans doubles the amount of time per spectrum but produces a spectrum with less noise. Since noise in the data is already an issue, these parameters have to be chosen carefully.

The previous settings had been a spectrum resolution of 2 cm^{-1} and 8 scans per spectrum. To balance the required increased spectral resolution sacrifices in time per scan and number of scans per spectrum had to be made. The spectral resolution was increased by a factor of 4 to 0.5 cm^{-1} and the number of scans was reduced to 4. This increase in resolution was chosen because it balanced the

decreased number of scans and kept the time per spectrum constant. No further resolutions were tested due to the acceptable data obtained.

At a resolution of 0.5 cm^{-1} it is possible to spot a few NO peaks in the spectrum, shown in Figure 2.16. However, there are very few locations where it is possible to draw a baseline. The optimal baseline has ends where both plots intersect; that ensures that the baseline remains in the same location whether or not NO is present. It is also desirable to choose a baseline with points in a trough as these points are less susceptible to variation due to a slight change in water concentration (noise). Beyond this criterion the best peak is the one with the highest amplitude over the baseline.

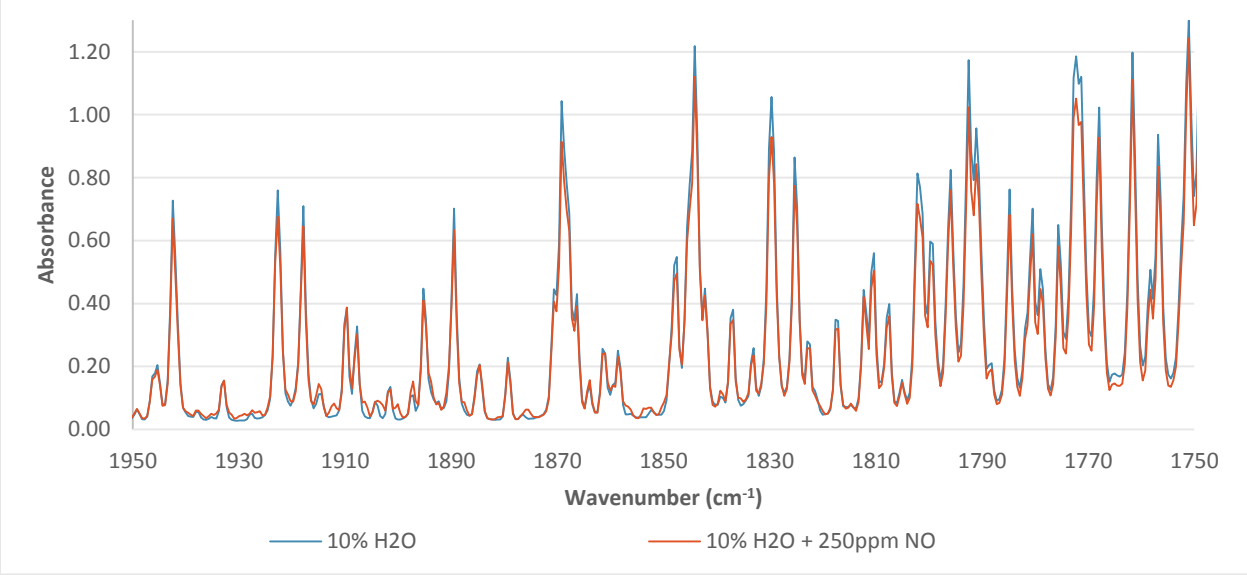

Figure 2.16: Comparison of the NO region when water is present

The peak at 1875.71 cm^{-1}, shown in Figure 2.17, represents the largest NO peak in a trough of a water peak. The NO peak still overlaps with water, but the baseline in the water trough is flat and is wider than the NO peak, which allows simple subtraction of water's influence. At this point, it was clear

that a higher spectral resolution was not needed, so the current settings are maintained for the course of experiments.

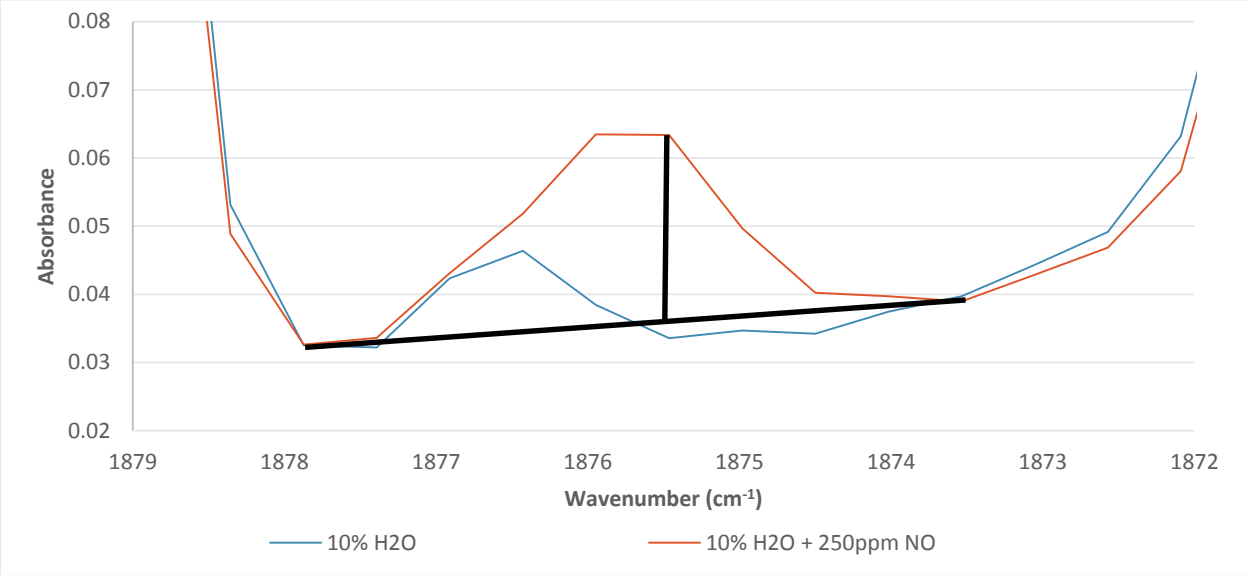

Figure 2.17: The NO peak showing baseline and amplitude

2.4.4 Increasing Signal to Noise Ratio

As discussed in the previous sections, the low signal to noise ratios of the NO and NO_2 data result in large errors in calculating their concentrations in a mixture, so techniques to improve this signal to noise ratio are implemented with varying success. One technique attempted is to increase the intensity of the IR light source in the spectrometer. This technique is achieved by increasing the aperture through which IR light passes before it is sent through the gas cell. The aperture is set to 17%, which according to the manufacturer is the largest recommended aperture for the spectral resolution chosen, and no attempt is made to increase this setting beyond manufacturer's recommendations.

It is thought that turbulence within the gas cell is responsible for some of the noise within the data. To resolve this turbulence, the rate of gas flow within the gas cell is reduced, but the gas flow in

the entire system has to remain constant. To achieve this reduction, an adjustable bypass of the spectrometer gas cell is added, as shown in Figure 2.18. The gas bypass system allows a continuous adjustment of the ratio of flow through the gas cell to the flow bypassing the gas cell. By the ideal gas law, gas flow at each leg of the bypass system is proportional to gas pressure of the leg; therefore, the ratio of flow rates is determined by the ratio of the pressures of each leg of the bypass system.

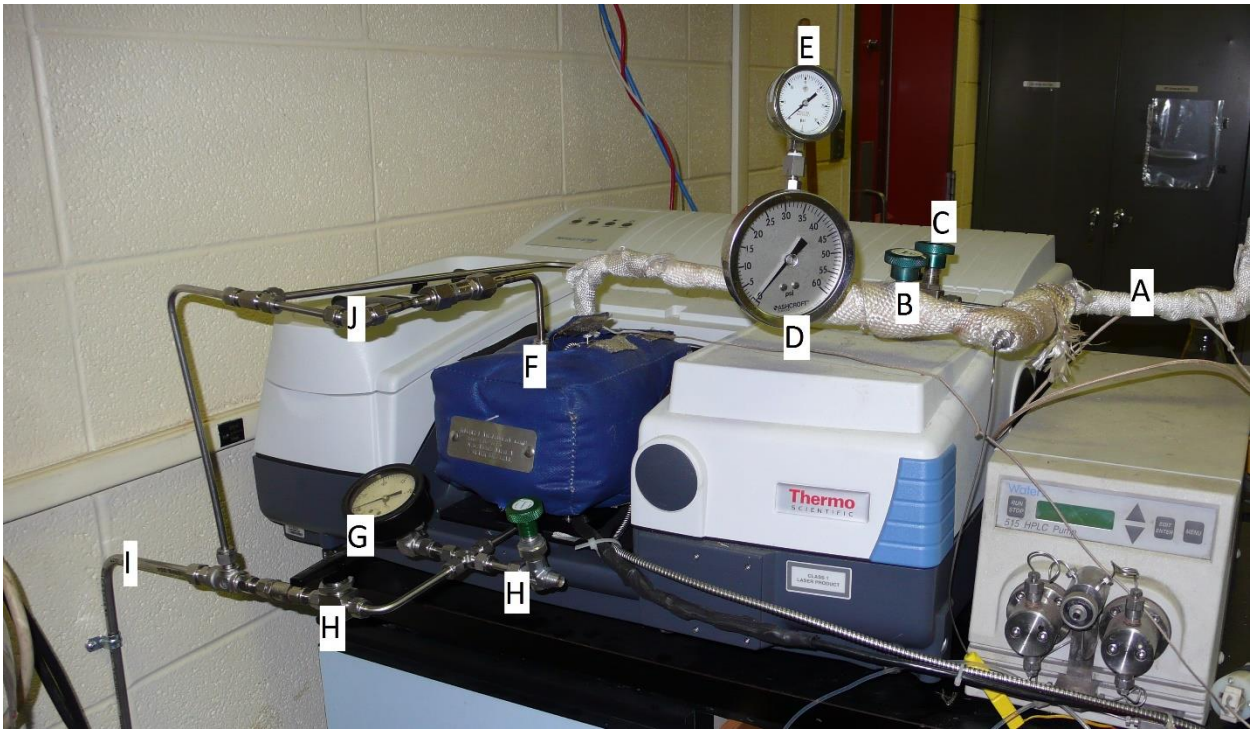

Figure 2.18: The analysis section including FT-IR spectrometer, gas cell, and bypass system showing gas inlet (A), gas cell gas flow control needle valve (B), bypass flow control needle valve (C), gas cell inlet pressure gauge (D), bypass pressure gauge (E), gas cell (with insulating jacket) (F), gas cell outlet pressure gauge(G), valves for obtaining gas samples (H), exhaust (I), and gas cell pressure relief valve (J). Also visible is the pump for the steam system.

The largest concern over this arrangement is that reducing the flow through the gas cell can negatively affect the experimental results. The gas cell acts as a continuously stirred tank with one inlet and one outlet; reducing the gas flow decreases the space velocity of the gas cell. The spectrometer performs 4 scans in 17 s, or 4.25 s per scan. To ensure each scan represents an independent analysis of the gas mixture not influenced by the previous scan, the gas cell has to replace its contents within this time frame.

At a space velocity of 40000 hr^{-1}, the total gas flow rate is 25.6 L/min for a standard cylindrical catalyst monolith of 3" length by 1" diameter. The volume of the spectrometer gas cell is about 200 mL. When all the gas is passing through the gas cell (no bypass), the space velocity of the gas cell is 1.7 s^{-1}. In the SCR experiments, determining gas concentration down to 1 in 10^6 or 1 ppm is an acceptable resolution. Assuming the full flow rate and perfect mixing, which is reasonable in a gas with high turbulence, only 6 in 10^{15} molecules in the gas cell are from the previous scan, which is well below the detection threshold. The gas cell's flow rate would have to be decreased to a space velocity of 0.75 s^{-1}, equivalent to a bypass to gas cell flow rate of 1.6:1, before the remaining gas in the gas cell would be detectable.

Therefore, the bypass is a reasonable option to reduce turbulence without affecting experimental results. While it would be optimal to make the gas cell flow rate as low as possible, the imprecision of the pressure gauges used necessitate that a more conservative value be chosen. In this system, it is determined that at 1:1 bypass to gas cell flow is an achievable value using the equipment available, which corresponds to a gas cell pressure of 3 psig during the experiment.

At this bypass flow rate, a tremendous reduction in noise is observed. Figure 2.19 shows a comparison of calibration data taken with the 1.6:1 bypassed gas cell compared to no bypass. For NO peak, the standard error without the bypass is 1.61%; with the bypass, the error drops to 0.36%, a 78% decrease. For the NO_2 peak, the standard error without the bypasses is 2.73%; with the bypass, the error drops to 0.80%, a 71% decrease.

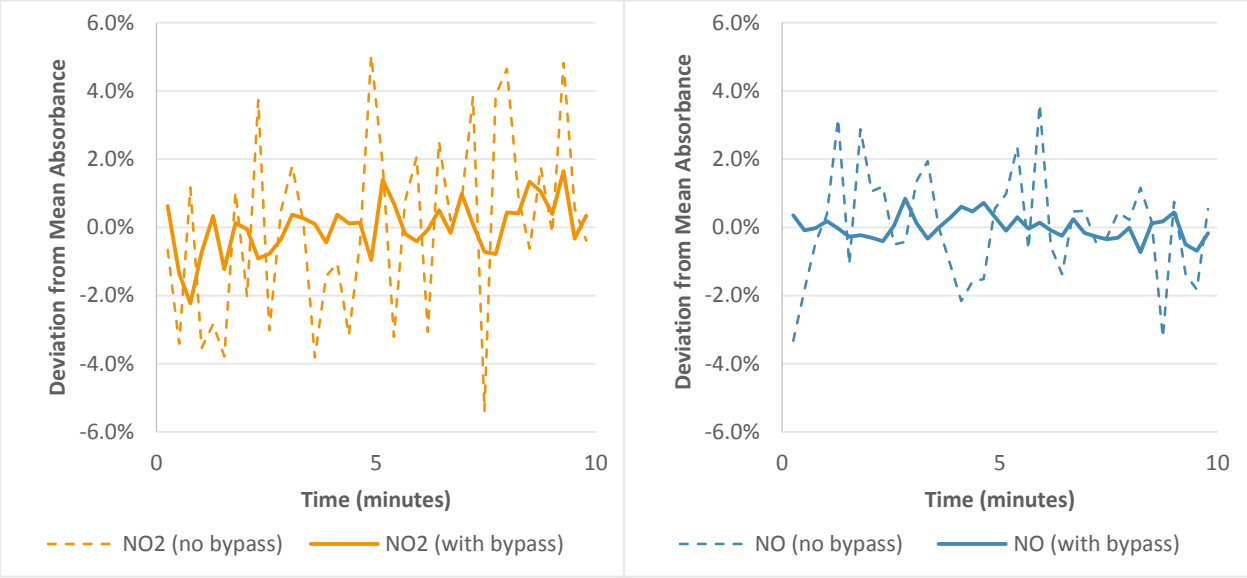

Figure 2.19: Comparison of data taken with and without the gas bypass

2.5 Control and Safety

2.5.1 Computer Control

The monolith testing apparatus is controlled through a mix of custom software, proprietary software, and manual operation. The focus of operation is a National Instruments LabView program created specifically for the catalyst monolith testing apparatus. This software controls all eight mass flow controllers and the heaters of the furnace in which the monolith is housed. It also monitors temperatures within the monolith and furnace and interfaces with the toxic gas sensor system to communicate safety information to the operator. The interface between the LabView software and the various system components is facilitated through the FieldPoint controller model CFP-2110 described earlier. The FieldPoint controller acts as an analog I/O interface generating the furnace and MFC set points as well as accepting thermocouple, MFC flow rate, and gas sensor inputs.

The software is divided into two sections – temperature control and gas flow control. For temperature control, the set points of the furnace can be adjusted and the monolith temperatures read to ensure that the monolith remains within experimental conditions. In the gas flow control section, a gas concentration table is filled out specifying a time profile of desired gas inlet compositions.

A goal of the SCR catalyst monolith testing system is to automate the system as much as possible to remove the necessity of an operator actively monitoring the system. In the current system, an operator has to first turn on the gas flow and heaters and set temperatures. Then, a catalyst monolith testing procedure including gas concentration and times can be entered into the computer. When the operator determines that the system is up to temperature, water flow can be turned on and left for around an hour until the steam flow is stable. The operator then collects a background sample for the spectrometer. Afterwards, testing can begin; the operator has to select to start recording data from the spectrometer software then select to start the testing procedure. Finally, the data generated is analyzed by combining the spectrographic data with the calibration curves and the output from the testing procedure program when each stage testing started.

2.5.2 Toxic Gas Monitoring

Three of the gases stored at high concentrations, NO, NO_2, and NH_3, are toxic at concentrations well below that of their containers. The Occupational Safety and Health Administration (OSHA) specifies a maximum continuous 8-hour permissible exposure limit of 25 ppm, 5 ppm, 50 ppm for NO, NO_2, and NH_3, respectively. OSHA also specifies a maximum 30-minute exposure limit of 50 ppm, 100 ppm, and 500 ppm for NO_2, NO, and NH_3, respectively. Since concentrations of the gases used exceeded these values, to maintain safety in the laboratory, a gas detection system that monitors NO, NO_2, and NH_3 levels within the laboratory is installed.

This system is based upon two Industrial Scientific iTrans2 gas monitoring systems with a custom built control box and additional components added on to expand the system's capabilities. The main control box and one sensor control unit is shown in Figure 2.20. The system is designed such that the iTrans2 system signals a control box when the atmospheric concentration of any of the three gases exceeds the OSHA daily exposure limits. At that point an amber warning light and flashing xenon strobe light (with amber lens) are activated to indicate that conditions within the laboratory are unsafe for long term operation and for the operator to check for and fix leaks in the system before continuing. This alarm signal is also sent to the main computer control system, which puts a message on screen alerting the operator to this condition should the operator somehow not notice the strobe light.

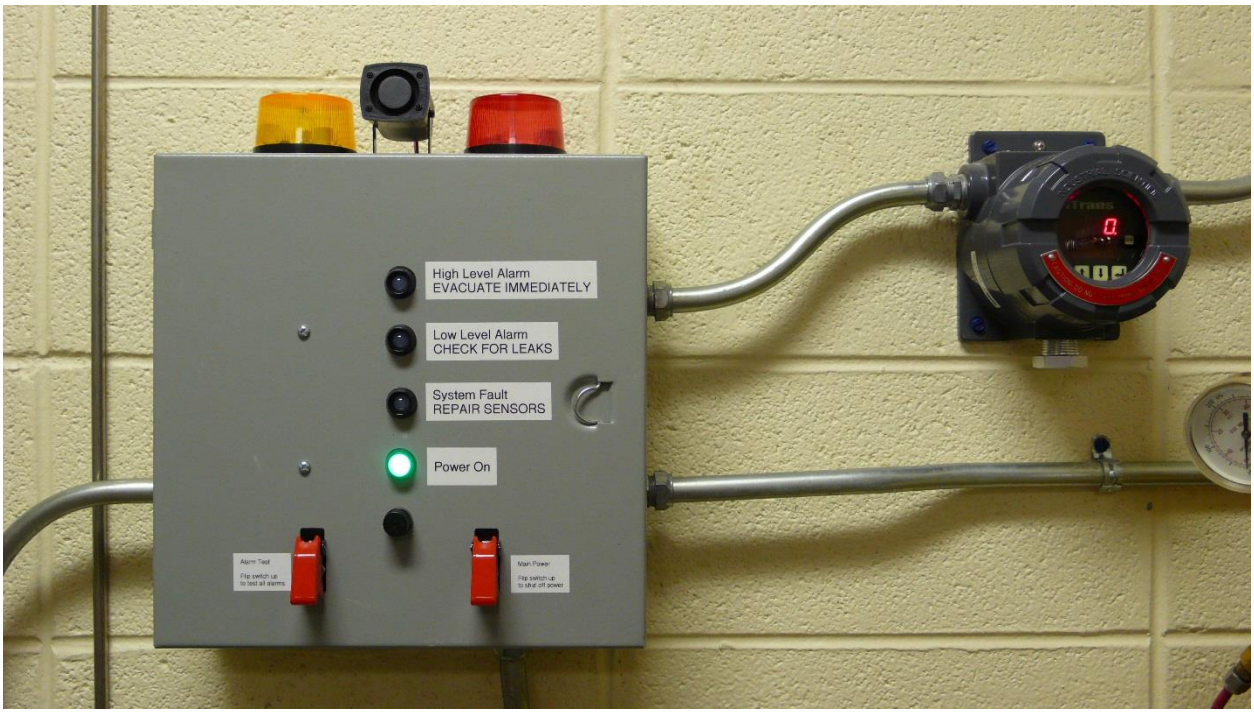

Figure 2.20: Gas detection system control box and NH_3 sensor control unit showing NH_3 concentration in ppm. Visible on the control box are the status indicator LEDs, on/off and alarm test switches, amber and red strobe lights, and siren. Not pictured are the NH_3, NO, and NO_2 sensors and the NO/NO_2 control unit.

When any of the gas concentrations exceeds one half of the OSHA 30-minute exposure limits, then the iTrans2 system sends a signal to the control box, which then turns on a red light, a flashing xenon strobe light (with red lens), and a 120dB siren. The system simultaneously activates solenoid

valves, which cut off the gas flow of NO, NO_2, and NH_3 at the gas regulators, and sends a signal to the main control system to activate a testing system shutdown procedure. The alarm value of one half the OSHA 30-minute exposure limit was chosen because it was assumed that should there be a leak, the gas concentration within the room would slowly build rather than immediately arrive at the 30 minute OSHA exposure limit, which would mean that the persons in the room would be exposed to cumulatively more gas than would be encountered in the specified 30-minute exposure.

2.6 Future Improvements

While at this time the catalyst monolith testing apparatus functions adequately, there is room for improvement. In particular, features need to be implemented through software to improve ease of use and reduce the necessity of an operator to constantly monitor the system.

The automation of the system could serve to be improved. While the gas concentrations can be set to automatically change based on a program, many other features of the apparatus must be manually controlled. While a single experiment can be run automatically, an operator must adjust system parameters between each experiment. Since a single monolith is tested multiple times under different conditions, if the system had completely automatic control, an operator could conceivably start the apparatus just before he or she left work and have all the tests complete by the morning.

The full automation of the system is primarily limited by the lack of ability to automatically adjust temperatures over time according to a set program. This is because the temperature controllers used for the heating tapes cannot be pre-programmed or remotely controlled; to change the tubing temperature the set points on these controllers have to be manually set at the controllers. Since all monoliths need to be tested at multiple temperatures to quantify their performance, this functionality is

essential to an automated system. Eight of the temperature controllers would have to be replaced to support automatic operation.

The system also does not support automatic adjustment of the steam flow rate since the HPLC pump also does not support remote set points; liquid flow rate has to be set manually or turned on/off at the unit itself. This pump would need to be replaced to support remote operation. However, very few experiments require adjustment of the steam concentration. The FT-IR spectrometer supports remote operation through its supplied OMNIC software; however, NI LabVIEW does not support this instrument through any available plugins and thus it cannot be controlled from a central program. Automatic data analysis converting spectrometer absorbance to gas concentration is not implemented due to time constraints, although this automated analysis should be possible through programming. A future goal of this system is to provide complete automation so that any operator can specify a test program, leave the system for multiple hours, and then come back to retrieve concentration results.

The final suggested improvement in the test apparatus is to make the user experience simpler. This is mainly solved through implementing code that calculates optimal settings. Currently, there are dozens of different input parameters that need to be set for a given experiment. For example, a person operating the apparatus needs to set 11 temperature set points even though the only temperature that matters to the results is that of the monolith. This can be particularly frustrating to a new user since none of these temperatures directly control for the monolith temperature; the monolith temperature depends on all 11 settings of the temperature controllers. In this case, if the operator could just input a desired monolith temperature and then have the software calculate the required temperature set points, the learning curve would be reduced significantly. Since this apparatus is intended to be used for years to come by many different researchers, simplifying the user experience is perhaps the most important improvement that can be made.

Chapter 3

Performance Testing and Catalytic Reactions

The industrial sponsor provided multiple iron zeolite SCR catalyst monoliths. One of these iron zeolite catalyst monoliths was selected for performance testing in this section. This section aims to probe the individual reactions that occur on a SCR catalyst including an attempt to correlate performance trends to specific reactions.

When performing SCR, along with the main NO_X reduction reactions, side reactions take place. To better understand and evaluate catalyst performance and probe catalyst aging mechanisms, it is important to have a good understanding of probable chemical reactions that take place and contribute to the overall performance. The testing procedure in this section aims to study the three main reactions on the catalyst individually – the standard NO reaction, the fast NO-NO_2 reaction, and the slow NO_2 reaction. In addition, side reactions are monitored including NO oxidation, NH_3 oxidation, and N_2O generation. Finally, NH_3 storage capacity is calculated.

3.1 SCR Testing Procedure

The goal of the testing procedure is to produce test conditions similar to that of an SCR catalyst monolith in automotive usage. Gases are fed at a space velocity of 40000 hr^{-1}, which is chosen by the industrial sponsor and represents an intermediate value of gas flow rates used in the literature [102, 103]. The monolith sample is a core of a commercial SCR catalyst monolith and measures 3” in length by 1” in diameter. At the chosen space velocity, this corresponds to a gas flow rate of 25.7 L/min. The catalyst monolith is tested in the presence of carbon dioxide and water since these components are present in the exhaust. The monolith is tested at three temperatures – 250 °C, 300 °C, and 400 °C. The

250 °C and 300 °C tests represent engine operation at normal operating conditions while the 400 °C test represents engine operation at high load [16, 104]. Tests at higher temperatures are not needed because it is known that higher temperatures do not represent steady-state operating conditions in real-world environments [16].

Tests are divided into multiple stages. Each test stage has different pollutant concentrations that are chosen to emphasize a specific performance characteristic of the catalyst, and the concentrations in each stage used will be discussed before each test. Prior to every experiment, the catalyst is purged of its stored NH_3 by heating to 450 °C and passing a mixture of air plus 500 ppm NO through the monolith. The outlet is monitored, and the purge is considered complete once NO outlet concentration matches NO inlet concentration for at least 10 minutes. Steady state results are produced by obtaining the mean concentration of each component for the final ten minutes of each stage.

3.2 Ammonia and NO Oxidation

The oxygen in the gas stream, while necessary for the SCR reactions, participates in side reactions as discussed in Chapter 1. Two of these side reactions are NH_3 oxidation and NO oxidation. Ammonia oxidation decreases the amount of NH_3 available for NO_X reduction, and NH_3 oxidation can also generate undesirable byproducts. In contrast, NO oxidation must be discussed in the context of the inlet since it is desirable to adjust $NO:NO_2$ to be as close to 1:1 as possible to favor the fast reaction.

The effects of NH_3 oxidation and NO oxidation are tested in stages 1 and 2, respectively, at each temperature using the procedure depicted in Table 3.1. The procedure replicates the nitrogen, oxygen, water, and carbon dioxide concentrations used throughout this chapter while introducing only one other component at a time.

Table 3.1: NH_3 and NO oxidation testing procedure

	Inlet Concentration (%)				Inlet Concentration (ppm)		
	N_2	O_2	H_2O	CO_2	NH_3	NO	NO_2
Stage 1	74	6	10	10	500	0	0
Stage 2	74	6	10	10	0	500	0

Since these two stages of the testing procedure were run before every SCR test (in Figure 3.1, Figure 3.2, and Figure 3.3), there are three tests each for NH_3 oxidation and NO oxidation at every temperature. The data presented in

Table 3.2 is the average of the three tests at each temperature.

Table 3.2: NH_3 and NO oxidation results

			Outlet Concentration (ppm)				
	Temperature	**NH_3 or NO Oxidized (%)**	**NH_3**	**NO**	**NO_2**	**N_2O**	**Total NO_X**
Stage 1: Steady State NH_3 Oxidation	250 °C	0.9	495.3	0.1	0.0	0.1	0.1
	300 °C	0.7	496.4	0.4	0.2	0.0	0.6
	400 °C	9.8	451.2	0.2	0.3	0.1	0.5
Stage 2: Steady State NO Oxidation	250 °C	1.8	0.0	491.0	7.7	0.0	498.7
	300 °C	1.9	0.1	485.4	15.0	0.1	500.4
	400 °C	5.5	0.0	472.7	28.0	0.2	500.7

None of the NH_3 oxidation tests produce significant amounts of NO, NO_2, or N_2O at steady state, which indicates that all NH_3 is being oxidized directly to N_2 and H_2O. The relative amount of NH_3 oxidation is very low at 200 and 300 °C with oxidation of 0.9 and 0.7%, respectively. At 400 °C, NH_3

oxidation becomes a significant issue with an average of 9.8% of NH_3 being lost to oxidation. This is consistent with previous studies which state that for iron-zeolite catalysts NH_3 oxidation only becomes significant at 400 °C and above [102].

NO oxidation increases with temperature with an average of 1.8% at 250 °C, 2.0% at 300 °C, and 5.5% at 400 °C. The only product of the reaction is NO_2, which is present in equivalent amount to the difference between the NO inlet and the NO outlet. Previous studies of new iron-zeolite catalysts have shown similar results with very little NO oxidation occurring and NO oxidation increasing to 7% at 400 °C [105]. Thus, NO oxidation is not very significant but should not be ignored.

3.3 Ammonia Storage

SCR is a heterogeneous catalytic reaction, so NH_3 must adsorb on the catalyst before it can reduce NO_X. Ammonia storage capacity scales with the number of Brønsted acid sites that adsorb NH_3 on the catalyst [106]. However, NH_3 storage capacity is only an indicator and not directly proportional to catalyst activity since only a fraction of the NH_3 storage sites are utilized during SCR reactions, and this fraction is dependent upon the NO_X composition [50]. For example, at the same overall NO_X inlet concentration, the reduction of a pure NO feed requires three times the number of adsorption sites on the catalyst compared to a 1:1 NO:NO_2 [50]

Ammonia storage capacity was tested by performing the two-step procedure presented in Table 3.3. After the normal NH_3 purge procedure, the monolith is heated to its temperature setting in an oxygen-free environment. In stage 1, 500 ppm of NH_3 is added. Ammonia adsorbs to the catalyst, and the NH_3 outlet concentration is monitored. Once the NH_3 outlet concentration matches the inlet concentration for at least ten minutes, stage 1 ends and stage 2 begins. In stage 2, the NH_3 supply is cut off and stored NH_3 desorbs from the catalyst. Once the NH_3 outlet drops below 5 ppm, the temperature

set point of the monolith is increased to 450 °C. The test is continued until two criteria are fulfilled: the monolith reaches the temperature set point and the concentration of NH_3 in the outlet is below 5 ppm.

Table 3.3: NH_3 storage capacity testing procedure

	Inlet Concentration (%)				Inlet Concentration (ppm)		
	N_2	**O_2**	**H_2O**	**CO_2**	**NH_3**	**NO**	**NO_2**
Stage 1	80	0	10	10	500	0	0
Stage 2	80	0	10	10	0	0	0

Table 3.4 reports the NH_3 storage results. As the lack of oxygen prevents NH_3 oxidation in this experiment, the NH_3 adsorption should be equal to the NH_3 desorption [64]. The results follow the expected trend of lower capacity at higher temperature [50, 106]. The difference between the adsorption and desorption numbers is a result of the necessity to integrate data points over a long period of time; error is accumulated in this integration.

Table 3.4: NH_3 storage results

Temperature (°C)	Adsorbed NH_3 (mmol)	Desorbed NH_3 (mmol)
250	1.350	1.610
300	0.943	0.918
400	0.198	0.245

This data is difficult to compare with other studies as the standard method of reporting NH_3 storage capacity is either through storage capacity per weight catalyst or storage capacity per volume catalyst. Since the item under investigation is a supported catalyst and there is no information from the manufacturer as to the weight or volume of the coating, it is not possible to put these results in context

with other studies. However, this NH_3 storage data will present a good reference point when discussing catalyst deactivation in Chapter 4.

3.4 Standard Reaction

The first program to test SCR performance focuses on the standard reaction, where NO is reduced by NH_3, and this procedure is presented in Table 3.5. The first two stages are those of the NH_3 and NO oxidation as described earlier. The standard reaction occurs in stage 3.

Table 3.5: Standard reaction testing procedure

	Inlet Concentration (%)				Inlet Concentration (ppm)		
	N_2	O_2	H_2O	CO_2	NH_3	NO	NO_2
Stage 1	74	6	10	10	500	0	0
Stage 2	74	6	10	10	0	500	0
Stage 3	74	6	10	10	500	500	0

The standard reaction test results are shown in Figure 3.1, and a summary of the stage 3 data is presented in Table 3.6. The results indicate that the rate of the standard reaction is highly correlated with temperature with NO reduction increasing from only 2.2% at 250 °C to 77.1% at 400 °C. This trend in NO reduction corresponds well with previous studies, which indicate poor performance of the standard reaction at low temperature on iron zeolite catalysts [102, 105].

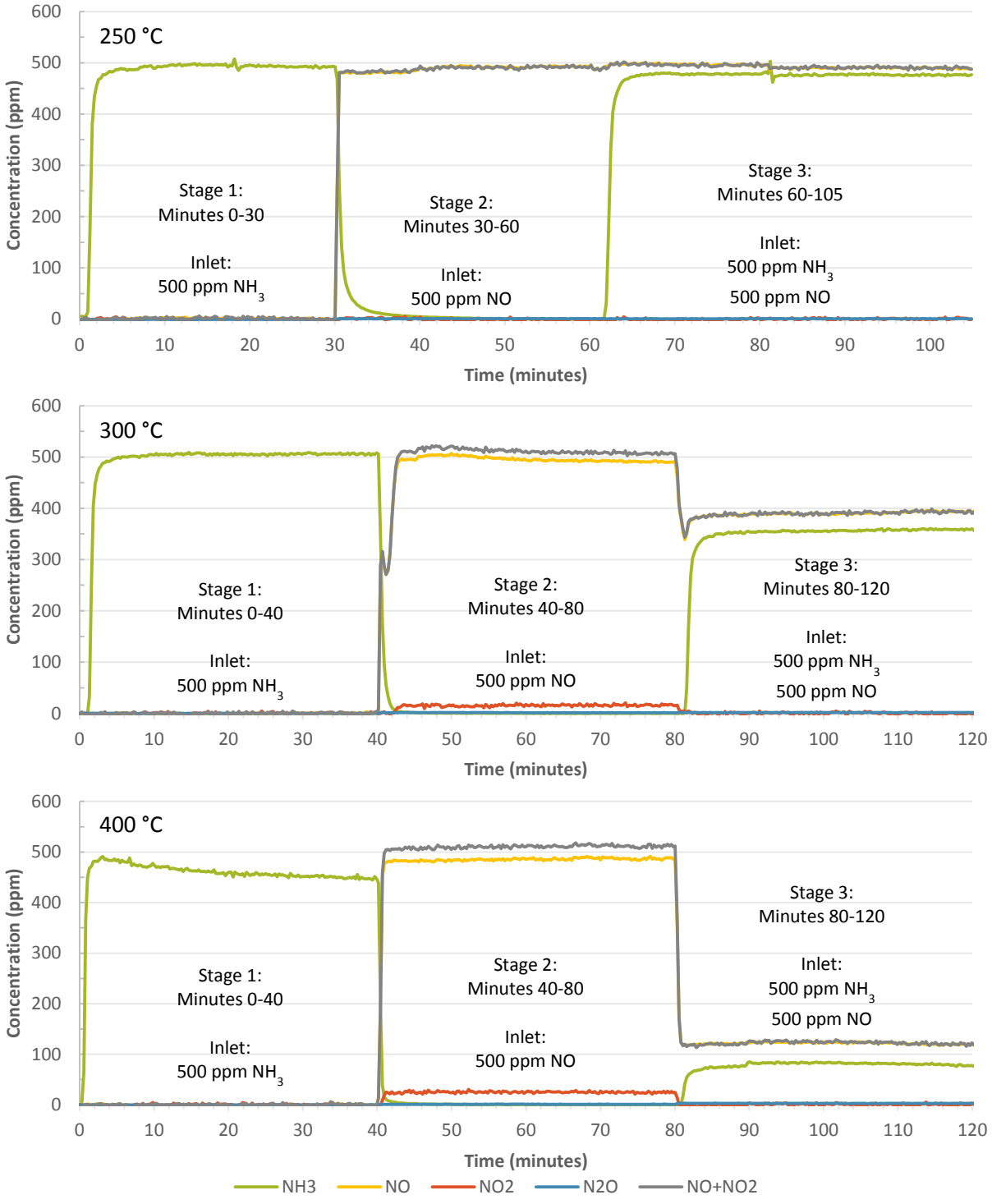

Figure 3.1: Performance of the catalyst monolith with parameters favoring the standard reaction at 250, 300, and 400 °C

Table 3.6: Standard reaction performance

Temperature (°C)	Equilibrium Concentration (ppm)					NH_3 Consumption (%)	NO_X Reduction (%)
	NH_3	NO	NO_2	N_2O	Total NO_X		
250	476.3	488.8	1.2	0.9	490.0	4.7	2.0
300	354.5	390.1	1.2	1.6	391.3	29.1	21.7
400	72.3	112.8	1.5	2.7	114.3	85.5	77.1

The NH_3 consumption closely tracks the NO_X reduction with differences of 2.7%, 7.4%, and 8.4% at 250, 300, and 400 °C, respectively. In this experiment, since there is minimal generation of N_2O, the majority of the extra NH_3 must oxidize to N_2 and H_2O.

In stage 2 of the 300 °C test there is a transient behavior of the NO immediately after the stage begins. When NH_3 is cut off and NO is turned on, the NO level increases nearly to the set point, drops, and then recovers to the set point. This effect is repeatable; the second stage of the 300 °C tests in Figure 3.2 and Figure 3.3, which are run at the exact same conditions, demonstrate the exact same behavior. In addition, a similar behavior occurs in stage 3 of the standard reaction test at 300 °C when the NH_3 is present.

Studies have reported identical transient behavior at low and intermediate temperatures in the same conditions [75, 105]. The behavior occurs when NH_3 is switched on or off in the presence of NO but without NO_2. This behavior has been attributed to NH_3 inhibiting the standard reaction, and it has been reported that the behavior is most marked in zeolite catalysts [75, 102, 105]. It has been suggested that the excess NH_3 is inhibiting the oxidation of NO to NO_2 on the surface of the catalyst [75], which is one of the steps of the standard reaction mechanism as described in Chapter 1. This behavior should also be present at colder temperatures [75, 105]. It does not clearly appear in the 250 °C results as there is so little NO reduction that the instrument is not sensitive enough to capture this phenomenon.

3.5 Fast Reaction

The second program focuses on testing the fast reaction, where NO_X in equal parts of NO and NO_2 is reduced by NH_3, and this procedure is presented in Table 3.7. This test represents the most desirable operating regime for a SCR catalyst since the fast reaction has the highest rate constant of the three primary SCR reactions. Therefore a given catalyst can achieve a higher NO_X reduction efficiency through the fast reaction compared to either the standard or slow reactions. Alternatively, if a SCR catalyst cannot meet specifications when performing the fast reaction, this indicates that the catalyst will also fail to effectively perform the standard and slow reactions. The reason for the indicator is that because those reactions' slower kinetics, more active sites are required for the same NO_X reduction efficiency at a given temperature compared to the fast reaction [50, 76, 91, 102].

Table 3.7: Fast reaction testing procedure

	Concentration (%)				Concentration (ppm)		
	N_2	O_2	H_2O	CO_2	NH_3	NO	NO_2
Stage 1	74	6	10	10	500	0	0
Stage 2	74	6	10	10	0	500	0
Stage 3	74	6	10	10	500	250	250

The fast reaction test results are shown in shown in Figure 3.2, and its steady state performance is summarized in Table 3.8. Unlike the standard reaction, NO_X reduction by the fast reaction is not highly correlated with temperature; NO_X reduction is excellent at all temperatures reaching 95.3% even at 250 °C and increasing to 97.8% at 400 °C. These results corroborate well with previous studies, which show similar very high NO_X reduction using the fast reaction with NO_X reduction always exceeding 90% [102, 105].

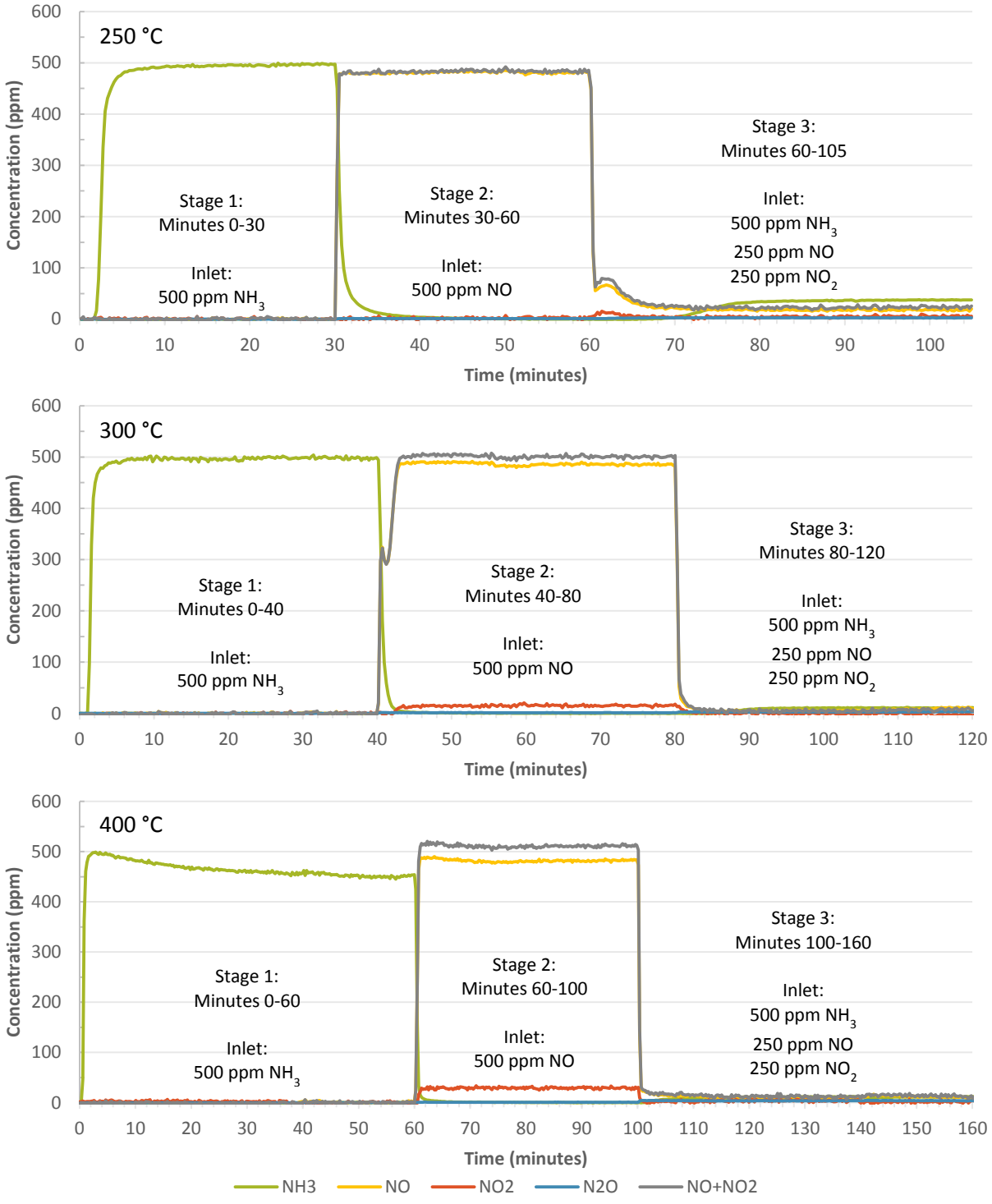

Figure 3.2: Performance of the catalyst monolith with parameters favoring the fast reaction at 250, 300, and 400 °C

Table 3.8: Fast reaction performance

Temperature (°C)	Equilibrium Concentration (ppm)					NH_3 Consumption (%)	NO_X Reduction (%)
	NH_3	NO	NO_2	N_2O	Total NO_X		
250	37.5	17.8	5.7	2.5	23.5	92.5	95.3
300	10.6	10.1	4.7	2.7	14.8	97.9	97.0
400	8.1	8.0	3.2	3.6	11.2	98.3	97.8

The NH_3 consumption does not track the NO_X reduction in the fast reaction tests as it did in the standard reaction tests. The difference between NH_3 consumption and NO_X reduction changes from of -2.8% at 250 °C to 0.9% at 300 °C and 0.5% at 400 °C. The higher NO_X reduction than NH_3 consumption at 250°C indicates that a reaction must be consuming a higher proportion of NO_X than NH_3. Since this behavior occurs only at 250 °C, the likely reason for the results is the generation of NH_4NO_3, reaction (19), and then decomposition of the ammonium nitrate into HNO_3 and NH_3, Reaction (21). These two reactions has previously been reported to occur at low temperature and in an environment with a high concentration of water and a low concentration of NO [99, 104, 107, 108] – the same conditions in which this test is run. The net result of Reactions (19) and (21) is Reaction (23):

$$NH_3 + 2\,NO_2 \rightarrow HNO_3 + N_2 + H_2O \qquad (23)$$

As this reaction consumes one mole of NH_3 for every two moles of NO_2, Reaction (23) can explain why at 250 °C there is more NH_3 than NO_X. This reaction can also explain why the highest consumption of NO_2 occurs at 250 °C. Further supporting the nitric acid hypothesis is that the 250 °C test shows transient behavior in stage 3. Transient behavior at low temperatures and with NO as well as NO_2 present has been previously reported in the literature citing the formation and destruction of ammonium nitrate as being responsible for this transient behavior [64, 94, 106].

Previous studies have shown that ammonium nitrate generation diminishes by 300 °C and ceases before 400 °C [64, 109]. This behavior is consistent with the results observed where NH_3

consumption becomes higher than NO_X reduction at 300 °C and 400 °C, which would correspond to decreased ammonium nitrate generation and increased NH_3 oxidation as temperature increases.

3.6 Slow Reaction

The third program focuses on testing the slow reaction where NO_2 is reduced by NH_3, and this procedure is presented in

Table 3.9. Unlike the standard reaction procedure, which contains only NO, the slow reaction procedure contains both NO and NO_2 in a 1:3 ratio. This ratio was requested by the industrial sponsor, and compared to using only NO_2 and no NO, 1:3 NO:NO_2 represents a much more realistic operating condition for this monolith as discussed in Chapter 1.

Table 3.9: Slow reaction testing procedure

	Concentration (%)				Concentration (ppm)		
	N_2	**O_2**	**H_2O**	**CO_2**	**NH_3**	**NO**	**NO_2**
Stage 1	74	6	10	10	500	0	0
Stage 2	74	6	10	10	0	500	0
Stage 3	74	6	10	10	500	125	375

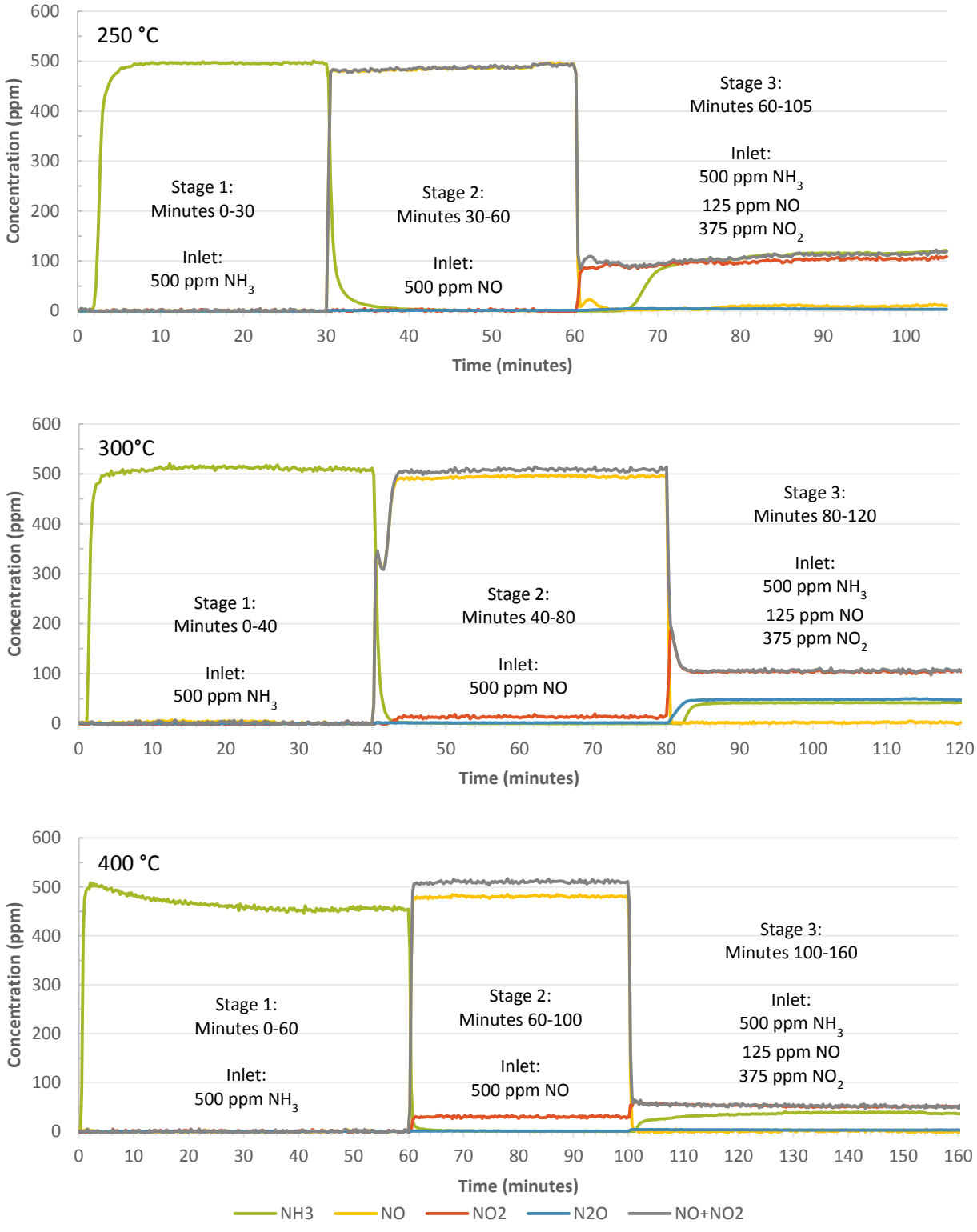

Figure 3.3: Performance of the catalyst monolith with parameters favoring the slow reaction at 250, 300, and 400 °C

The slow reaction test provides some very interesting results as presented in Table 3.10. NO_2 reduction is 71.7% at 250 °C, increases slightly to 72.2% at 300 °C, and increases greatly to 86.7% at 400 °C. NO reduction at 250 °C is 91.0% and increases to 99.5 % at 300 °C and remains at 98.5% at 400 °C.

Table 3.10: Slow reaction performance

Temperature (°C)	Equilibrium Concentration (ppm)					NH_3 Consumption (%)	NO_X Reduction (%)
	NH_3	NO	NO_2	N_2O	Total NO_X		
250	119.5	11.3	106.0	3.2	117.3	76.1	76.5
300	42.0	0.6	104.2	45.5	104.8	91.6	79.0
400	38.4	1.9	49.9	2.6	51.8	92.3	89.6

The drastic reduction in NO at 250 °C is likely due to the fast reaction because the previous data shows that at 250 °C the standard reaction is only 2.2% effective at reducing NO while the fast reaction is 95.3% effective. NO_X reduction is 0.4% higher than NH_3 consumption at 250 °C indicating that HNO_3 formation is occurring just as in the 250 °C fast reaction test. The majority of the remainder of the consumed NO_2 must be reacted through the slow reaction because the catalyst is not generating enough N_2O to account for the missing NO_2. The prevalence of the slow reaction would also explain why the difference between NH_3 consumption and NO_X reduction is not as great in the 250 °C slow reaction test as it is in the 250 °C fast reaction test.

The slow reaction requires 4:3 NH_3:NO_2 while the HNO_3 generation reaction requires 1:2 NH_3:NO_2. Assuming that all of the consumed NO is through the fast reaction in a 1:1 ratio with NH_3 and accounting for the NH_3 remaining at steady state, then a combination of the HNO_3 generation and the slow reactions must consume 155 ppm NO_2 and 142 ppm NH_3. Using reaction stoichiometry, 20% of the NH_3 or 29 ppm is being consumed in HNO_3 generation with the remainder being consumed through the

slow reaction. This value is within reason considering that the difference in NH_3 consumption and NO_X reduction in the 250 °C fast reaction experiment is 14 ppm.

At 300 °C, the most prominent difference is the appearance of N_2O, which is present at 45.5 ppm. However, 300 °C is the only temperature where large amounts of N_2O are generated in all the experiments; N_2O is not in high concentration in the 250 °C tests or 400 °C tests or in any of the standard or fast reaction tests. This high N_2O generation at 300 °C corresponds very well with previous studies of iron zeolite catalysts, which report that in an environment with a low $NO:NO_2$ ratio, N_2O generation peaks at between 275 °C and 325 °C [94, 105]. The high N_2O generation also corresponds well with the difference between NH_3 consumption and NO_X reduction, which at 12.6% is the largest of all the tests performed.

At 400 °C, NO_2 reduction increases compared to 300 °C and the difference between NH_3 consumption and NO_X reduction decreases to 2.8%. Consistent with the N_2O studies, the amount of N_2O generated at 400 °C declines below that of 300 °C, although the literature reviewed generally shows a small amount of N_2O at 400 °C [94, 105] whereas this experiment shows no N_2O. A possible reason for this discrepancy is that the experiments cited used NO_2 and no NO while this experiment uses 1:3 $NO:NO_2$.

3.7 Performance Summary

In summary, the catalyst monolith tested in this section has features that corroborate well with the established literature on iron-zeolite catalysts. The catalyst monolith is highly resistant to NH_3 oxidation at 250 °C and 300 °C but oxidizes 9.8% of the NH_3 at 400 °C. The catalyst monolith's NO reducing performance is very low at 2.2% at 250 °C but increases greatly to 77.4% at 400 °C. The catalyst monolith's fast reaction performance is very high at all temperatures with NO_X reduction

reaching 95.3% even at 250 °C. However, at 250 °C in the fast reaction a higher proportion of NO_X is reduced than NH_3 consumed indicating generation of HNO_3. In an environment with an excess of NO_2, the catalyst monolith's performance also indicates HNO_3 generation at 250 °C. Large amounts of N_2O – 45.5 ppm – are generated at 300 °C but this N_2O generation is lower at other temperatures. Ammonia storage capacity decreases with increasing temperature in contrast to the general trend of increased NO_X reduction performance at higher temperatures supporting a previous study that only a fraction of active sites are used for NO_X reduction.

In looking at future experiments, it is important to consider the side reactions that can occur. The tests presented in this chapter indicate that the side reactions occur in the presence of NO_2. Therefore, when characterizing the performance of additional monoliths, it will be important to look at how the catalyst reacts to NO_2 – whether the catalyst will have the desired performance and reduce the NO_2 through the fast and slow reactions or whether the NO_2 will be consumed in NH_4NO_3 generation and decomposition as well as N_2O generation.

Chapter 4

Catalyst Deactivation

The industrial sponsor for this project provided two catalyst monoliths: one monolith was a fresh catalyst monolith with no previous use, and the other monolith was used in a diesel truck. Having two monoliths with different aging presents an opportunity to compare these monoliths' performance, composition, and structure. Comparing two monoliths also offered a chance to study SCR catalyst aging on a coated monolith; while there are many studies of diesel SCR catalyst aging, studies of aging of SCR catalysts coated on supports are uncommon. The goal of this section is to first study the SCR performance of the catalyst monoliths and then explain the causes for the difference in performance between the two monoliths by using physical characterization of the monoliths.

4.1 Background

The monoliths used in this research are coated in zeolite catalysts; the two most commonly cited deactivation mechanisms for zeolite SCR catalysts are dealumination and promoter metal deactivation [76]. These are classified as hydrothermal mechanisms – deactivation mechanisms that are a result of the catalyst being exposed to high temperature in the presence of water over long periods of time.

Dealumination is the loss of framework aluminum from the zeolite structure. As the substitution of aluminum in the zeolite structure produces the Brønsted acid sites on the catalyst, dealumination reduces the number of Brønsted acid sites on the catalyst [110]. Since the Brønsted acid sites adsorb NH_3, testing for NH_3 storage capacity represents a way to check the Brønsted acidity of the catalyst [111]. It is also possible to directly check the aluminum concentration within the catalyst to

measure the extent of dealumination [112]. However, both characterization methods can be prone to error. Other deactivation mechanisms may be responsible for a loss of Brønsted acidity, and the aluminum does not need to be removed from the catalyst to become inactive; aluminum sites have been shown to change to an inactive form as the catalyst ages [110, 112].

Promoter metal deactivation refers to the removal of the promoter metal from the zeolite structure and change into an inactive oxidation state [113, 114]. In the process of deactivation, the metal can form large agglomerates on the catalyst surface or be removed from the catalyst surface. This deactivation mechanism is different from sintering, where metals also aggregate into large particles. Sintering deactivates metal and metal oxide catalysts through reducing the surface area of the metal catalyst. In contrast, promoter metal deactivation in zeolite catalysts is primarily caused by the change in oxidation state; the formation of large metal agglomerates is secondary. The presence of metal agglomerates does not necessarily mean that the catalyst is suffering from this deactivation mechanism; certain SCR catalysts are designed to have metal aggregates as part of their structure [115]. The growth of metal aggregates only suggests the deactivation mechanism.

Mechanical failure of the catalyst coating is another aging mechanism. Through thermal cycling, the catalyst coating can crack and then separate from the support resulting in a loss of catalytic material [116]. In addition, catalyst aggregation can occur where the catalyst coating itself agglomerates into particles [117]. This mechanism results in a loss of surface area and thus a loss of catalytic activity similar to sintering.

Carbon deposits can degrade catalyst activity through coking. The carbon deposits bind preferentially to strong acid sites masking them from the reactants [118]. The effects of coking are reversible on zeolite SCR catalysts; studies have tested catalysts with up to 10.9% carbon (weight basis) and have reported that heating a carbon-coked SCR catalyst to 500 °C for two hours in the presence of oxygen restores original catalyst functionality [85, 118].

Finally, catalyst poisoning can occur through reaction with various elements. The most commonly cited elements are sulfur and phosphorous [80, 119-122] as sulfur is present in ppm concentrations in diesel fuel [43], and phosphorous is present in engine lubricating oils [121], although there are dozens of possible compounds that can deactivate a catalyst. The mechanism behind poisoning is that the elements or compounds irreversibly bind to active sites rendering the sites permanently inactive [117].

4.2 Catalyst Performance

The first aspect to be analyzed is the monoliths' NO_X reduction performance. Two aspects of the catalyst monoliths' performance are to be characterized - NH_3 storage capacity and SCR activity. A testing procedure consisting of three stages and three temperatures was developed to analyze performance.

4.2.1 SCR Testing Procedure

Similar to the procedure described in the previous chapter, the testing procedure used in this chapter has the goal to produce conditions similar to that of an SCR catalyst monolith in automotive usage. However, compared to the previous chapter, this chapter uses an abbreviated procedure to reduce the amount of time required for testing.

As in Chapter 3, the gases are fed at a space velocity of 40000 hr^{-1}, and the monolith samples are cores of commercial SCR monoliths measuring 3" in length by 1" in diameter. At the chosen space velocity, this corresponds to a gas flow rate of 25.7 L/min. The catalyst monoliths are tested in the

presence of carbon dioxide and water since these components are present in the exhaust. Each catalyst monolith is tested at three temperatures: 250, 300, and 400 °C.

The test consists of three consecutive stages as shown in Table 4.1. The purpose of the first stage is to quantify NH_3 storage capacity. When quantifying NH_3 storage capacity, NH_3 cannot be consumed in side reactions, so no oxidants such as O_2 or NO_X are allowed in the inlet gas. In this stage, a fixed concentration of NH_3 is sent to the catalyst monolith. For a short period of time, NH_3 adsorbs onto the monolith, and the gases exiting the monolith are devoid of NH_3. After a period of time, the monolith becomes saturated with NH_3 and NH_3 is detected in the gases leaving the monolith. Once the gases exiting the catalyst monolith have the same concentration as the inlet, the catalyst is fully saturated with NH_3. The test is run for an additional five minutes to confirm the saturation and then the stage is complete. To quantify NH_3 storage from these results, the amount of NH_3 detected after the catalyst monolith is integrated throughout the entire stage. This is subtracted from the integral of the NH_3 fed to the monolith. The difference of these values is the amount of NH_3 adsorbed on the catalyst.

Table 4.1: Catalyst monolith performance testing procedure

	Concentration (%)				Concentration (ppm)		
	N_2	**O_2**	**H_2O**	**CO_2**	**NH_3**	**NO**	**NO_2**
Stage 1	90	0	5	5	500	0	0
Stage 2	80	10	5	5	0	500	0
Stage 3	80	10	5	5	500	250	250

In the second stage, the quantities of NH_3 that desorb and react are tested. The NH_3 feed is cut off and replaced by NO allowing reduction of pre-adsorbed NH_3 by NO. In addition, 10% oxygen is added to replicate exhaust conditions and test NO oxidation. The NH_3 stored on the catalyst desorbs, oxidizes, or reacts with NO_X, and the monolith outlet initially shows no NO_X. After a period of time,

there is no more NH_3 stored on the catalyst, SCR reactions cannot occur, and NO_X levels return to match the inlet feed. The test is run for an additional five minutes to confirm the consumption of all the NH_3, and then the stage is complete. The steady state performance of stage 2 can be used to describe NO oxidation, and the amount of NH_3 that desorbs from the catalyst without reacting can also be calculated by integrating the NH_3 concentration throughout stage 2. To calculate the amount of adsorbed NH_3 that reacts with NO_X, the amount of NO_X detected after the monolith is integrated throughout the entire stage. This is subtracted from the integral of the NO_X fed to the monolith, and the difference of these values is the amount of NO_X that reacted with NH_3.

In the third stage, steady state SCR performance is tested. 1:1 NO_X:NH_3 is sent to the monolith. The NO_X consists of 1:1 NO:NO_2 encouraging the fast NO_X reaction. As in stage 2 10% oxygen is added to replicate exhaust conditions.

4.2.2 SCR Testing Results

The results of the testing of the new catalyst monolith is presented in

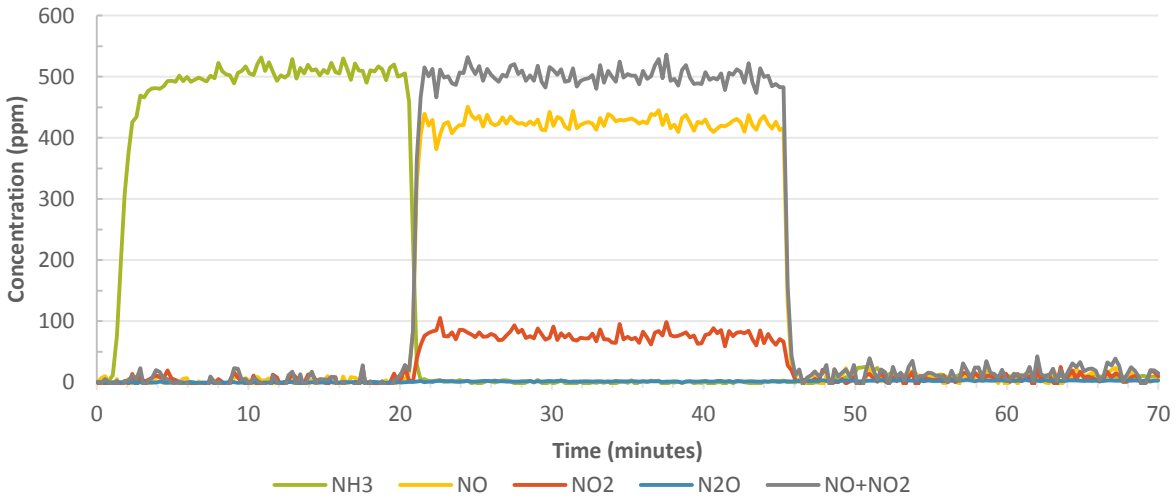

Figure 4.1, and the testing of the used catalyst monolith is presented in Figure 4.2

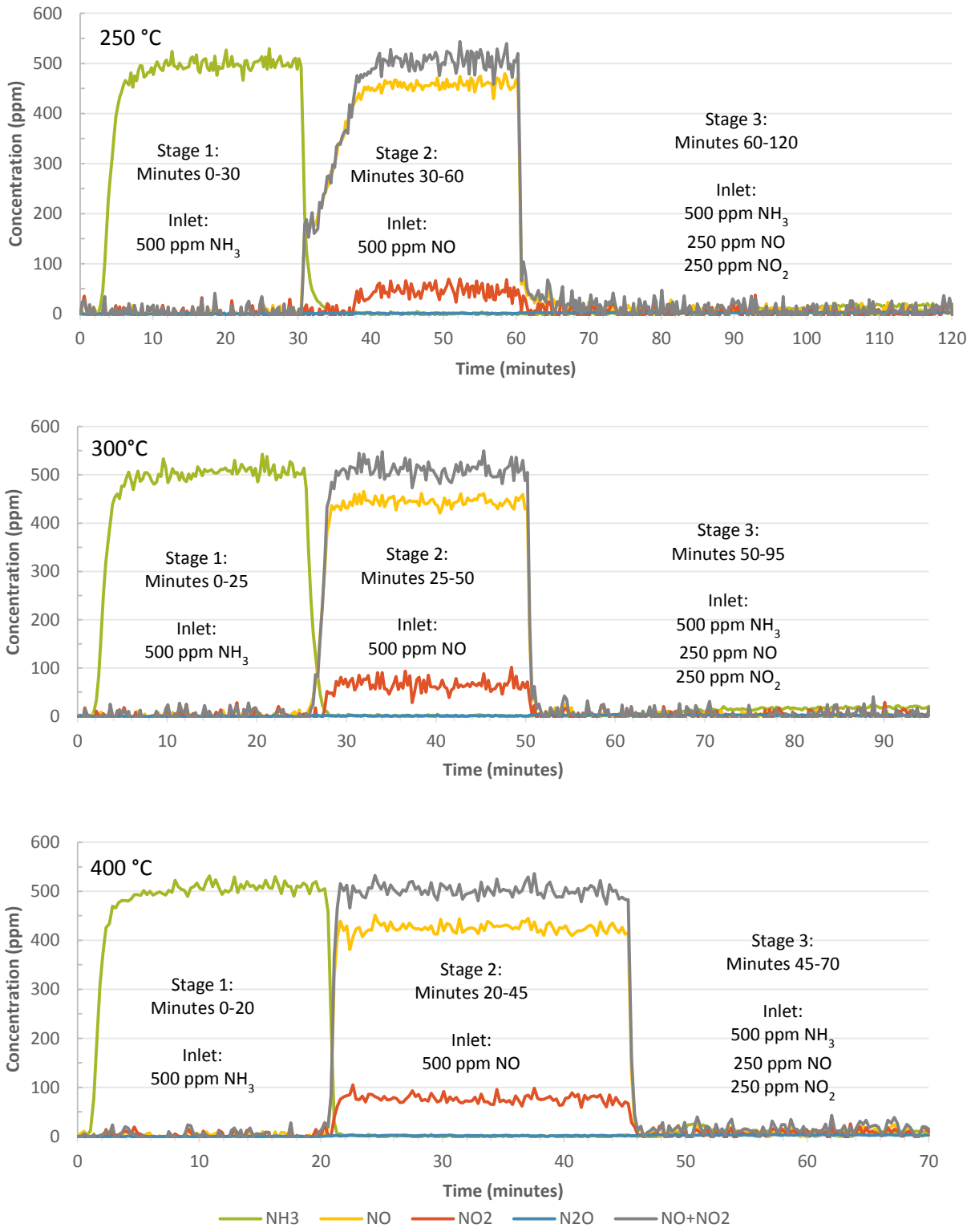

Figure 4.1: Performance of the new catalyst monolith at 250, 300, and 400 °C.

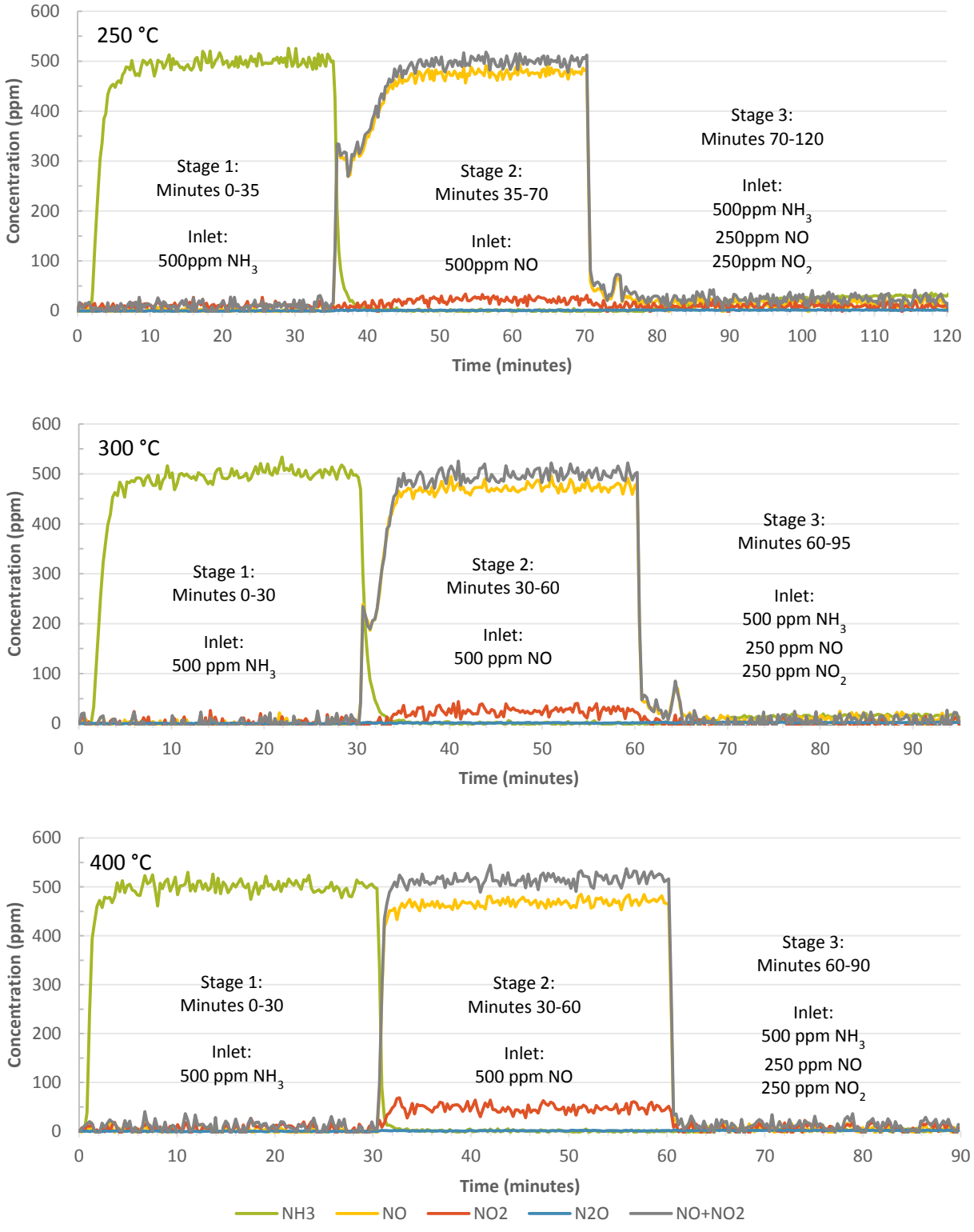

Figure 4.2: Performance of the used catalyst monolith at 250, 300, and 400 °C.

From the stage 1 results in

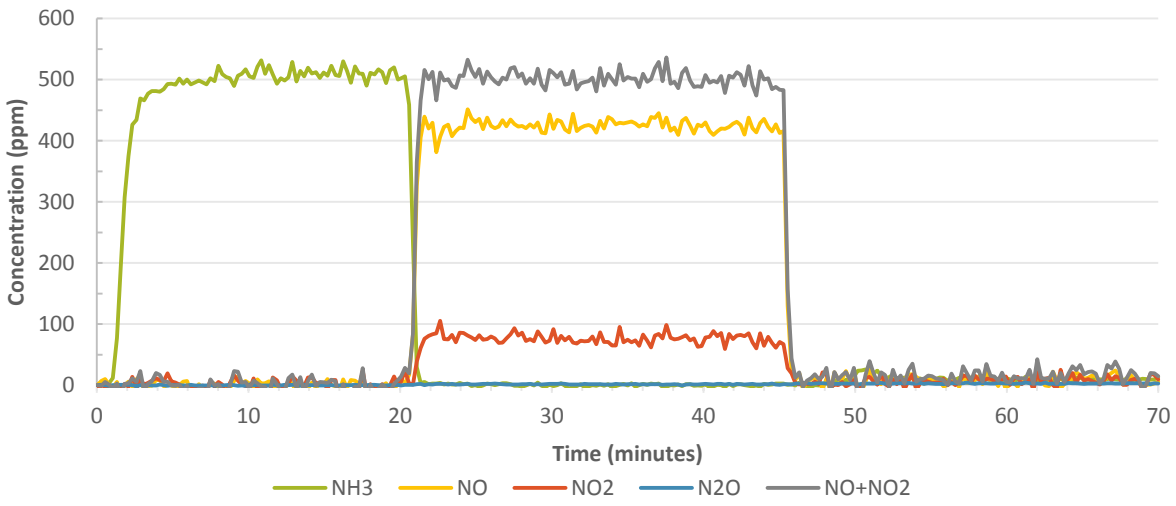

Figure 4.1 and Figure 4.2, NH_3 storage capacity is calculated. Due to some variation in the calibration of the mass flow controllers, the NH_3 and total NO_X concentrations are offset from the desired 500 ppm. The exact concentrations of NH_3 and NO_X in the inlet are taken into account using the steady state concentrations at the end of stages 1 and 2, respectively. The NH_3 storage data are presented in Table 4.2.

Table 4.2: NH_3 storage of the new and used monoliths

Temperature	250 °C		300 °C		400 °C	
	NH_3 Adsorbed	NH_3 Desorbed + NO_X reacted	NH_3 Adsorbed	NH_3 Desorbed + NO_X reacted	NH_3 Adsorbed	NH_3 Desorbed + NO_X reacted
New monolith (mmol)	2.64	2.67	1.93	1.87	1.29	1.12
Used monolith (mmol)	2.07	2.04	1.74	1.70	0.75	0.54
% Increase Over New	-21.6	-23.6	-9.8	-9.0	-41.9	-51.8

The NH_3 storage results show that both monoliths store less NH_3 as temperature increases, which is in alignment with the thermodynamics of adsorption and previous studies [102, 105]. Moreover, the used monolith stores less NH_3 than the new monolith at all temperatures with the used

monolith storing up to 42% less NH_3 than the new monolith. This lower NH_3 storage suggests that the used monolith is suffering from dealumination.

At 250 °C, the amount of NH_3 that either desorbs or reacts with NO_X is similar to the amount adsorbed respectively for each monolith indicating that mass is conserved. However, as temperature increases, the sum of NH_3 desorbed and NO_X reacted trends lower than the amount of NH_3 adsorbed. At 400 °C, the NH_3 desorbing and reacting with NO_X is 13.1% lower than the NH_3 adsorbed on the new monolith and 28.0% lower than the NH_3 adsorbed on the used monolith. This result indicates that the NH_3 is being consumed through some other mechanism not quantifiable in this test, which is most likely NH_3 oxidation, although side reactions not involving a 1:1 stoichiometry of NO_X:NH_3 can also contribute to this discrepancy. This result also indicates that the used monolith is oxidizing NH_3 at a much higher rate than the new monolith, which will be further investigated later in this section.

The NO oxidation over the monoliths can be quantified by using the steady state performance data in stage 2. Table 4.3 shows the equilibrium concentration of NO and NO_2 at different temperatures. The used monolith performs less NO oxidation at all temperatures – from 52.1% less NO_2 at 250 °C to 64.9% less NO_2 at 400 °C. Since NO oxidation is the rate limiting step in SCR as discussed in chapter 1, this result suggests that the NO_X reduction performance should be lower on the used monolith compared to the new monolith. In addition, since NO oxidation occurs on the promoter metal, the lower NO oxidation on the used monolith implies that promoter metal deactivation has occurred.

Table 4.3: NO conversion performance of the new and used monoliths

Temperature	Monolith	NO Oxidation (Stage 2) Equilibrium Concentration (ppm) NO	NO_2
250 °C	New	461.1	44.9
	Used	477.4	21.5
	% Increase Over New	3.5	-52.1
300 °C	New	444.8	66.1
	Used	473.8	26.1
	% Increase Over New	6.1	-60.5
400 °C	New	422.8	75.0
	Used	462.7	48.7
	% Increase Over New	9.4	-64.9

Table 4.4 shows the stage 3 fast reaction results where both monoliths perform NO_X reduction of at least 93.6% at all temperatures with balanced performance reducing both NO and NO_2. This result corresponds well with the fast reaction data presented in Chapter 3, which reports at least 95.3% reduction in the same conditions. While their performance is similar, the used monolith has lower NO_X reduction performance than the new monolith at all temperatures tested ranging from 2.5% lower at 250 °C to 3.0% lower at 400 °C.

Table 4.4: NO_X reduction performance of the new and used monoliths

Temperature	Monolith	Fast Reaction (Stage 3) Equilibrium Concentration (ppm) NH_3	NO	NO_2	N_2O	Total NO_X	NH_3 Consumption (%)	NO_X Reduction (%)
250 °C	New	36.7	1.9	6.0	0.2	7.9	92.7	98.4
	Used	31.5	9.6	10.2	1.7	19.8	93.7	96.0
	% Increase Over New	-14.2	405.3	70.0	750.0	150.6	0.5	-2.4
300 °C	New	18.9	4.5	5.2	2.4	9.7	96.2	98.1
	Used	12.9	7.1	7.1	1.9	14.2	96.8	97.2
	% Increase Over New	-31.7	57.8	36.5	-20.8	46.4	0.6	-0.9
400 °C	New	9.9	9.5	8.1	2.8	17.6	98.0	96.5
	Used	3.2	14.3	17.5	1.9	31.8	99.4	93.6
	% Increase Over New	-67.7	50.5	116.0	-32.1	80.7	1.4	-3.0

Nitrous oxide production is low on both monoliths at all temperatures with no cases exceeding 3 ppm N_2O. Although the production of N_2O is greater on the used monolith compared to the new monolith at 250 °C, the trend reverses at 300 and 400 °C with the new monolith producing more N_2O than the used monolith, a counterintuitive result. This unexpected behavior is likely due to the NH_3 concentration. The used monolith consumes more NH_3 than the new monolith at all temperatures even though the NO_X reduction of the used monolith is always lower than that of the new monolith. This result implies that the used monolith is oxidizing more NH_3 than the new monolith. Because the reactions that produce N_2O are reliant on an NH_3 input, a lower NH_3 concentration should result in less N_2O produced. In this case, the effects of the lower NH_3 concentration appear to outweigh the used monolith's propensity to produce additional N_2O. From this result, it can be concluded that when designing a SCR system using these monoliths, it is important to control the NH_3 slip and not inject excess NH_3 to prevent it from being converted to N_2O.

While the NH_3 stored decreases by up to 42%, the decline in NO_X reduction performance is only at most 3%. A study has shown that the required NH_3 storage capacity for the fast reaction is only a fraction of the available capacity on the catalyst [50]. Based upon the NO_X reduction results, it is likely that the NH_3 storage capacity on the used monolith is more than enough for the fast reaction and the additional NH_3 storage capacity on the new monolith is not fully used.

4.3 Catalyst Characterization

Physical analysis of the "new" and "used" monolith samples was performed using X-Ray Diffraction (XRD), X-ray Photoelectron Spectroscopy (XPS), and Scanning Electron Microscopy (SEM) with Energy Dispersive X-ray Spectroscopy (EDS). The XPS and XRD samples were prepared by taking the front portion of the monolith and crushing it into a powder. Although XPS is a surface technique, the preparation method means that the XPS results represent the bulk composition of the catalyst and structural support.

XPS was performed using an aluminum Kα source. Sample charging was corrected by aligning the carbon 1s peak to 285 eV. Survey scans of the new and used catalyst monoliths, shown in Figure 4.3, show only minor differences between the samples.

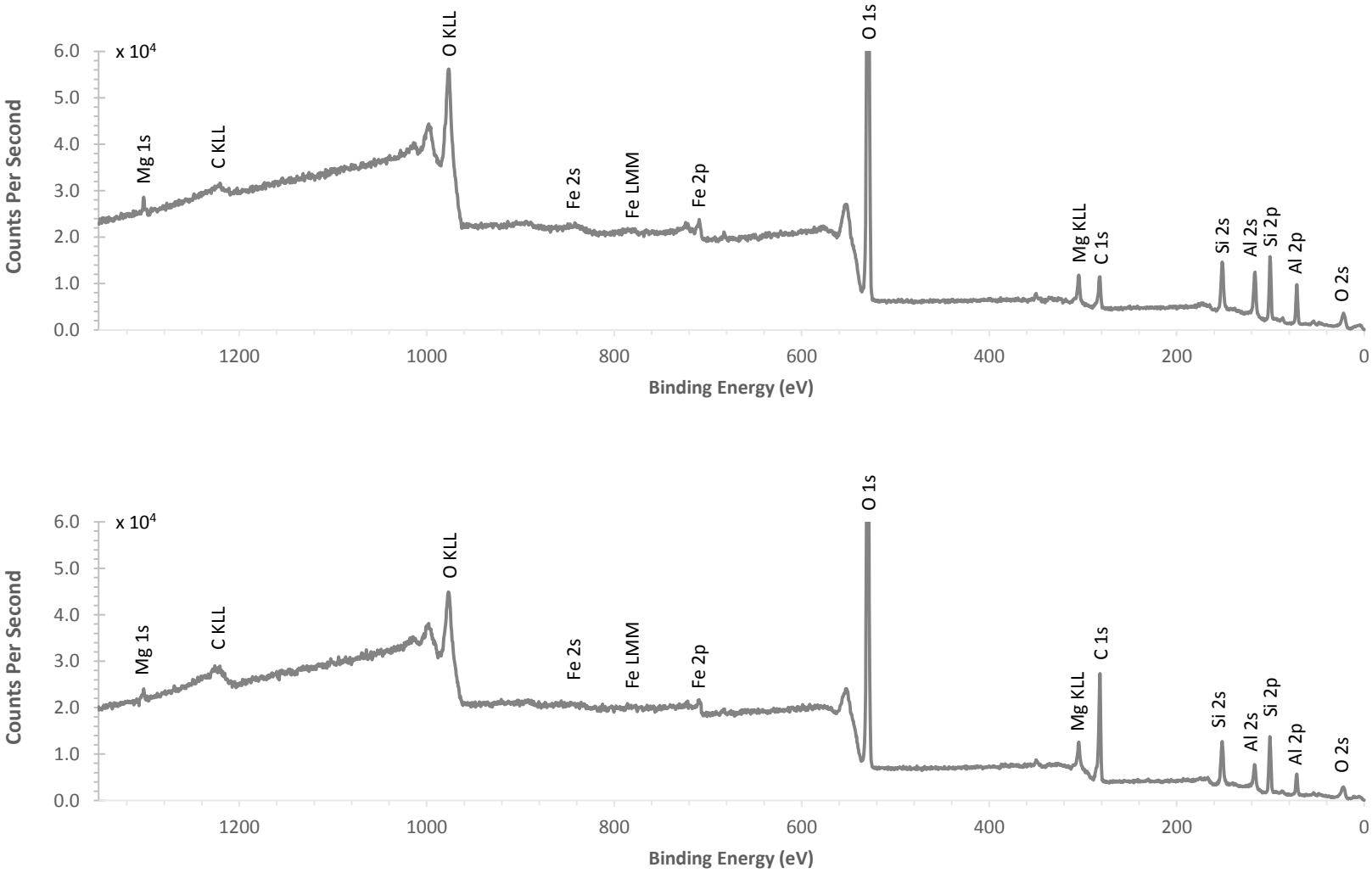

Figure 4.3: XPS spectra of the new monolith (top) and used monolith (bottom)

The data were analyzed for atomic composition using Casa XPS's reference library and sensitivity factors, and these results are presented in Table 4.5. Only six elements were detected – oxygen, aluminum, silicon, magnesium, carbon, and iron. In both samples carbon represents a significant portion of the sample composition. While there are studies of activated carbon as a catalyst support [123], a search reveals no evidence of commercial SCR catalysts containing carbon in either the catalyst or support making it likely that carbon is a not originally part of these monoliths.

Table 4.5: Atomic composition of the monoliths

Element	O	Si	Al	Mg	Fe	C
Peak Used for Analysis	1s	2s	2s	1s	2p	1s
New Monolith Atomic Concentration (%)	56.6	14.8	17.1	0.4	0.5	10.7
Used Monolith Atomic Concentration (%)	46.0	14.2	10.5	0.4	0.8	28.1

Other than being part of the original catalyst, carbon can become part of the sample in two ways. *Adventitious carbon* is a contaminant of samples caused by the catalyst's adsorption of carbon containing molecules from the atmosphere [124]. Carbon is also a component of diesel fuel, and as discussed earlier, can become coked on the catalysts. The SEM analysis is needed to confirm coking rather than sample contamination.

By excluding carbon, new atomic compositions can be obtained in Table 4.6. When excluding carbon, the composition of both monoliths is even more similar.

Table 4.6: Atomic composition of the monolith samples (excluding carbon)

Element	O	Si	Al	Mg	Fe
Peak Used for Analysis	1s	2s	2s	1s	2p
New Monolith Atomic Concentration (%) (excluding carbon)	63.4	16.6	19.1	0.4	0.6
Used Monolith Atomic Concentration (%) (excluding carbon)	64.0	19.7	14.6	0.6	1.1

Based upon the elemental composition and a comparison with literature studying SCR catalysts, conclusions can be made as to the class of catalyst. As stated in Chapter 1, the common catalysts used are alumina (Al_2O_3), titania (TiO_2), and zeolites. There is no evidence of titanium, ruling out titania as a support. There is presence of aluminum, but it is likely that the sample is not using alumina as a support. If the catalysts were using alumina as a support, then the large presence of silicon could not be explained. The large presence of silicon in addition to the aluminum supports the aluminum substituted zeolite.

The zeolites tested in literature are silicon with small substitutions of aluminum on the order of a few percent of the silicon composition [84, 90, 102, 105, 125]; however, the ratio of Al to Si obtained from XPS on the new and used catalysts is closer to 1:1. There is also a small amount of magnesium present, which is a component not found in any common SCR catalyst, which indicates that the structural support contains a large portion of aluminum as well as some magnesium and potentially the other metals.

The used monolith contains 4.5% less aluminum than the used monolith indicating dealumination as a cause of loss of catalyst activity. This result corresponds well with the NH_3 storage results, which showed reduced NH_3 storage at all temperatures on the used monolith. The XPS data also shows the presence of iron and of no other common active SCR metals such as copper or manganese, which strongly indicates that this catalyst's active metal ion is iron.

XRD analysis was performed on both samples using a Cu Kα X-ray source, and the results are presented in Figure 4.4. Comparing the XRD results to spectrums of common catalyst supports reveals cordierite, whose spectrum [126] is compared with the tested monoliths in Figure 4.4. The presence of cordierite is not unexpected as it is a very common support in environments that experience thermal cycling such as those used in automobiles. Cordierite has an extremely low coefficient of thermal expansion, which makes the catalyst coating resistant to cracking during thermal cycling [127, 128].

Cordierite's molecular formula is $(Mg,Fe)_2Al_3Si_5O_{18}$. The presence of cordierite can explain the presence of magnesium in the XPS data as well as the high Al:Si ratio.

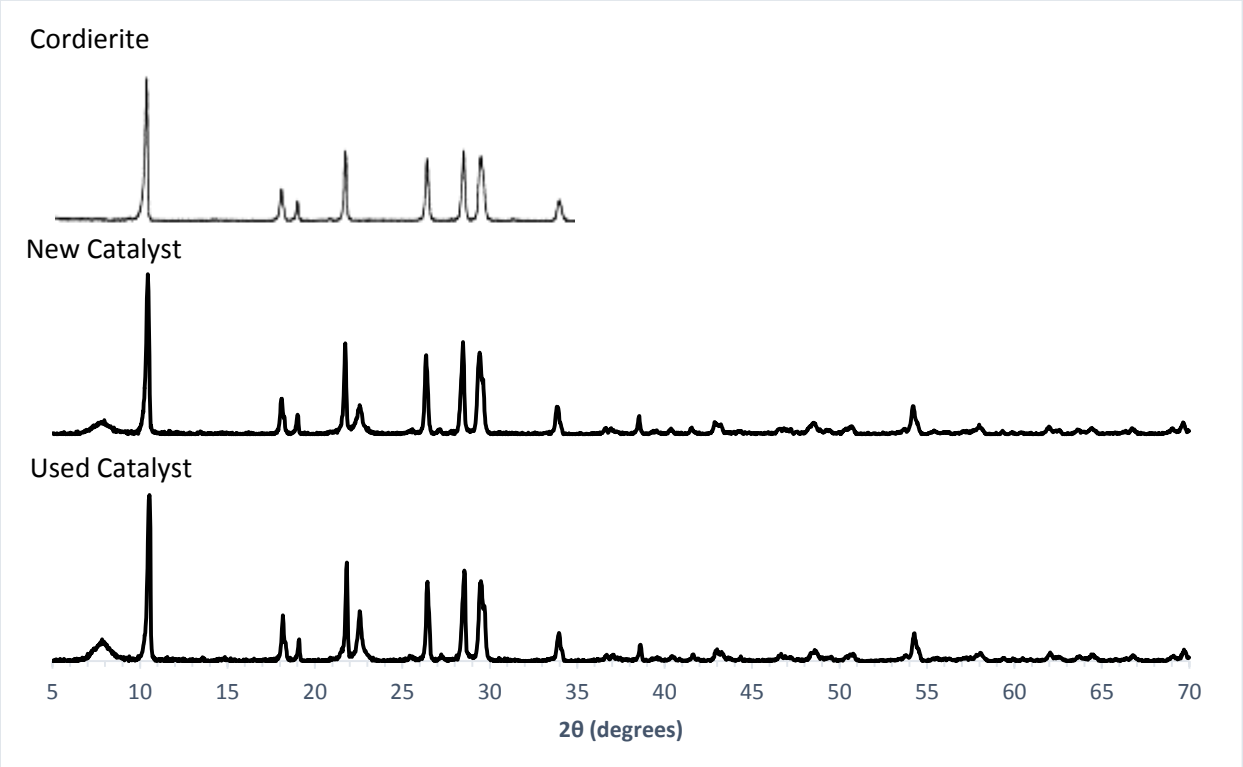

Figure 4.4: XRD Analysis of the monoliths. Cordierite data is from [126]

The similarity of the height and width of cordierite peaks between the new and used samples indicates that support has not changed during aging. The available cordierite data stretches to 35°, but it is likely that the higher angle data also represents the support; the high angle peaks' locations, heights, and widths do not change between the new and used monoliths, the same behavior as the lower angle cordierite peaks.

Below 35°, there are two peaks that cannot be attributed to cordierite, which are present at 8° and 22.5°. These two peaks likely are the zeolite catalyst itself. In contrast to the peaks of the cordierite, the 8° and 22.5° peaks become narrower and taller in the used monolith when compared to the new monolith. This result indicates that the catalyst's domains are growing as the catalyst ages.

In addition, the XRD data does not show any new peaks appearing on the used monolith sample. Iron oxide peaks would appear as a result of iron agglomerates on the surface of the catalyst coating as a side effect of promoter metal deactivation [129]; however, such peaks are not visible in the scan of the used monolith sample. If iron agglomeration is occurring, the iron particle size is not yet large enough to be detectable by XRD.

Scanning Electron Microscopy (SEM) was performed on the catalysts to image surface structure and was used in conjunction with Energy-Dispersive X-ray Spectroscopy (EDS) to analyze elemental composition. Unlike XPS, EDS is a bulk technique and gives more reliable bulk compositions of the samples.

Figure 4.5 shows images of the front faces of the new and used monoliths. The new monolith has some cracks in the surface coating, but its surface appears smooth. In comparison, the used monolith not only has surface cracks but appears to be missing coating in certain places revealing the jagged surface of the structural support. This lack of catalyst coating could indicate mechanical failure of the coating, but since the ends of these monoliths are also subject to mechanical wear from handling, this lack of coating could also be wear incurred during the extraction of the monolith core from the larger monolith during sample preparation. A second set of samples is studied later in this section to eliminate the possibility of wear from handling.

In Figure 4.5, a higher resolution scan is performed on the catalyst coatings of the front faces of both monoliths. Points within each micrograph (indicated in Figure 4.6) are selected for EDS analysis, which is presented in Table 4.7. At least three elemental analyses are taken from points on the flat surface and at least three elemental analyses from cracks in the surface in addition to the elemental analyses of other interesting features observed. The results show that the catalyst coating on the front faces of both the new and used have non-uniform compositions, which is potentially to be due to sample contamination. The catalyst coating on the new monolith's front face (points 1-4) ranges from

7.77 to 26.91% carbon, while no carbon should be expected on a new sample. In conflict with the XPS results, the catalyst coating on the used monolith's front face (points 8-10) shows less carbon than the new sample with only 6.95-8.51% carbon. The composition of the cracks of the new monolith's coating (point 5-7) does not deviate significantly from that of the rest of the surface (points 1-4) with a carbon concentration around 11% at all points; in contrast, the cracks in the used monolith's coating (points 8-10) do consistently have two to three times the carbon concentration of the rest of the surface (points 11-14).

Two large bright spots appear in the used monolith sample (points 15-17), which has the highest carbon concentration of all points scanned with up to 61.47% carbon. Similar features on other parts of either monolith could not be found, supporting that these objects in points 15-17 are contaminants and that the carbon is a result of sample contamination rather than coking.

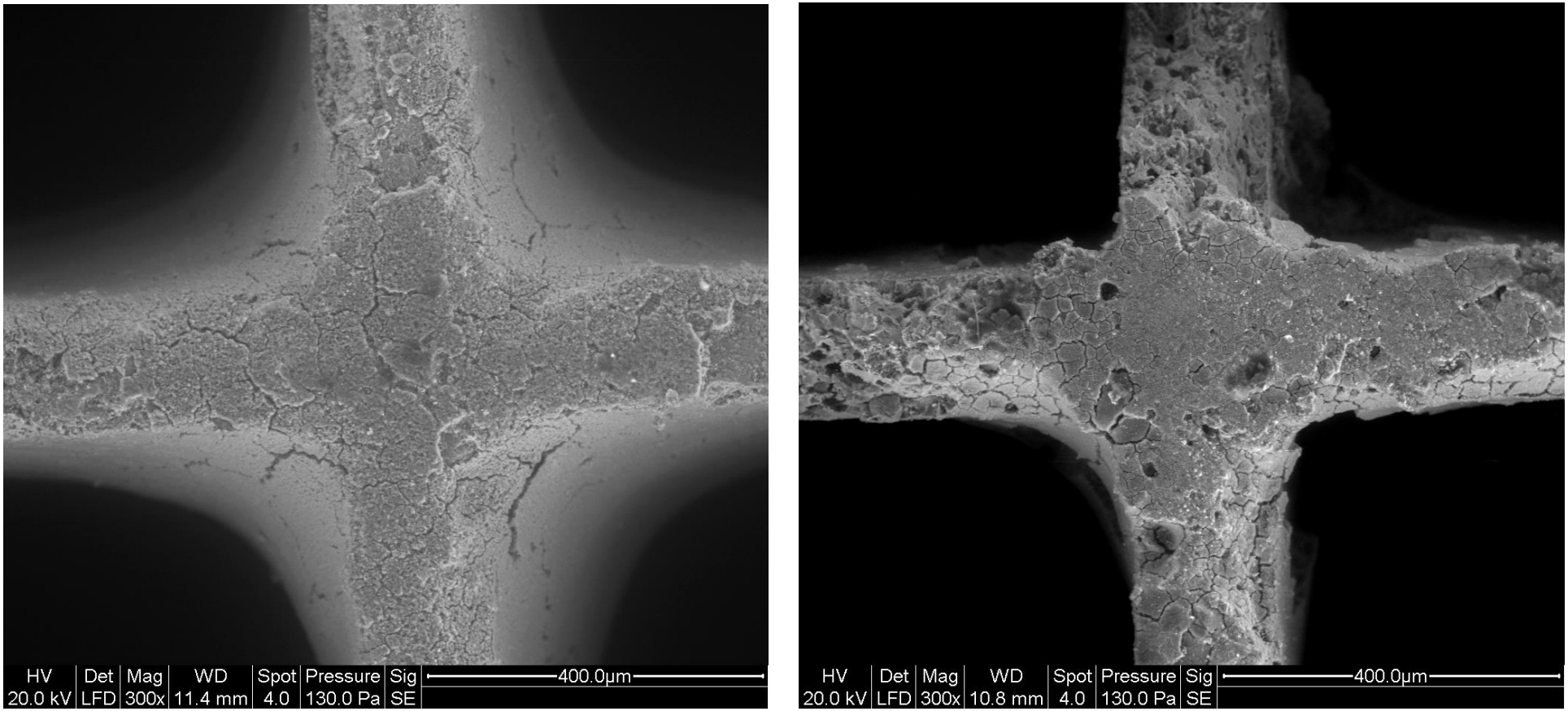

Figure 4.5: SEM images of the front faces of the new monolith (left) and the used monolith (right). The additional material that appears in the corners of the new monolith micrograph is part of the vertical surface and is a visual artifact. A different contrast and gamma setting is necessary in the used monolith micrograph, which enhances the image of the horizontal surface but in turn obscures the vertical surfaces.

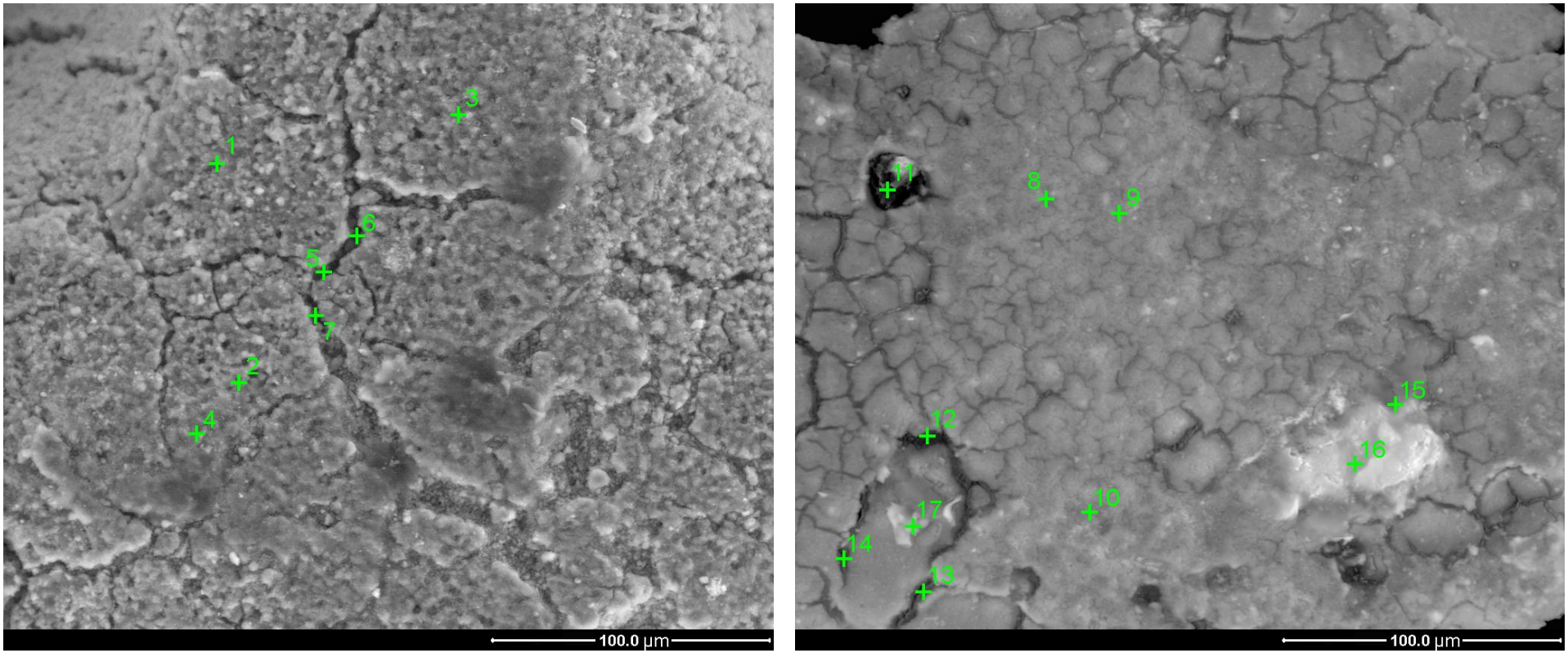

Figure 4.6: SEM images of the catalyst coating of the front faces of the new monolith (left) and the used monolith (right).
The green crosses are points probed for elemental composition using EDS (sample number indicated next to each point), the results of which are presented in Table 4.7.

Table 4.7: Elemental compositions of the selected sites from the front monolith faces

Site Number	Monolith Tested	Special Feature	Elemental Composition (Atomic %)							
			C	O	Mg	Al	Si	P	S	Fe
1	New		7.77	65.76	0.16	6.22	16.10	0.01	0.14	3.83
2	New		10.96	66.73	0.16	5.19	13.90	0.08	0.13	2.84
3	New		11.47	63.52	0.18	5.93	14.68	0.03	0.15	4.04
4	New		26.91	53.15	0.14	5.37	11.05	0.07	0.14	3.18
5	New	Crack	11.52	62.88	0.19	6.61	14.76	0.03	0.14	3.86
6	New	Crack	9.14	66.46	0.17	6.06	14.68	0.01	0.16	3.30
7	New	Crack	10.67	67.23	0.20	5.27	13.44	0.07	0.14	2.98
8	Used		8.51	62.03	3.33	7.86	16.18	0.15	0.50	1.44
9	Used		6.95	62.82	4.20	8.98	15.67	0.10	0.37	0.92
10	Used		7.89	62.61	4.22	8.91	15.16	0.09	0.29	0.84
11	Used	Crack	16.66	57.18	2.18	5.56	13.73	0.14	0.76	3.81
12	Used	Crack	21.37	54.73	1.66	4.87	13.46	0.15	0.71	3.05
13	Used	Crack	16.60	57.02	1.73	5.06	15.53	0.15	0.74	3.16
14	Used	Crack	15.31	57.97	1.46	4.82	16.42	0.14	0.74	3.14
15	Used	Bright spot	61.47	29.13	0.52	1.65	5.91	0.09	0.39	0.84
16	Used	Bright spot	58.98	30.95	0.92	2.52	5.75	0.05	0.23	0.60
17	Used	Bright spot	33.99	44.28	2.94	6.44	11.14	0.05	0.31	0.84

One consistent result is the difference in sulfur and phosphorous composition between the catalyst coatings of the new and used monoliths. The new monolith's coating (points 1-7) has an average sulfur concentration of 0.14% while the used monolith's coating (points 8-14, excluding the high carbon bright spot) has over quadruple the sulfur concentration with an average sulfur concentration of 0.59%. Similarly, the new monolith's coating (points 1-7) has an average phosphorous concentration of 0.04% while the used monolith's coating (points 8-14, excluding the high carbon bright spot) has over triple the phosphorous concentration with an average phosphorous concentration of 0.13%.

Since the ends of the monoliths have non-uniform compositions (particularly regarding carbon) and are likely contaminated, a micrograph of a section inaccessible to abrasion from handling and far away from the faces where contaminants could enter is needed to confirm whether or not the observed change in composition and lack of coating is related to aging. To exclude any potential effects of

improper handling in the past, interior surfaces of both the used and new catalysts are analyzed. The monoliths are cut parallel to their channels exposing the interiors of these channels. The micrographs presented in Figure 4.7 are interior channels of each monolith 0.25" from its respective front face. When looking at these images, keep in mind that the channels are in the shape of a "U", which results in distortion of the image since the left and right sides are closer to the detector than the middle. Therefore, the length scale presented in each micrograph is only calibrated to the center of the image.

While both monoliths have surface cracks, the new monolith exhibits only small, scattered cracks less than 400 μm in length while the used monolith exhibits a well formed network of cracks spanning the entire width of the channel. This evidence supports that the catalyst coating is mechanically wearing as the catalyst ages.

In Figure 4.8, a higher resolution scan is performed on the catalyst coatings of the channels of both monoliths. Using the same procedure as for the front faces, points within each micrograph (indicated in Figure 4.8) are selected for EDS analysis, which is presented in Table 4.8. Unlike the coatings of the faces of the monoliths, the coatings of the channels have uniform compositions for each monolith supporting that this sample is free from contamination. Like the used monolith's front face, the new monolith's channel has a bright particle (point 26). However, unlike the bright spots on the used monolith's front face, the bright spot on the used monolith's channel has a similar composition to the rest of the channel's surface indicating this is not a sample contaminant. This uniform composition and lack of contamination supports that the EDS results obtained in the channels should be representative of the catalyst coatings of the entire monoliths.

.

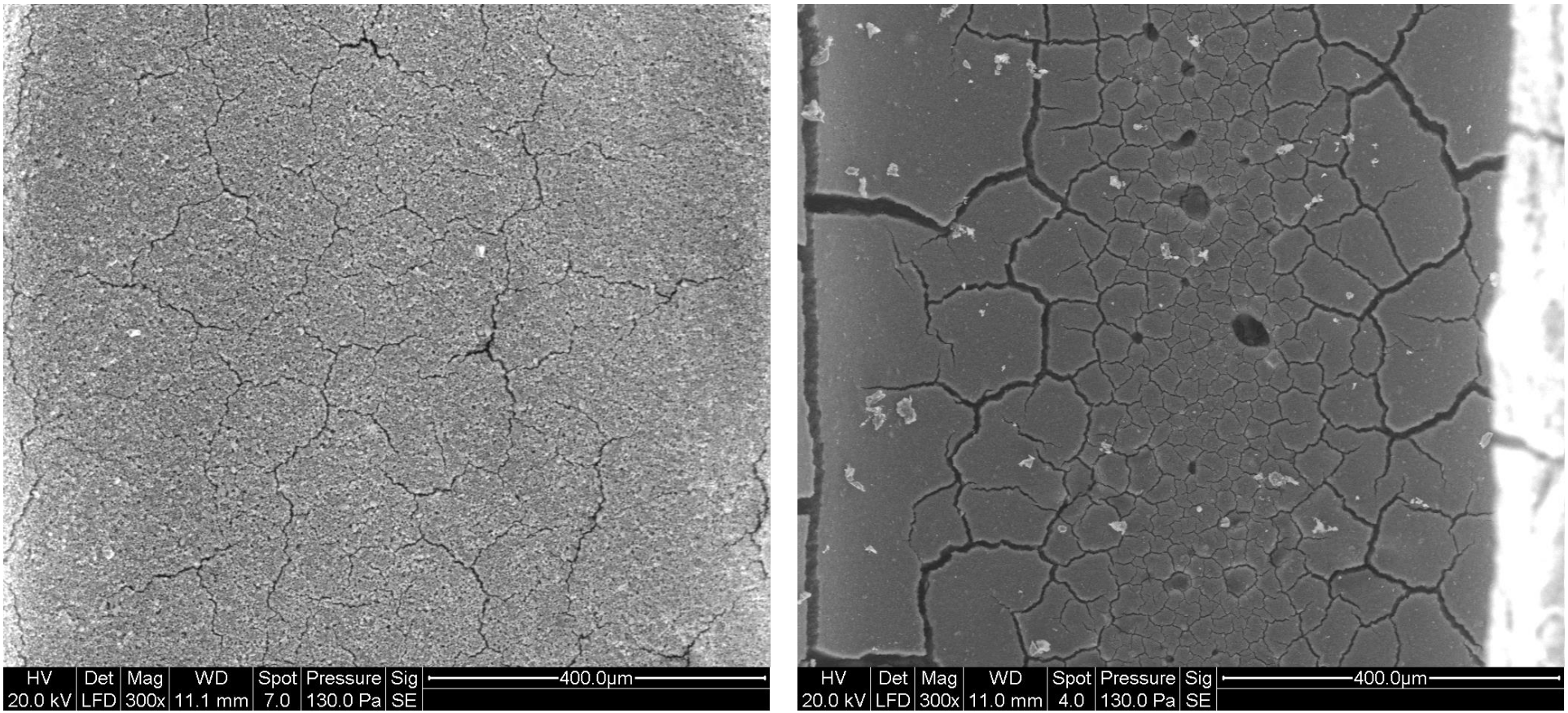

Figure 4.7: SEM images of channels within the new monolith (left) and the used monolith (right). Keep in mind that the channels are in the shape of a "U", which results in distortion of the image since the left and right sides are closer to the image sensor than the middle. Therefore, the length scale presented in each micrograph is only calibrated to the center of the image.

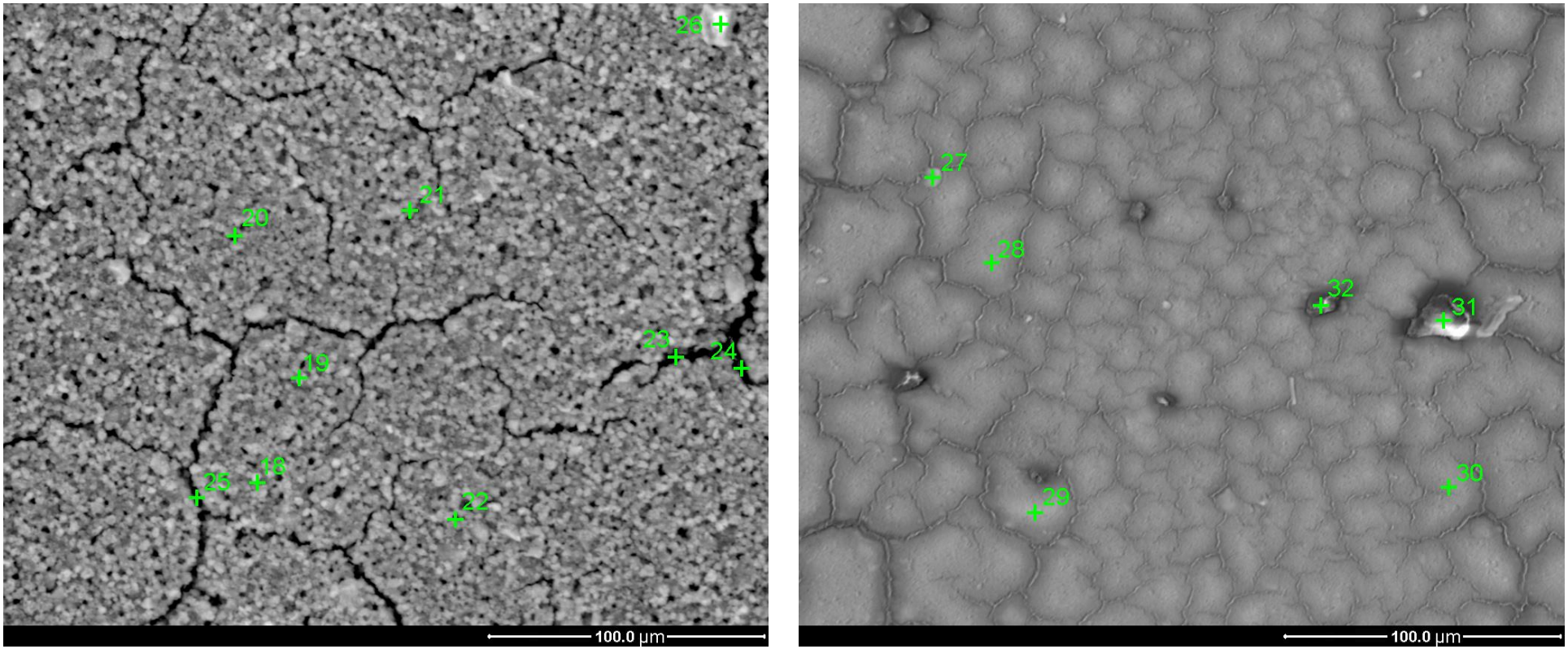

Figure 4.8: SEM images of the catalyst coating of the channels within the new monolith (left) and the new monolith (right).
The green crosses are points probed for elemental composition using EDS (sample number indicated next to each point), the results of which are presented in Table 4.8

Table 4.8: Elemental compositions of the selected sites from the monolith channels

Site Number	Monolith Tested	Special Feature	Elemental Composition (Atomic %)							
			C	O	Mg	Al	Si	P	S	Fe
18	New		3.01	68.21	0.38	6.16	17.23	0.03	0.00	4.98
19	New		3.17	68.53	0.43	6.16	17.04	0.03	0.01	4.63
20	New		3.09	67.80	0.38	6.25	17.56	0.03	0.01	4.88
21	New		3.52	69.06	0.49	6.23	16.94	0.03	0.00	3.75
22	New		3.39	70.30	0.52	6.11	16.97	0.03	0.00	2.68
23	New	Crack	3.48	70.51	0.68	6.24	16.85	0.03	0.01	2.21
24	New	Crack	3.42	70.71	0.73	6.28	16.78	0.05	0.01	2.03
25	New	Crack	3.01	67.70	0.34	6.24	17.89	0.04	0.00	4.77
26	New	Bright spot	3.43	70.72	0.68	6.30	16.78	0.04	0.00	2.05
27	Used		2.50	67.22	0.70	6.13	20.86	0.05	0.43	2.11
28	Used		2.80	67.34	2.56	7.71	18.53	0.05	0.30	0.71
29	Used		2.42	67.88	0.38	5.52	22.16	0.05	0.45	1.13
30	Used		2.47	68.31	0.35	4.61	22.56	0.07	0.44	1.19
31	Used	Crack	2.36	67.33	0.80	6.27	20.88	0.06	0.43	1.88
32	Used	Crack	2.08	67.08	0.39	5.67	22.97	0.06	0.50	1.25

With an average of 3.28% carbon, the carbon concentration in the new monolith's catalyst coating (points 18-26) is on average 0.84% higher than the used monolith's catalyst coating (points 27-32). The uniformity of the samples tested combined with the low carbon concentration provides strong evidence that the carbon present on the monoliths is adventitious carbon and not coking. The higher concentration on the new catalyst is likely due to the history of the sample. The used monolith had in the past been heated to 500 °C to purge NH_3, which as referenced earlier is also hot enough to burn off carbon coking. In contrast, the new monolith had never been heated in a furnace prior to taking the EDS samples (to ensure that the heating would not degrade the sample), so it is reasonable to expect that the new, unheated sample would have extra carbon contamination. By excluding carbon, new elemental compositions are calculated in Table 4.9.

Table 4.9: Elemental compositions of the selected sites from the monolith channels excluding carbon

Site Number	Monolith Tested	Special Feature	Elemental Composition (Atomic %) (Excluding Carbon)						
			O	Mg	Al	Si	P	S	Fe
18	New		70.33	0.39	6.35	17.76	0.03	0.00	5.13
19	New		70.77	0.44	6.36	17.60	0.03	0.01	4.78
20	New		69.96	0.39	6.45	18.12	0.03	0.01	5.04
21	New		71.58	0.51	6.46	17.56	0.03	0.00	3.89
22	New		72.77	0.54	6.32	17.57	0.03	0.00	2.77
23	New	Crack	73.05	0.70	6.46	17.46	0.03	0.01	2.29
24	New	Crack	73.21	0.76	6.50	17.37	0.05	0.01	2.10
25	New	Crack	69.80	0.35	6.43	18.45	0.04	0.00	4.92
26	New	Bright spot	73.23	0.70	6.52	17.38	0.04	0.00	2.12
27	Used		68.94	0.72	6.29	21.39	0.05	0.44	2.16
28	Used		69.28	2.63	7.93	19.06	0.05	0.31	0.73
29	Used		69.56	0.39	5.66	22.71	0.05	0.46	1.16
30	Used		70.04	0.36	4.73	23.13	0.07	0.45	1.22
31	Used	Chipped	68.96	0.82	6.42	21.38	0.06	0.44	1.93
32	Used	Chipped	68.50	0.40	5.79	23.46	0.06	0.51	1.28

The previously noted trend in the sulfur and phosphorous composition increasing in the used monolith's coating becomes even more noticeable in the interior channels. Excluding carbon, the new monolith's catalyst coating (points 18-26) has a negligible sulfur concentration below 0.01% while the used monolith's catalyst coating's (points 27-32) has a significant average sulfur concentration of 0.44%. Following the same trend, excluding carbon, the new monolith's catalyst coating (points 18-26) has an average phosphorous concentration of 0.03% while the used monolith's catalyst coating (points 27-32) has double the phosphorous with an average phosphorous concentration of 0.06%.

While the XPS data did not detect sulfur and phosphorous, the lack of detection was likely caused by the low detection sensitivity of the XPS technique. It has been previously reported that iron-zeolite catalysts are more resistant to sulfur poisoning than copper-zeolite catalysts [80, 119]; however, zeolite catalysts have been shown to be susceptible to phosphorous poisoning resulting in a decrease in NO_X reduction [120]. Based upon this evidence of sulfur and phosphorous, it is likely that the catalyst is

suffering from poisoning, although based upon the SCR performance results, the resulting reduction performance is not significant enough to be noticeable in real world scenarios.

Another consistent trend among all the points analyzed is the reduction in iron content in the used monolith's catalyst coating. The new monolith's catalyst coating has an average iron concentration of 3.67% (excluding carbon) while the used monolith's catalyst coating has 62% less iron with an average iron concentration of 1.41% (excluding carbon). Previous studies have indicated that a large amount of iron, usually at least 2.5% Fe (although the exact amount is debated [130, 131]), is needed for maximum catalyst activity, and loss of iron is responsible for decreased catalyst activity. With only half the optimal iron content, research shows NO_X conversion rates over 50% lower at 300 °C [132]. While the used monolith did not have appreciably lower NO_X reduction performance than the new monolith, it did have lower NO oxidation capability compared to the new monolith, which was probably caused by the lack of iron.

While dealumination was indicated by lower NH_3 storage capacity of the used monolith and the 4.5% lack of aluminum in the XPS scan of the used monolith, the EDS results show a much smaller difference of 0.30% less aluminum in the used monolith's catalyst coating compared to new. However, the EDS results do indicate a large variation in aluminum concentration across the used monolith's catalyst coating especially when compared to the new monolith's catalyst coating. In the new monolith's catalyst coating, the highest aluminum concentration over the nine points sampled is only 3.16% greater than the lowest aluminum concentration. In the used monolith's catalyst coating, the highest aluminum concentration over the six points sampled is 79.01% greater than the lowest aluminum concentration. The results indicate that dealumination is occurring but the aluminum is not being removed from the monolith. The aluminum atoms are being removed from the zeolite structure and deposited elsewhere on the catalyst in an inactive state rather than being completely removed from the monolith.

4.4 Catalyst Deactivation Mechanisms

SCR performance data indicates that both the new and used monoliths perform comparably in NO_X reduction to the monolith in section 3. The main differences are that unlike the new monolith, the used monolith is oxidizing the NH_3 slip. The lack of change in NO_X reduction performance is likely due to the new monolith being overdesigned for the real-world SCR application. Because the monolith must maintain its NO_X performance over a long time period, excess catalyst is applied so that even after years of degradation there is still enough catalytic material to meet environmental regulations for NO_X reduction. If the experimental program deviated from real world conditions by increasing the NO_X load, it is likely that a large difference in SCR performance between the two monoliths would emerge.

Of the five deactivation mechanisms cited – dealumination, promoter metal deactivation, mechanical failure, coking, and catalyst poisoning – all except coking have evidence supporting their presence. Evidence of dealumination includes the 25% lower NH_3 storage capacity of the used monolith, XPS and EDS data showing lower aluminum concentration in the used samples, and the EDS data showing increased variation of aluminum concentration across the catalyst coating of the used monolith. Evidence of promoter metal deactivation includes the lower NO oxidation capability of the used monolith compared to the new monolith at all temperatures and EDS results showing 62% less of the promoter metal iron on the used monolith's catalyst coating compared to the new monolith's catalyst coating. Mechanical failure is evidenced by the SEM images of the high level of cracking of the used monolith's catalyst coating and mechanical abrasion of the front face of the used monolith, and catalyst poisoning is evidenced with the 0.50% sulfur concentration of the new monolith's catalyst coating (compared to 0.01% of the new sample) and doubling of the phosphorous concentration of the used sample compared to new. Catalyst coking is not supported as a cause of deactivation since the excess carbon observed in the XPS samples and the EDS samples of the catalyst faces is not present

throughout the catalyst coating; the interior surfaces less prone to sample contamination show low carbon concentrations (3%) consistent with adventitious carbon.

Chapter 5

Conclusions and Future Work

This study set out to analyze the selective catalytic reduction (SCR) reactions and deactivation mechanisms on zeolite catalysts. The project aimed to achieve three goals: 1) to quantify the NO_X reduction performance of a SCR catalyst coated monolith and correlate performance at different temperatures and NO:NO_2 ratios to the reactions occurring on the catalyst, 2) to study the important SCR reactions, significant side reactions, and NH_3 adsorption, and 3) to study the catalyst deactivation mechanisms and their effects on SCR performance.

5.1 Observations on Experimental Design

The construction of a testing apparatus to analyze catalyst performance in real time was successful. Key findings include:

1. At low water flow rates, stable steam generation cannot be achieved through boiling of pools of water. Achieving a stable supply of steam at these low flow rates is primarily dependent on breaking the surface tension of liquid water. Generation of a water mist along with a high carrier gas flow rate is necessary to achieve a stable supply of steam.
2. Fourier-transformed infrared spectroscopy can be used to quantify the concentrations of pollutant gases. The resolution of the infrared spectrometer must be 0.5 cm^{-1} or better to allow the separation of the spectra of water and NO. In addition, sending only a portion of the gas stream to the spectrometer reduces the experimental error in the infrared spectra collected while not reducing validity of the data.

5.2 Observations on SCR Reactions

Testing of a zeolite catalyst monolith to investigate the SCR reactions shows that:

1. Side reactions cannot be ignored when designing a SCR system. When supplied with 1:1 and 1:3 ratios of NO:NO_2 at 250 °C, the catalyst monolith reduced more NO_X than NH_3 suggesting that part of the NO_X reduction was proceeding through an ammonium nitrate intermediate and generating nitric acid. When provided a low ratio of NO:NO_2, the catalyst monolith generates high levels of nitrous oxide at intermediate temperature.
2. Transient catalyst effects must be considered when designing a SCR system that is intended to operate in continuously variable conditions. A transient drop in catalyst performance was observed at all temperatures upon NH_3 injection in the presence of NO but not NO_2, which is believed to be related to an inhibition effect of NH_3 previously reported in literature. A different transient behavior believed to be due to the formation of ammonium nitrate is also observed only at low temperature when NH_3 is turned on in the presence of NO_2.

5.3 Observations on Catalyst Deactivation

The comparison of two catalyst monoliths reached the following conclusions:

1. SCR testing reports that the used catalyst monolith exhibited similar NO_X reduction performance (less than 3% difference) compared to the new catalyst monolith at all reaction conditions. However, the used catalyst monolith showed lower NO oxidation and NH_3 stored at all temperatures compared to the new catalyst monolith with at least 50% less NO_2 being generated and at least 25% less NH_3 being stored.
2. X-ray Photoelectron Spectroscopy (XPS), X-Ray Diffraction (XRD), and Scanning Electron Microscopy (SEM) with Energy Dispersive X-ray Spectroscopy (EDS) analysis of the samples

indicate that dealumination of the catalyst is the main catalyst aging mechanism of the used catalyst monolith. Promoter metal deactivation, poisoning by sulfur and phosphorous, and mechanical failure of the catalyst coating also contribute to aging effects. Carbon coking does not appear on the catalyst monoliths tested.

3. The similar NO_X reduction performance of the two catalyst monoliths despite all the evidence of catalyst aging on the used catalyst monolith suggests that the catalyst monoliths were overdesigned for its intended feed conditions. However, the 1.41% average iron concentration on the used monolith's catalyst coating, 62% lower than the new monolith's catalyst coating and lower than the 2.5% recommended by previous studies, suggests that the used monolith is at end of life.

5.4 Suggestions for Future Work

Future work can improve the usability of the testing apparatus, elucidate catalyst reactions, and provide additional insight on the correlation between catalyst structure and deactivation mechanisms. Some suggestions include:

1. The catalyst testing apparatus should be refined by programming software to simplify the user interface and reduce the number of variables that need to be entered to perform an experiment. In addition, the current temperature control system should be upgraded with one that is centrally controlled by a computer enabling automation of the temperature control system.
2. The transient behavior of the catalyst at 250 °C when NH_3 is tuned on with both NO and NO_2 present should be investigated. This behavior is not adequately explained in the literature,

and experimentation into the conditions that cause the phenomenon can provide insight into the reactions occurring on the catalyst.

3. Additional physical characterization studies should be performed on the new and used catalysts to further elucidate the chemistry of the deactivation mechanisms. A study of iron through a fine XPS scan at the Fe 2p region as well as X-ray Absorbance Near Edge Structure (XANES) experiments would provide insight into the state of the iron atoms on the catalyst. In addition, nuclear magnetic resonance (NMR) could probe the state of dealumination that was indicated by the XPS and EDS scans.

References

[1] M. Jianzhong, X. Xiaobin, Z. Chunsheng and Y. Peng, "A Review of Atmospheric Chemistry Research in China: Photochemical Smog, Haze Pollution, and Gas-Aerosol Interactions," *Advances in Atmospheric Sciences,* vol. 29, no. 5, pp. 1006-1025, 2012.

[2] M. Greenstone, "The Impacts of Environmental Regulations on Industrial Activity: Evidence from the 1970 and 1977 Clean Air Act Amendments and the Census of Manufactures.," *Journal of Political Economy,* vol. 110, no. 6, pp. 1175-1219, 2002.

[3] A. Lloyd and T. Cackette, "Diesel Engines: Environmental Impact and Control," *Journal of the Air & Waste Management Association,* vol. 51, no. 6, pp. 809-847, 2001.

[4] A. Walker, "Controlling Particulate Emissions from Diesel Vehicles," *Topics in Catalysis,* vol. 28, no. 1-4, pp. 165-170, 2004.

[5] L. Schipper, "Automobile Use, Fuel Economy, and CO2 Emissions in Industrialized Countries: Encouraging Trends Through 2008?".

[6] U.S. Energy Information Administration, "Annual Energy Outlook 2013," Washington D.C., 2013.

[7] ExxonMobil, "The Outlook for Energy: A View to 2040," 2013.

[8] International Energy Agency, "World Energy Outlook 2012," 2012.

[9] R. Sawyer, R. Harley, S. Cadle, J. Norbeck, ,. R. Slott and H. Bravo, "Mobile Sources Critical Review: 1998 NARSTO Assessment," *Atmospheric Environment,* vol. 34, no. 12-14, pp. 2161-2181, 2000.

[10] J. Calvert, J. Heywood, R. Sawyer and J. Seinfeld, "Achieving Acceptable Air Quality: Some Reflections on Controlling Vehicle Emissions," *Science,* vol. 261, no. 5117, pp. 37-45, 1993.

[11] H. L. MacLean and L. B. Lave, "Evaluating Automobile Fuel/Propulsion System Technologies," *Progress in Energy and Combustion Science,* vol. 29, no. 1, pp. 1-69, 2003.

[12] X. Qin, L. Chen, F. Sun and C. Wu, "The Universal Power and Efficiency Characteristics for Irreversible Reciprocating Heat Engine Cycles," *European Journal of Physics,* vol. 24, no. 4, pp. 359-366, 2003.

[13] J. E. Dec, "Advanced Compression Ignition Engines - Understanding the In-Cylinder Processes," *Proceedings of the Combustion Institute,* vol. 32, no. 2, pp. 2727-2742, 2009.

[14] X. Zhen, Y. Wang, X. Shuaiqing, Y. Zhu, C. Tao, T. Xu and M. Song, "The Engine Knock Analysis - An Overview," *Applied Energy,* pp. 628-636, 2012.

[15] Y. Shiao and L. Dat, "Efficiency Improvement for an Unthrottled SI Engine at Part Load," *International Journal of Automotive Technology,* vol. 13, no. 6, pp. 885-893, 2012.

[16] M. V. Twigg, "Progress and Future Challenges in Controlling Automotive Exhaust Gas Emissions," *Applied Catalysis B: Environmental,* no. 70, pp. 2-15, 2007.

[17] X. Lu, D. Han and Z. Huang, "Fuel Design and Management for the Control of Advanced Compression-Ignition Combustion Engines," *Progress in Energy and Combustion Science,* vol. 37, no. 6, pp. 741-783, 2011.

[18] C. Arciumanis, C. Bae, R. Crookes and E. Kinoshita, "The Potential of Di-Methyl Ether (DME) as an Alternative Fuel for Compression-Ignition Engines: A Review," *Fuel,* vol. 87, no. 7, pp. 1014-1030, 2008.

[19] M. Yaho, Z. Zheng and H. Liu, "Progress and Recent Trends in Homogeneous Charge Compression Ignition (HCCI) Engines," *Progress in Energy and Combustion Science,* vol. 35, no. 5, pp. 398-437, 2009.

[20] M. Yao, Z. Zheng and H. Liu, "Progress and Recent Trends in Homogeneous Charge Compression Ignition (HCCI) Engines," *Progress in Energy and Combustion Science,* vol. 35, no. 5, pp. 398-437, 2009.

[21] L. Prockop and R. Chichkova, "Carbon Monoxide Intoxication: An Updated Review," *Journal of the Neurological Sciences,* vol. 262, no. 1-2, pp. 122-130, 2007.

[22] S. T. Omaye, "Metabolic Modulation of Carbon Monoxide Toxicity," *Toxicology,* vol. 180, no. 2, pp. 139-150, 2002.

[23] M. E. Jenkin, S. M. Saunders and M. J. Pilling, "The Tropospheric Degredation of Volatile Organic Compounds: A Protocol for Mechanism Development," *Atmospheric Environment,* vol. 31, no. 1, pp. 81-104, 1996.

[24] E. S. Wright, D. Dziedzic and C. S. Wheeler, "Cellular, Biochemical and Functional Effects of Ozone: New Research and Perspectives on Ozone Health Effects," *Toxicology Letters,* vol. 51, pp. 125-145, 1990.

[25] A. Sydbom, A. Blomberg, S. Parnia, N. Stenfors, T. Sandstron and S.-E. Dahlen, "Health Effects of Diesel Exhaust Emissions," *European Respiratory Journal,* vol. 17, pp. 733-746, 2001.

[26] J. P.A. Neeft, M. Makkee and J. A. Moulijn, "Diesel Particulate Emissions Control," *Fuel Processing Technology,* vol. 47, pp. 1-69, 1996.

[27] O. I. Smith, "Fundamentals of Soot Formation in Flames with Application to Diesel Engine Particulate Emissions," *Progress in Energy and Combustion Science,* vol. 7, no. 4, pp. 275-291, 1981.

[28] B. Brunekreef, "Air Pollution and Health," *Lancet,* vol. 362, no. 9341, pp. 1233-1242, 2002.

[29] M. Gomez-Garcia, V. Pitchon and A. Kiennemann, "Pollution by Nitrogen Oxides: An Approach to NOx Abatement by Using Sorbing Catalytic Materials," *Environment International,* vol. 31, no. 3, pp. 445-467, 2004.

[30] D. H. Ehhalt and J. W. Drummond, "The Tropospheric Cycle of NOx," in *Chemistry of the Polluted and Unpolluted Troposphere*, Springer Netherlands, 1982, pp. 219-251.

[31] R. Atkinson, "Atmospheric Chemistry of VOCs and NOx," *Atmospheric Environment,* vol. 34, no. 12-24, pp. 2063-2101, 2000.

[32] J. A. Camagro and A. Alonso, "Ecological and Toxicological Effects of Inorganic Nitrogen Pollution in Aquatic Ecosystems: A Global Assessment," *Environment International,* vol. 32, no. 6, pp. 831-849, 2006.

[33] E. Franzoni and E. Sassoni, "Correlation Between Microstructural Characteristics and Weight Loss of Natural Stones Exposed to Simulated Acid Rain," *Science of the Total Environment,* vol. 412, pp. 278-285, 2011.

[34] S. Hill and L. D. Smoot, "Modeling of Nitrogen Oxides Formation and Destruction in Combustion Systems," *Progress in Energy and Combustion Science,* vol. 26, pp. 417-458, 2000.

[35] L.-Y. Jiang and I. Campbell, "A Critical Evaluation of NOx Modeling in a Model Combustor," *Journal of Engineering for Gas Turbines and Power,* vol. 127, no. 3, pp. 483-491, 2005.

[36] P. Glarborg, A. Jensen and J. Johnsson, "Fuel Nitrogen Conversion in Solid Fuel Fired Systems," *Progress in Energy and Combustion Science,* vol. 29, no. 2, pp. 89-113, 2003.

[37] M. Galbati, A. Cavigiolo, A. Effuggi, D. Gelosa and R. Rota, "Mild Combustion for Fuel-NOx Reduction," *Combustion Science and Technology,* vol. 176, no. 7, pp. 1035-1054, 2004.

[38] J. Miler, "Theory and Modeling in Combustion Chemistry," in *Twenty-Sixth Symposium (International) on Combustion, Vols. 1 and 2*, Naples, Italy, 1996.

[39] A. Williams, P. M, J. Jones and L. Rowlands, "A Review of NOx Formation and Reduction Mechanisms in Combustion Systems, with Particular Reference to Coal," *Journal of the Institute of Energy,* vol. 70, no. 484, pp. 102-113, 1997.

[40] U.S. Environmental Protection Agency, "2013 Revisions to the Greenhouse Gas Reporting Rule and Final Confidentiality: Determinations for New or Substantially Revised Data Elements," Washington, D.C., 2013.

[41] J. Kim, X. Ma, A. Zhou and C. Song, "Ultra-Deep Desulfurization and Denitrogenation of Diesel Fuel by Selective Adsorption over Three Different Adsorbents: A Study on Adsorptive Selectivity and Mechanism," *Catalysis Today,* vol. 111, no. 1-2, pp. 74-83, 2006.

[42] S. J. Smith, "Global and Regional Anthropogenic Sulfur Dioxide Emissions," *Global and Planetary Change,* vol. 29, no. 1-2, pp. 99-119, 2001.

[43] A. Stanislaus, A. Marafi and M. S. Rana, "Recent Advances in the Science and Technology of Ultra Low Sulfur Diesel (ULSD) Production," *Catalysis Today,* vol. 153, no. 1-2, pp. 1-68, 2010.

[44] B. CH, "Mechanisms of Catalyst Deactivation," *Applied Catalysis A: General,* vol. 212, no. 1-2, pp. 17-60, 2001.

[45] L. Muzio and G. Quartuxy, "Implementing NOX control: Research to Application," *Progress in Energy and Combstion Science,* vol. 23, pp. 233-266, 1996.

[46] T. Johnson, "Diesel Engine Emissions and Their Control: An Overview," *Platinum Metals Review,* vol. 52, no. 1, pp. 23-37, 2008.

[47] J. E. McCarthy, "Clean Air Act: A Summary of the Act and Its Major Requirements," 9 May 2005. [Online]. Available: http://fpc.state.gov/documents/organization/47810.pdf. [Accessed 5 June 2014].

[48] United States Environmental Protection Agency, "Heavy-Duty Highway Compression-Ignition Engines And Urban Buses -- Exhaust Emission Standards," [Online]. Available: http://www.epa.gov/otaq/standards/heavy-duty/hdci-exhaust.htm. [Accessed 10 04 2014].

[49] V. Vestreng, L. Ntziachristos, A. Semb, S. Reis and I. Isaksen, "Evolution of NOx Emissions in Europe with Focus on Road Transport Control Measure," *Atmospheric Chemistry and Physics,* vol. 9, no. 4, pp. 1503-1520, 2009.

[50] K. Kamasamudram, N. W. Currier, X. Chen and A. Yezerets, "Overview of the Practically Important Behaviors of Zeolite-Based Urea-SCR Catalysts, Using Compact Experimental Protocol," *Catalysis Today,* vol. 151, no. 3-4, pp. 212-222, 2010.

[51] S. Bennett, Modern Diesel Technology: Diesel Engines, Clifton Park, New York: Cengage Learning, 2010.

[52] J. Kaspar, P. Fornasiero and N. Hickey, "Automotive Catalytic Converters: Current Status and Some Perspectives," *Catalysis Today,* vol. 77, no. 4, pp. 419-449, 2003.

[53] V. Papadakis, C. Pliangos, I. Yentekakis, X. Verykios and C. Vayenas, "Development of High Performance, Pd-Based, Three Way Catalysts," *Catalysis Today,* vol. 29, no. 1-4, pp. 71-75, 1996.

[54] D. R. Tree and K. I. Svensson, "Soot Processes in Compression Ignition Engines," *Progress in Energy and Combustion Science,* vol. 33, no. 3, pp. 272-309, 2007.

[55] J. Neeft, M. Makkee and J. Moulijn, "Catalysts for the Oxidation of Soot from Diesel Exhaust Gases .1. An Exploratory Study," *Applied Catalysis B: Environmental,* vol. 8, no. 1, pp. 57-78, 1996.

[56] B. Van Setten, M. Makkee and J. Moulijn, "Science and Technology of Catalytic Diesel Particulate Filters," *Catalysis Reviews - Science and Engineering,* vol. 43, no. 4, pp. 489-564, 2001.

[57] K. Skalska, J. S. Miller and S. Ledakowicz, "Trends in NOX abatement: A review," *Science of the Total Environment,* pp. 3976-3989, 2010.

[58] M. Zheng, G. T. Reader and J. G. Hawley, "Diesel Engine Exhaust Gas Recirculation-A Review on Advanced and Novel Concepts," *Energy Conversion and Management,* vol. 45, pp. 883-900, 2004.

[59] G. Abd-Alla, "Using Exhaust Gas Recirculation in Internal Combustion Engines: A Review," *Energy Conversion and Management,* vol. 43, no. 8, pp. 1027-1042, 2002.

[60] M. Marciq, "Diesel Engine Exhaust Gas Recirculation - A Review on Advanced and Novel Concepts," *Energy Conversion and Management,* vol. 45, no. 6, pp. 883-900, 2004.

[61] R. Heck, "Catalytic Abatement of Nitrogen Oxides - Stationary Applications," *Catalysis Today,* vol. 53, no. 4, pp. 519-523, 1999.

[62] T. Rhoads, J. Marks and P. Siebert, "Overview of Industrial Source Control for Nitrogen Oxides," *Environmental Progress,* vol. 9, pp. 126-130, 2006.

[63] M. Buzanowski and R. Yang, "Simple Design of Monolith Reactor for Selective Catalytic Reduction of NO for Power Plant Emissions Control," *Industrial & Engineering Chemistry Research,* vol. 29, no. 10, pp. 2074-2078, 1990.

[64] A. Grossale, I. Nova, E. Tronconi, D. Chatterjee and M. Weibel, "The Chemistry of the NO/NO2=NH3 Fast SCR Reaction Over Fe-ZSM5 Investigated by Transient Reaction Analysis," *Journal of Catalysis,* vol. 256, no. 2, pp. 312-322, 2008.

[65] Y. Traa, B. Burger and J. Weitkamp, "Zeolite-Based Materials for the Selective Catalytic Reduction of NOx with Hydrocarbons," *Microporous and Mesoporous Materials,* vol. 30, pp. 3-41, 1999.

[66] M. T. Javed, N. Irfan and B. M. Gibbs, "Control of Combustion-Generated Nitrogen Oxides by Selective Non-Ctalytic Reduction," *Journal of Environmental Management,* vol. 83, no. 3, pp. 251-289, 2007.

[67] S. W. Bae, S. A. Roh and S. D. Kim, "NO Removal by Reducing Agents and Additives in the Selective Non-Catalytic Reduction (SNCR) Process," *Chemosphere,* vol. 65, no. 1, pp. 170-175, 2006.

[68] S. Zandaryaa, G. R, F. Lombardi and A. Fiore, "Nitrogen Oxides from Waste Incineration: Control by Selective Non-Catakytic Reduction," *Chemosphere,* vol. 42, no. 5-7, pp. 491-497, 2001.

[69] M. Iwamoto and H. Hamada, "Removal of Nitrogen Monoxide from Exhaust Gases Through Novel Catalytic Processes," *Catalysis Today,* vol. 10, no. 1, pp. 57-71, 1991.

[70] R. Burch, J. Breen and F. Meunier, "A Review of the Selective Reduction of NOx with Hydrocarbons Under Lean-Burn Conditions with Non-Zeolitic Oxide and Platinum Group Metal Catalysts," *Applied Catalysis B: Environmental,* vol. 39, pp. 283-303, 2002.

[71] F. Kapteijn, J. Rodriguez-Mirasol and J. A. Moulijn, "Heterogeneous Catalyic Decomposition of Nitrous Oxide," *Applied Catalysis B - Environmental,* vol. 9, no. 1-4, pp. 25-64, 1996.

[72] M. Shelef, "Selective Catalytic Reduction of NOx with N-Free Reductants," *Chemical Reviews,* vol. 95, no. 1, pp. 209-225, 1995.

[73] F. Meunier, J. Breen, V. Zuzaniuk, M. Olsson and J. Ross, "Mechanistic Aspects of the Selective Reduction of NO by Propsne over Alumina and Silver-Alumina Catalysts," *Journal of Catalysis,* vol. 187, pp. 493-505, 1999.

[74] Z. Liu and S. I. Woo, "Recent Advances in Catalytic DeNOx Science and Technology," *Catalysis Reviews: Science and Engineering,* vol. 43, no. 1, pp. 43-89, 2007.

[75] M. Wallin, C.-J. Karlsson, M. Skoglundh and A. Palmqvist, "Selective Catalytic Reduction of NOX with NH3 Over Zeolite H-ZSM-5: Influence of Transient Ammonia Supply," *Journal of Catalysis,* vol. 218, pp. 354-364, 2003.

[76] J. Li, H. Chang, L. Ma, J. Hao and R. T. Yang, "Low-Temperature Selective Catalytic Reduction of NOx with NH3 Over Metal Oxide and Zeolite Catalysis - A Review," *Catalysis Today,* vol. 175, pp. 147-156, 2011.

[77] H. L. Fang and H. F. M. DaCosta, "Urea Thermolysis and NOx Reduction With and Without SCR Catalysts," *Applied Catalysis B: Environmental,* vol. 46, no. 1, pp. 17-34, 2003.

[78] J. Li, R. Zhu, Y. Cheng, C. K. Lambert and R. T. Yang, "Mechanism of Propene Poisoning on Fe-ZSM-5 for Selective Catalytic Reduction of NOx with Ammonia," *Environmental Science and Technology,* vol. 44, pp. 1799-1805, 2010.

[79] H. Chongheng, Y. Wang, Y. Cheng, C. K. Lambert and R. T. Yang, "Activity, Stability and Hydrocarbon Deactivation of Fe/Beta Catalyst for SCR of NO with Ammonia," *Applied Catalysis A: General,* vol. 368, pp. 121-126, 2009.

[80] Y. Cheng, C. Lambert, D. H. Kim, J. H. Kwak, S. J. Cho and C. H. F. Peden, "The Different Impacts of SO2 and SO3 on Cu/Zeolite SCR Catalysts," *Catalysis Today,* vol. 151, no. 3-4, pp. 266-270, 2010.

[81] G. Bond and S. Tahir, "Vanadium-oxide Monolayer Catalysts - Preparation, Characterization, and Catalytic Activity," *Applied Catalysis,* vol. 71, no. 1, pp. 1-31, 1991.

[82] J. Chen and R. Yang, "Role of WO3 in Mixed V2O5-WO3/TiO2 Catalysts for Selective Catalytic Reduction of Nitric Oxide with Ammonia," *Applied Catalysis A: General,* vol. 80, no. 1, pp. 135-148, 1992.

[83] A. Burkardt, W. Weisweiler, J. van der Tillaart, A. Schäfer-Sindlinger and E. Lox, "Influence of the V2O5 Loading on the Structure and Activity of V2O5/TiO2 SCR Catalysts for Vehicle Application," *Topics in Catalysis,* Vols. 16-17, pp. 369-375, 2004.

[84] G. Qi, Y. Wang and R. T. Yang, "Selective Catalytic Reduction of Nitric Oxide with Ammonia over ZSM-5 Based Catalysts for Diesel Engine Applications," *Catalysis Letters,* vol. 121, no. 1-2, pp. 111-117, 2008.

[85] H. Chen and W. Sachtler, "Activity and Durability of Fe/ZSM-5 Catalysts for Lean Burn NOx Reduction in the Presence of Water Vapor," *Catalysis Today,* vol. 42, no. 1-2, pp. 73-83, 1998.

[86] F. Xiaobing and W. K. Hall, "FeZSM-5: A Durable SCR Catalyst for NOX Removal from Combustion Streams," *Journal of Catalysis,* no. 166, pp. 368-376, 1997.

[87] S. Brandenberger, O. Kröcher, A. Tissler and R. Althoff, "The State of the Art in Selective Catalytic Reduction of NOx by Ammonia Using Metal-Exchanged Zeolite Catalysts," *Catalysis Reviews: Science and Engineering,* vol. 50, no. 4, pp. 492-531, 2008.

[88] P. S. Metkar, N. Salazar, R. Muncrief, V. Balakotaiah and M. P. Harold, "Selective Catalytic Reduction of NO with NH3 on Iron Zeolite Monolithic Catalysts: Steady-State and Transient Kinetics".

[89] N.-Y. Topsøe, "Mechanism of the Selective Catalytic Reduction of Nitric Oxide by Ammonia Elucidated by in Situ On-Line Fourier Transform Infrared Spectroscopy," *Science,* vol. 265, pp. 1217-1219, 1994.

[90] G. Delahay, D. Valade, A. Guzmán-Vargas and B. Coq, "Selective Catalytic Reduction of Nitric Oxide with Ammonia on Fe-ZSM-5 Catalysts Prepared by Different Methods," *Applied Catalysts B: Environmental,* vol. 55, no. 2, pp. 149-155, 2005.

[91] J. Eng and C. H. Bartholomew, "Kinetic and Mechanistic Study of NOx Reduction by NH3 over H-Form Zeolites," *Journal of Catalysis,* vol. 171, pp. 27-44, 1997.

[92] M. P. Ruggeri, I. Nova and E. Tronconi, "Experimental Study of the NO Oxidation to NO2 Over Metal Promoted Zeolites Aimed at the Identification of the Standard SCR Rate Determining Step," *Topics in Catalysis,* vol. 56, pp. 109-113, 2013.

[93] M. Koebel, M. Elsener and G. Madia, "Reaction Pathways in the Selective Catalytic Reduction Process with NO and NO2 at Low Temperatures," *Industrial and Engineering Chemistry Research,* vol. 40, no. 1, pp. 52-59, 2001.

[94] A. Grossale, I. Nova, Tronconi and Enrico, "Ammonia Blocking of the “Fast SCR” Reactivity Over a Commercial Fe-Zeolite Catalyst for Diesel Exhaust Aftertreatment," *Journal of Catalysis,* vol. 265, no. 2, pp. 141-147, 2009.

[95] H. Huang, R. Long and R. Yang, "Kinetics of Selective Catalytic Reduction with NH3 on Fe-ZSM-5 Catalyst," *Applied Catalysis A: General,* vol. 235, no. 1-2, pp. 241-251, 2002.

[96] A. Kato, S. Matsuda, T. Kamo, F. Nakajima, H. Kuroda and T. Narita, "Reaction Between Nitrogen Oxide (NOx) and Ammonia on Iron Oxide-Titanium Oxide Catalyst," *Journal of Physical Chemistry,* vol. 85, no. 26, pp. 4099-4102, 1981.

[97] M. Koebel, G. Madia and M. Elsner, "Selective Catalytic Reduction of NO and NO2 at Low Temperatures," *Catalysis Today,* vol. 73, no. 3-4, pp. 239-247, 2002.

[98] I. Nova, C. Ciardelli, E. Tronconi, D. Chatterjee and B. Bandi-Konrad, "NH3–NO/NO2 Chemistry Over V-based Catalysts and Its Role in the Mechanism of the Fast SCR Reaction," *Catalysis Today,* vol. 114, no. 1, pp. 3-12, 2006.

[99] C. Ciardelli, I. Nova, E. Tronconi, D. Chatterjee, T. Burkhardt and M. Weibel, "NH3 SCR of NOX for Diesel Exhausts Aftertreatment: Role of NO2 in Catalytic Mechanism, Unsteady

Kinetics, and Monolith Converter Modelling," *Chemical Engineering Science,* vol. 62, no. 18-20, pp. 5001-5006, 2007.

[100] Sierra Instruments, "SideTrack 840 Technical Specifications," [Online]. Available: http://www.sierrainstruments.com/userfiles/file/datasheets/830-840-datasheet.pdf. [Accessed 10 04 2014].

[101] S. C.-P. Hsu, "Infrared Spectroscopy," in *Handbook of Instrumental Techniques for Analytical Chemistry*, Prentice Hall, 1997, pp. 247-283.

[102] M. Colombo, I. Nova and E. Tronconi, "A Comparative Study of the NH3-SCR Reactions Over a Cu-Zeolite and a Fe-Zeoline Catalyst," *Catalysis Today,* vol. 151, no. 3-4, pp. 223-230, 2010.

[103] O. Krocher, "Aspects of Catalyst Development for Mobile Urea-SCR Systems - From Vanadia-Titania Catalysts to Metal-Exchanged Zeoltites," in *Past and Present in DeNOX Catalysis: From Molecular Modelling to Chemical Engineering*, P. Granger and V. Parvulescu, Eds., Amsterdam, Elsevier Science BV, 2007, pp. 261-289.

[104] M. Koebel, M. Elsener and M. Kleemann, "Urea-SCR: A Promising Technique to Reduce NOX Emissions from Automotive Diesel Engines," *Catalysis Today,* vol. 59, no. 3-4, pp. 335-345, 2000.

[105] A. Grossale, I. Nova and E. Tronconi, "Study of a Fe-Zeolite-Based System as NH3-SCR Catalyst for Diesel Exhaust Aftertreatment," *Catalysis Today,* vol. 136, no. 1-2, pp. 18-27, 2008.

[106] H. Sjovall, R. J. Blint and L. Olsson, "Detailed Kinetic Modeling of NH3 and H2O Adsorption, and NH3 Oxidation Over Cu-ZSM-5," *Journal of Physical Chemistry C,* vol. 113, pp. 1393-1405, 2009.

[107] A. Savara, M.-J. Li, W. M. Sachtler and E. Weitz, "Catalytic Reduction of NH4NO3 by NO: Effects of Solid Acids and Implications for Low Temperature DrNOX Processes," *Applied Catalysis B: Environmental,* vol. 81, no. 3-4, pp. 251-257, 2008.

[108] M. Colombo, I. Nova, E. Tronconi, V. Schmeiber, B. Bandi-Konrad and L. Zimmermann, "NO/NO2/N2O-NH3 SCR Reactions Over a Commercial Fe-Zeolite Catalyst for Diesel Exhaust Aftertreatment: Intrinsic Kinetics and Monolith Converter Modelling," *Applied Catalysis B: Environmental,* Vols. 111-112, pp. 106-118, 2012.

[109] J. Despres, M. Koebel, O. Krocher, M. Elsener and A. Wokaun, "Adsorption and Desorption of NO and NO2 on Cu-ZSM-5," *Microporous and Mesoporous Material,* vol. 58, no. 2, pp. 175-183, 2003.

[110] S. Brandenberger, O. Krocher, M. Casapu, A. Tissler and R. Althoff, "Hydrothermal Deactivation of Fe-ZSM-5 Catalysts for the Selective Catalytic Reduction of NO with NH3," *Applied Catalysis B - Environmental,* vol. 101, no. 3-4, pp. 649-659, 2011.

[111] S. J. Schmieg, S. H. Oh, C. H. Kim, D. B. Brown, J. H. Lee, C. H. F. Pededn and D. H. Kim, "Thermal Durability of Cu-CHA NH3-SCR Catalysis for Diesel NOX Reduction," *Catalysis Today,* vol. 184, no. 1, pp. 252-261, 184.

[112] M. Muller, G. Harvey and R. Prins, "Comparison of the Dealumination of Zeolites Beta, Mordenite, ZSM-5, and Ferrierite by Thermal Treatment, Leaching with Oxalic Acid, and

Treatment with SiCl4 by 1H, 29Si, and 27Al MAS NMR," *Microporous and Mesoporous Materials,* vol. 34, no. 2, pp. 135-147, 2000.

[113] M. Hoj, M. J. Beier, J.-D. Grunwaldt and S. Dahl, "The Role of Monomeric Iron During the Selective Catalytic Reduction of NOX by NH3 over Fe-BEA Zeolite Catalysts," *Applied Catalysis B: Environmental,* vol. 93, no. 1-2, pp. 166-176, 2009.

[114] K. Krishna and M. Makkee, "Preparation of Fe-ZSM-5 with Enhanced Activity and Stability for SCR of NOX," *Catalysis Today,* vol. 114, pp. 23-30, 2006.

[115] F. Heinrich, C. Schmidt, E. Loffler, M. Menzel and W. Grunert, "Fe-ZSM-5 Catalysts for the Selective Reduction fo NO by Isobutane - The Problem of Active Sites," *Journal of Catalysis,* vol. 212, pp. 157-172, 2002.

[116] C. Eul Hun, "Thermal and CHemical Degredation Behavior of a Catalytic Ceramic Filter for Dust/NOx Removal," *Journal of Ceramic Processing Research,* vol. 10, no. 1, p. 73, 2009.

[117] D. Eley and H. Pines, Advances in Catalysis, San Diego: Elsevier, 1993.

[118] C. He, Y. Wang, Y. Cheng, C. K. Lambert and R. T. Yang, "Activity, Stability, and Hydrocarbon Deactivation of Fe/Beta Catalyst for SCR of NO with Ammonia," *Applied Catalysis A: General,* vol. 368, no. 1-2, pp. 121-126, 2009.

[119] C.-K. Seo, B. Choi, H. Kim, C.-H. Lee and C.-B. Lee, "Effect of ZrO2 Addition on de-NOx Performance of Cu-ZSM-5 for SCR Catalyst," *Chemical Engineering Journal,* vol. 191, pp. 331-340, 2012.

[120] S. Shwan, J. Jansson, L. Olsson and M. Skoglundh, "Chemical Deactivation of Fe-BEA as NH3-SCR Catalyst - Effect of Phosphorous," *Applied Catalysis B - Environmental,* vol. 147, pp. 111-123, 2014.

[121] O. Krocher and M. Elsener, "Chemical Deactivation of V2O5/WO3–TiO2 SCR Catalysts by Additives and Impurities from Fuels, Lubrication Oils, and Urea Solution I. Catalytic Studies," *Applied Catalysis B: Environmental,* vol. 75, pp. 215-227, 2008.

[122] S. Andonova, E. Vovk, J. Sjoblom, E. Ozensoy and L. Olsson, "Chemical Deactivation by Phosphorous Under Lean Hydrothermal Conditions Over Cu/BEA NH3-SCR Catalysts," *Applied Catalysis B: Environmental,* vol. 147, pp. 251-263, 2014.

[123] A. Boyano, M. Lazaro, C. Cristani, F. Maldonado-Hodar, P. Forzatti and R. Moliner, "A Comparative Study Of V2O5/AC and V2O5/Al2O3 Catalysts for the Selective Catalytic Reduction of NO by NH3," *Chemical Engineering Journal,* vol. 149, no. 1-3, pp. 173-182, 2009.

[124] T. L. Barr and S. Seal, "Nature of the Use of Adventitious Carbon as a Binding Energy Standard," *Journal of Vacuum Science and Technology A,* vol. 13, pp. 1239-1246, 1995.

[125] H. Sjovall, R. J. Blint and L. Olsson, "Detailed Kinetic Modeling of NH3 SCR Over Cu-ZSM-5," *Applied Catalysis B: Environmental,* vol. 92, no. 1-2, pp. 138-159, 2009.

[126] L. Li, J. Chen, S. Zhang, N. Guan, M. Richter, R. Eckelt and R. Fricke, "Study on Metal-MFI/Cordierite as Promising Catalysts for Selective Catalytic Reduction of Nitric Oxide by Propane in Excess Oxygen," *Journal of Catalysis,* vol. 228, pp. 12-23, 2004.

[127] V. Meille, "Review on Methods to Deposit Catalysts on Structured Surfaces," *Applied Catalysis A - General,* vol. 315, pp. 1-17, 2006.

[128] P. Avilia, M. Montes and E. Miro, "Monolithic Reactors for Environmental Applications - A Review on Preparation Technologies," *Chemical Engineering Journal,* vol. 109, no. 1-3, pp. 11-36, 2005.

[129] P. Balle, B. Geiger and S. Kureti, "Selective Catalystic Reduction of NOX by NH3 on Fe/HNEA Zeolite Catalysts in Oxygen-Rich Exhaust," *Applied Catalysis B: Environmental,* vol. 85, no. 3-4, pp. 109-119, 2009.

[130] M. Schwidder, M. Kumar, K. Klementiev, M. Pohl, A. Bruckner and W. Grunert, "Selective Reduction of NO with Fe-ZSM5 Catalysts of Low Fe Content -I. Relations Between Active Site Structure and Catalytic Performance," *Journal of Catalysis,* vol. 231, no. 2, pp. 314-330, 2005.

[131] M. Iwasaki, K. Yamazaki, K. Banno and H. Sinjoh, "Characterization of Fe/ZEM-5 DeNO(x) Catalysts Prepared by Different Methods: Relationships Between Active Fe Sites and NH3-SCR Performance," *Journal of Catalysis,* vol. 260, no. 2, pp. 205-216, 2008.

[132] G. Qi and R. Yang, "Ultra-Active Fe/ZSM-5 Catalyst for Selective Catalytic Reduction of Nitric Oxide with Ammonia," *Applied Catalysis B-Environmental,* vol. 60, no. 1-2, pp. 13-22, 2005.

[133] S. Devahasdin, C. Fan Jr., K. Li and D. H. Chen, "TiO2 Photocatalytic Oxidation of Nitric Oxide: Transient Behavior and Reaction Kinetics," *Journal of Photochemistry and Photobiology A: Chemistry,* vol. 156, no. 1-3, pp. 161-170, 2003.

[134] M. F. Irfan, J. H. Goo and S. D. Kim, "Co3O4 Based Catalysts for NO Oxidation and NOX Reduction in Fast SCR Process," *Applied Catalysis B-Environmental,* vol. 78, no. 3-4, pp. 267-274, 2008.

[135] Q. Ye, L. Wang and R. T. Yang, "Activity, Propene Poisoning Resistance and Hydrothermal Stability of Copper Exchanged Chabazite-Like Zeolite Catalysts For SCR of NO with

Ammonia in Comparison to Cu/ZSM-5," *Applied Catalysis A: General,* Vols. 427-428, pp. 24-34, 2012.

[136] C. Ericson, "NOX Modelling of a Complete Diesel Engine/SCR System," Media-Tryck, Lund, Sweden, 2007.

[137] "Combining Filtration and Catalytic Combustion in Patriculate Traps for Diesel Exhaust Treatment," *Ambrogio, Michele; Saracco, Guido; Specchia, Vito,* vol. 56, no. 4, pp. 1613-1621, 2001.

[138] S. Ayuthaya, N. Mongkolsiri, N. Praserthdam and P. Silveston, "Carbon Deposits Effects on the Selective Catalytic Reduction of NO over Zeolites Using Temperature Programmed Oxidation Technique," *Applied Catalysis B-Environmental,* vol. 43, no. 1, pp. 1-12, 2003.

[139] R. Q. Long and R. Yang, "Selective Catalytic Oxidation of Ammonia to Nitrogen Over Fe-Exchanged Zeolites," *Journal of Catalysis,* vol. 201, no. 1, pp. 145-152, 2001.

[140] M. S. Kumar, M. Schwidder, W. Grunert and A. Bruckner, "On the Nature of Different Iron Sites and Their Catalytic Role in Fe-ZSM-5 DeNOx Catalysts: New Insights By a Combined EPR and UV/VIS Spectroscopic Approach," *Journal of Catalysis,* vol. 227, no. 2, pp. 384-397, 2004.

[141] H. Sjovall, R. J. Blint, A. Gopinath and L. Olsson, "A Kinetic Model for the Selective Catalytic Reduction of NOx with NH3 over an Fe-zeolite Catalyst," *Industrial & Engineering Chemistry Research,* vol. 49, no. 1, pp. 39-52, 2010.

[142] J. Gary and G. Handwerk, Petroleum Refining: Technology and Economics, 2nd ed., New York, 1984.